Silver-based antibacterial surfaces for bone implants

Bogdan Stefan Necula

Silver-based antibacterial surfaces for bone implants

Proefschrift

ter verkrijging van de graad van doctor
aan de Technische Universiteit Delft,
op gezag van de Rector Magnificus prof. ir. K.C.A.M. Luyben,
voorzitter van het College voor Promoties,
in het openbaar te verdedigen op woensdag 6 november 2013 om 10:00 uur
door

Bogdan Stefan NECULA

Master of Science
"Gh. Asachi" Technical University Iasi, Romania

geboren te Piatra Neamt, Romania

Dit proefschrift is goedgekeurd door de promotor:
Prof. ir. L. Katgerman

Copromotor: Dr. ir. I. Apachitei

Samenstelling promotiecommissie:

Rector Magnificus,	voorzitter
Prof. ir. L. Katgerman,	Technische Universiteit Delft, promotor
Dr. ir. I. Apachitei,	Technische Universiteit Delft, copromotor
Prof. dr. F.C.T. van der Helm,	Technische Universiteit Delft
Dr. S.A.J. Zaat,	Academisch MC, Universiteit van Amsterdam
Prof. dr. G.J.V.M. van Osch,	Erasmus MC, Universitair Medisch Centrum Rotterdam
Prof. dr. ir. J. Sietsma,	Technische Universiteit Delft
Prof. dr. ir. H. Terryn,	Vrije Universiteit Brussels

Keywords: antibacterial coatings, bone implants, titanium dioxide, porous coatings, silver nanoparticles, *in vitro* evaluation.

ISBN: 978-94-6186-233-4

"Every operation is an experiment in bacteriology"

- Berkeley George Andrew Moynihan

Contents


1 cm

Chapter 1

Infections associated with bone implants: etiology, incidence, treatment and prevention strategies

An introduction to the problem of implant associated infections and the need of antibacterial cementless implants.

1.1. Treatment of joint diseases using implantable devices

1.1.1. Joint diseases

Today, the most frequent chronic musculoskeletal disorder and the leading cause of disability in the elderly is osteoarthritis (OA). OA is a chronic disease involving the joints, especially those bearing the weight (*e.g.,* hip, knee), characterized by destruction of articular cartilage, which results in severe pain, loss of motion, and occasionally, an angular deformity of the extremity. Unlike bone, cartilage has a very limited capacity for repair, therefore, when exposed to a severe mechanical, chemical, or metabolic injury, the damage is permanent [1].

Epidemiological studies estimate that approximately 43 million people in the United States and 15% of the world population are affected by OA [2, 3]. Due to demographic changes, the incidence of OA is rapidly increasing, leading to social, psychological and economical burdens in patients and consequently substantial costs to the healthcare systems [2, 4]. The risk of mobility impairments caused by knee OA alone is greater

than due to any other disease in people over 65 [5]. The factors that increase the risk of OA include: older age, gender (women are more likely to develop OA), genetic predisposition, joint injuries, obesity, increased mechanical stress, greater bone density and lifestyle [4]. Other joint diseases, like rheumatoid arthritis, avascular necrosis, congenital dislocation of the hip joint and acetabular dysplasia (shallow hip socket) can also lead to severe pain and loss of function of the affected joints.

1.1.2. Treatment of osteoarthritis

To date, a medical cure for OA does not exist and, most likely, the disease will get worse over time. Over-the-counter pain relievers and nonsteroidal anti-inflammatory drugs (*e.g.,* acetaminophen, aspirin, ibuprofen and naproxen) can reduce inflammation and relieve pain. However, these drugs may cause severe complications to older people (*i.e.,* stomach upset, cardiovascular problems, liver and kidney damage).

Life-style changes like getting exercise, loosing weight, eating a healthy, balanced diet might take some stress off the joints, and relieve some of the pain. Regular exercise can increase the endurance and strengthen the muscles around the joints, making them more stable, while loosing weight might decrease the stress on the weight-bearing joints.

However, a significant advance in the treatment of painful and disabling OA, that greatly improved the symptoms, restore mobility and quality of life, represents total joint replacement (TJR) surgery or total joint arthroplasty (TJA). TJR surgery is an orthopaedic surgery in which an arthritic, dysfunctional or traumatized joint is replaced with an orthopaedic prosthesis. Such surgery can be performed on any joints of the body, including the hip, knee, ankle, foot, shoulder, elbow, wrist, and fingers. Among these procedures, hip and knee joint arthroplasties are by far the most common.

1.1.3. Prosthetic designs and biomaterial combinations

Decades of *in vivo* research and clinical experimentation have resulted in a large number of prosthetic designs and biomaterial combinations.

In this section, two of the most encountered procedures, *i.e.,* total hip replacement (THR) and total knee replacement (TKR) will be covered with respect to fixation method and material combinations. The development of a stable, permanent fixation method of implants to bone has been an incredible challenge in the field. Up to date,

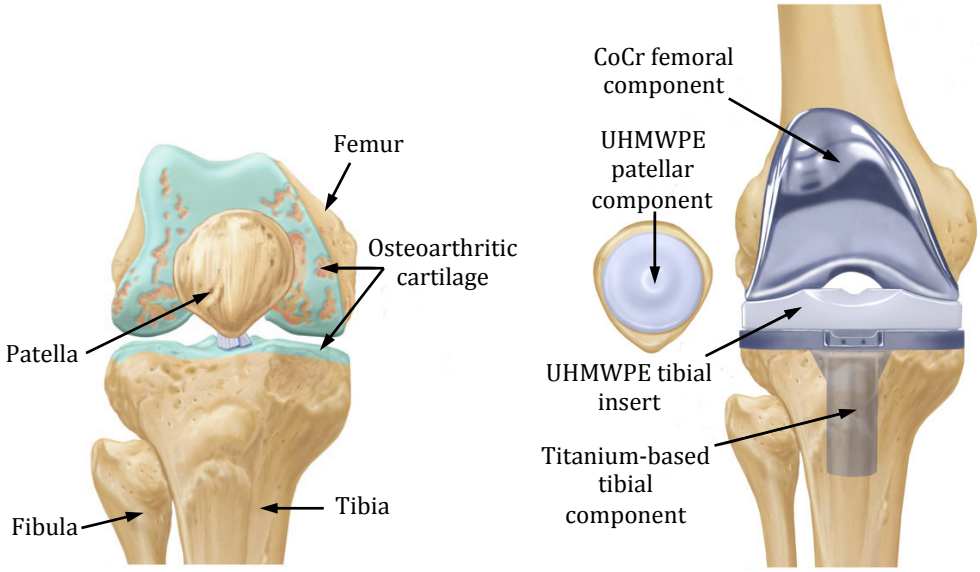

Fig. 1.1. Schematic representation of an osteoarthritic knee (a) with the corresponding components of a total knee replacement (b). Where: CoCr -Cobalt Chrome alloy; UHMWPE - Ultra-High Molecular Weight Polyethylene. Adapted from St. Francis Orthopaedic Institute website [6].

there are two types of fixation methods: (i) cemented, most commonly achieved using polymethylmethacrylate (PMMA), called bone cement, to mechanically fix the implant to the bone and (ii) cementless, biological fixation, which is achieved through bone ingrowth directly into the porous structure of the implant and osseointegration [7].

Fixation of implants using PMMA provides immediate stability, allowing the patients to bear all their weight on the implant at once. However, this method has several drawbacks. It creates two types of interface (*i.e.,* bone-cement and cement-implant) and therefore loosening might occur at either one. Furthermore, a thin fibrous membrane may appear at the interface with the bone leading to macro-motion, bone loss and implant loosening [8].

Cementless implant fixation is used preferably in young patients in order to preserve as much bone stock as possible. This is an important factor in order to maximize implant stability on both short and long-term. On short-term, the implant support and stable fixation will benefit from mechanically healthy host bone and, on long-term, it

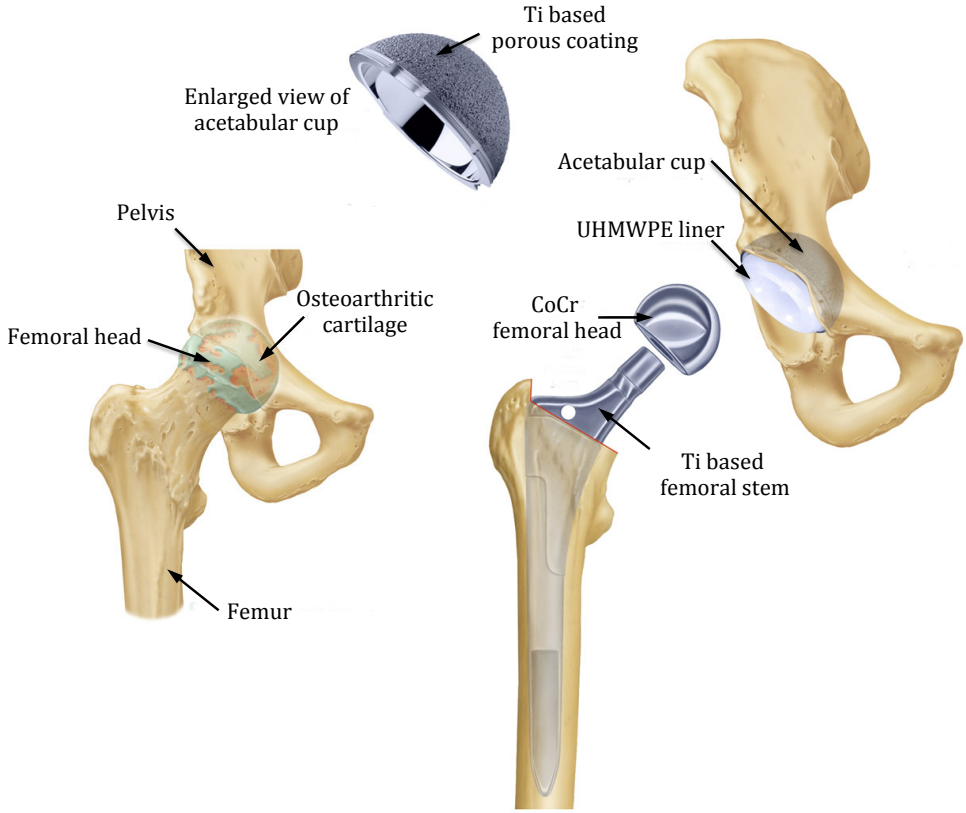

Fig. 1.2. Schematic representation of an osteoarthritic hip (a) with the corresponding components of a total hip replacement (b). Adapted from St. Francis Orthopaedic Institute website [9].

is preferred to have as much host bone as possible should a revision surgery be required.

A cementless TKR prosthesis consists of femoral, tibial, and/or patellar components (Fig. 1.1). The femoral component is typically made of CoCr alloy whereas the polymeric tibial insert is assembled on a titanium-based stemmed tibial component. The tibial and patellar components are made of Ultra-High Molecular Weight Polyethylene (UHMWPE) [10]. The prosthesis for a cementless THR consists of a femoral component and an acetabular component (Fig. 1.2). The femoral component (stem) is divided into head, neck, and shaft. The stem is press-fitted into the medullary canal and is made almost exclusively from a Ti alloy. The femoral head is

made of one of the following materials: CoCr alloy, alumina or zirconia-alumina. The acetabular component consists of an UHMWPE insert and a titanium shell [10].

All the biomaterials used in THR and TKR should meet several criteria in order to perform successfully in the body. They must be biocompatible, performing *in vivo* without producing a harmful local or systemic response. They must be resistant to corrosion and chemical degradation, so that the *in vivo* environment does not adversely affect any of their properties. In addition, the biomaterials must possess sufficient mechanical strength since they must withstand the large forces that are transmitted across all of the articular joints in the body. Finally, materials for use in bearing surfaces must be wear resistant over tens of millions of cycles of use with a minimal release of particulate debris [11].

1.1.4. Failure and complications

The causes of implant failure may be classified, in general, as short-term (intra-operative), medium-term and long-term. Other classification may include factors related to the surgeon (technique or wrong implant), patient (inappropriate use) or manufacturer (design or material).

Intra-operative risks include mal-positioning of the components, limb shortening, instability/dislocation, loss of range of motion, fracture of the adjacent bone, nerve damage and damage of the blood vessels. Immediate risks after surgery are generally associated with superficial or deep wound infections, wound healing abnormalities, prosthesis instability and dysfunction of the peripheral nerves. Medium-term risks include infection, dislocation, persistent pain, loss of range of motion and weakness. Longer-term problems are less directly associated with the surgical trauma and intervention but are linked more to the patient and performance of the prosthesis. Serious complications, leading to implant loosening may be classified as (i) aseptic due to the wear of the components leading to particle disease (osteolysis or polyethylene synovitis) and (ii) septic due to *implant associated infections (IAI)*.

1.2. Implant associated infections

1.2.1. Etiology

A key factor that will determine the occurrence of IAI is the chance that infectious bacteria will reach the implant surface. Bacteria, from different sources, can reach the surface of the implant in several ways at different time points. Deep prosthetic

infections can be subdivided into: (i) early infection, if becomes apparent during the early post-operative period, which may range between 1 and 3 months; (ii) delayed infections, usually appear within 3 months and two years after surgery; and (iii) late or haematogenous infections that appear > 2 years after implantation [12]. For both early and delayed infections the contamination with bacteria is thought to have happened either during surgery or during early post-operative period, while haematogenous infections are caused by bacteria from infections elsewhere in the body, like the urinary tract, skin or dental sepsis. According to Babiak and Górecki [13], during the decade 1994–2003, early infections constituted 25%, delayed and after revisions 69%, and haematogenous 6% from totally 112 treated septic hip prostheses.

The main sources of contamination for early and delayed infections appear to be from the airborne particles from the operating theater, the skin of the patient, the hands of the surgical personnel and the instruments used during surgery [14-16]. Airborne bacteria, which can be present in the operating theater, can colonize the open wound and consequently, the surface of the implant during surgery. Also, during insertion of the prosthesis, microorganisms from the patient skin can be pushed towards the implant surface. Furthermore, microorganisms present on the patient skin can contaminate the operation wound and reach the implant surface through diffusion, active movement or blood transport [17].

Bacteria can reach the implant surface also via the blood stream causing so called haematogenous infections. The presence of bacteria in the blood, called bacteremia, is usually a consequence of skin infections, dental interventions, abscesses, infections of the urinary tract or pneumonia. It is believed that some strains of bacteria might survive within macrophages [18] and thus potentially being transported to the implant surface as the biomaterials surface elicits a foreign body reaction [17].

Surgical related factors involved in the contamination include duration of the procedure, the number of personnel in the operating theatre and use of strong antibiotic prophylaxis, vertical laminar air flow and body exhaust suits [14, 19, 20]. Host factors predisposing to infection are older age, poor nutritional status, underlying joint disease (rheumatoid arthritis, psoriasis), obesity, diabetes, prior native joint infection, and HIV infection [12].

The combination of tissue trauma and the presence of a large foreign body (*i.e.,* the implant) will lead to the inability of the host defense mechanisms to act in the neighborhood of the prosthesis. This will significantly compromise the local tissue ability to fight against infection. It has been shown that the presence of a foreign body decreases >100,000-fold the minimal infecting dose of bacteria [12]. For example, it

was showed [21] that the presence of subcutaneous suture would reduce the required inoculum to produce infection with *Staphylococcus aureus* from 10^6 to only 200 colony forming units (CFU). Furthermore, the *Staphylococcus epidermidis*, a relatively avirulent bacteria, normally not capable of producing infection, is the most common infecting bacteria in IAI [22].

1.2.2. Biofilm formation

Immediately after implantation, the prosthesis is instantly covered by a proteinaceous conditioning film precipitating from tissue fluids, ruptured cells, and blood [23]. This film alters the surface characteristics of the implant allowing attachment of bacteria that may otherwise not attach to the bare surface [24].

Planktonic bacteria present in the wound can be transported to the surface of the prosthesis through an interaction of physical and chemical forces such as: Brownian motion, sedimentation due to differences in specific gravity between the bacteria and the body fluid or convective mass transport, through which bacteria cells are physically transported towards the surface by the movement of the bulk fluid [25]. When the bacteria have reached the surface of the implant, initial attachment occurs (Fig. 1.3). The attachment is mediated by specific or non-specific interaction forces between the microbial proteins known as "microbial surface components recognizing adhesive matrix molecules" and specific host-tissue ligands in the conditioning film, like fibronectin, fibrinogen and collagen. The non-specific interaction forces, such as Van der Waals forces, surface tension, acid-base interactions and electrostatic forces have a long-range character while the specific interactions act on highly localized regions, over distances smaller than 5 nm, irreversibly binding a bacterium to the implant surface [17, 26]. Once the microorganisms are attached to the implant surface they are protected against phagocytosis, as the bacteria and implant together are too large to be ingested [17]. The initial phase of adherence to the biomaterials surface is followed by a rapid proliferation phase, during which bacterial cells start dividing and secrete a matrix of polysaccharides on the bacterial membrane that facilitate multilayered intercellular adhesion and formation of a *biofilm* [12, 27]. The extracellular polysaccharide matrix retains nutrients and protects the microorganisms from the immune response. With the protective polysaccharide shell and sequestered nutrients, bacteria in biofilms exhibit extreme resistance to antibiotics [28]. To kill biofilm bacteria high dosages of antibiotics are needed *i.e.,* approximately 1000 times the dose necessary to kill the same amount in a planktonic state [29, 30]. The last stage is biofilm maturation and detachment of single cells or groups of cells, which may travel to other sites and start the whole process of biofilm

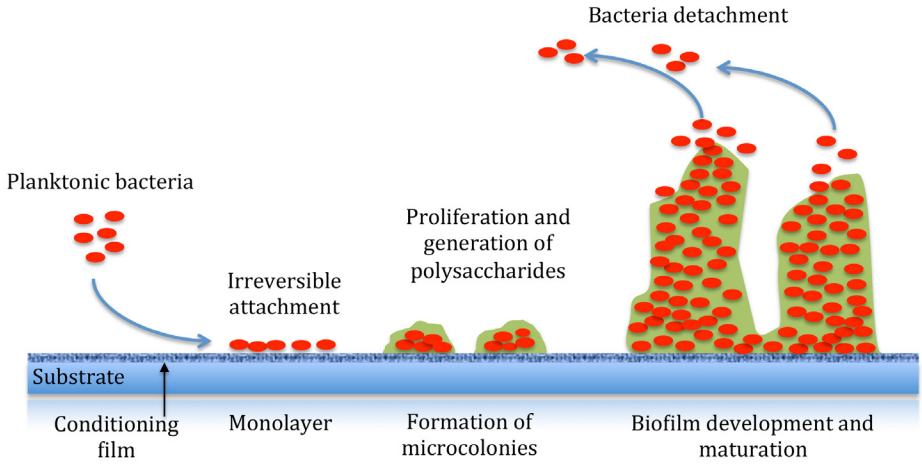

Fig. 1.3. Representation of bacterial adhesion to a biomaterial substrate with subsequent formation of a biofilm.

formation elsewhere [31, 32]. Once a mature biofilm has formed on the surface of the implant, an IAI with all its complications, including ultimately removal of the prosthesis, is almost inevitable.

1.2.3. Current treatment

IAI do not heal only by applying systemic therapy with antibiotics. Up to date, there are different strategies for treatment of IAI depending on the anatomic location of the prosthesis and on the severity of the infection *i.e.,* permanent removal of prosthesis, two-stage replacement of the prosthesis, one-stage replacement of the prosthesis, arthrodesis, amputation and suppressive antimicrobial chemotherapy. The most common type of treatment is the two-stage revision, as it allows a better debridement, preserves bone stock and allows the use of cementless prosthesis [33]. During the first step of the two-stage revision procedure, the old prosthesis is removed, soft tissues are debrided and in many cases a local antibiotic carrier is left *in situ*. During this time interval the systemic antibiotics should further cure the infection and, at the second stage, when the infection is cured, a new prosthesis is implanted.

These are long, traumatic and expensive procedures for the patients. The costs of treatment for a single infected prosthesis differ between national medical care systems. For example, the costs of one infected case of hip prosthesis in the USA, in

2000, were between $60,000 and $75,000. Similar costs, in 2003, were €50,000 per case in Germany and €75,000 in Great Britain [34, 35].

1.2.4. Prevention measures

General measures to prevent the contamination of implanted materials with microorganisms can be organized into pre-operative, per-operative and post-operative.

Pre-operative, considerable effort has to be taken on improvement of the host resistance to infection by setting up the right body temperature, glucose level and nutritional state [36]. Prior to the surgery, removal of operative site hair at the time of operation using clippers rather than a razor as well as skin preparation with 10% povidone-iodine solution and application of an iodine-impregnated drape to the skin are well established preventive measures [26]. In order to prevent acquisition of antibiotic resistant skin flora avoidance of prolonged pre-operative hospital stay is recommended. Systemic administration of antibiotics is considered to be the most effective measure to reduce surgical site infections by about 80% [37]. Mannien *et al.* [38] suggested that antibiotics must been given intravenously 15–45 minutes before incision.

Per-operative measures to reduce the contamination of the wound include factors related to the operating room environment such as the use of adequate laminar airflow ventilation, body exhaust systems, minimizing operating room traffic and administration of prophylactic antibiotics with proper redose if the operation is prolonged [36, 39].

Post-operative measures may include antimicrobial prophylaxis for another 24 hours after procedure and monitoring of the surgical wound for the development of infection [36].

1.2.5. Incidence

Although application of prophylactic antibiotics and better operation hygiene has reduced the incidence of IAI, still a significant number of patients suffer from these infections. In the Netherlands, post-operative surgical infection rates are documented in a registry called 'PREZIES' (PREventie ZIEkenhuisinfecties door Surveillance). This register shows that infection rates of about 2.3% and 1.8% are obtained for total hip and knee arthroplasties, respectively [40]. For revision cases, these numbers increase rapidly, with 4.5% for total hip arthroplasty and 5.0% for total knee arthroplasty. The

United Kingdom National Joint Registry reports that in England and Wales between 2010 and 2011 there were approximately 179,000 THR and TKR procedures, from which 1,019 revision hip arthroplasty procedures and 1168 knee revision procedures were performed due to IAI [41]. In USA, according to the Medicare system for people aged 65 or over, the incidence of infection in hip replacements was 1.63% within 2 years and 0.59% from years 2 to 10, while in total knee replacements it was 1.55% within 2 years and 0.46% between years 2 and 10 [42, 43]. Worldwide, the number of infections associated with all implantable biomedical devices approaches one million cases per year [44].

Future strategies to prevent IAI should focus on providing antimicrobial capability to the implant itself by incorporation of a bioactive into the surface of the implant to be released at the site of implantation. Local delivery of an antibacterial agent should prevent bacterial colonization and biofilm formation on the implant surface.

1.3. Biomaterial strategies to prevent implant associated infections

Clinically, cemented implant procedures may use drug/antibiotic-loaded cements as a strategy to reduce the incidence of IAI. However, for cementless implants, no suitable strategies for local antibacterial delivery are currently available in clinics. As the cementless implant has to interact with the surrounding bone to obtain a stable fixation, the surface properties are extremely important. A potential antibacterial surface will be at the interface with the living bone and therefore should be biocompatible and allow wound healing and osseointegration. In this regard, the choice of the antibacterial agent and the potential carrier/coating is very important. Such agent should not be toxic for the bone cells and should kill a wide range of bacterial strains. Furthermore, it should have a controlled and sustained release over a long time without the risk of developing bacterial resistance. The carrier should be at least inert if not promote osteoinduction and osseointegration. Creating an antibacterial surface often results in addition of coatings/layers or changing the chemical composition of the targeted surface. Such coatings or layers should be able to withstand the significant forces that are often applied to orthopaedic implants during insertion. Good adhesion of the layer with the substrate should prevent delamination during the arthroplasty procedure and should have the mechanical strength necessary for everyday load bearing. One crucial requirement for cementless implants is mechanical interlocking with the surrounding bone, achieved by osseointegration. For this, rough and porous surfaces are used by means of a plasma

sprayed process. An antibacterial surface should add up to this requirement, hence should cover closely the complex geometry of plasma sprayed implant surfaces.

Many *in vitro* and *in vivo* studies on the synthesis of antibacterial coatings for medical devices have been published. The main two research approaches are based on (i) reducing or inhibiting the bacteria ability to adhere and colonize the implanted device (passive approach) and (ii) providing an antibacterial function to the implanted device that will kill any adherent bacteria (active approach). For the former approach, surface modifications to prevent bacteria colonization have been examined by using hydrophilic polyurethanes, polyo(ethylene glycol), and poly(ethylene oxide) brushes [45-49]. These passive coatings can reduce bacterial adhesion on the implant but they do not eliminate the risk of infection in the surrounding wound.

The active approach is based on surfaces that continuously release antibacterial agents at the site of implantation. Local delivery of antibacterials maximizes their effect where they are required, reduces potential systemic toxicity (high local doses can be administered without exceeding the systemic toxicity level of the drug) and increases cost efficiency. Such delivery also allows for the tailored selection of the antibacterial drug toward specific pathogens associated with implant infections, avoiding potentially harmful side reactions in other parts of the body.

To generate antibacterial surfaces on orthopaedic implants several surface modification techniques can be used. Considering the depth, place and type of interaction of the surface modification to the original substrate (Fig. 1.4) the antibacterial layers can be classified as:

a) layers deposited on top of the substrate (with little interaction with the substrate);

b) layers deposited on top of the substrate with formation of an interaction layer at the interface with the substrate;

c) layers formed by conversion of the outmost surface of the original substrate into a more desirable chemistry and/or topography;

d) layers created by diffusion treatment of the substrate that does not add new material on top of the original substrate but changes the chemical composition of the outmost surface of the substrate material.

Antibacterial drugs and biomolecules can be deposited on the implant surfaces directly or by means of polymeric, ceramic or metallic coatings. This usually involves low temperature processes and therefore little interaction takes place with the

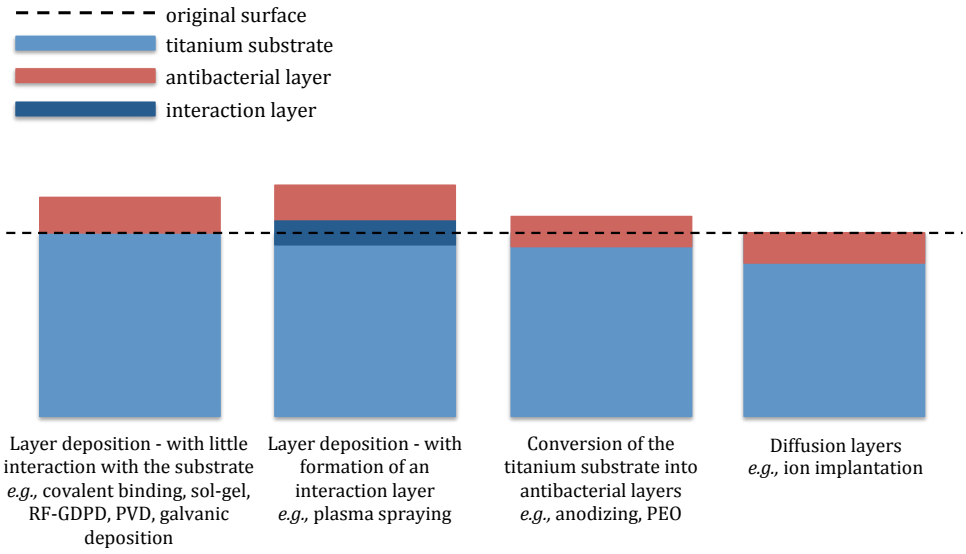

Fig. 1.4. Classification of surface modification processes by the depth and place of the antibacterial layer. Adapted from [50].

substrate material (*i.e.,* no chemical and/or physical change of the original substrate). One approach involves the immobilization of antibacterial agents directly onto biomaterials surfaces for example, the covalent binding of antibiotics or antimicrobial peptides onto the titanium surfaces [51-58]. Although there are very obvious advantages for these systems, they also have their weaknesses. Coatings tend to be thin and fragile resulting in limited availability of the antibacterial agent and scraping of the coating during surgical insertion. The use of biocompatible polymer coatings (*e.g.,* polyurethane, silicone rubber, polyamide, polyhydroxyalkanoates, *etc.*) loaded with antibiotics (*i.e.,* vancomycin, tobramycin, rifampicin, cefamandol, cephalothin, carbenicillin, amoxicillin, and gentamicin) [59-62], Ag ions [63, 64], Ag nanoparticles [65], nitric oxide (NO) [66-69] and antimicrobial peptides [52, 70-72] represents another strategy for local antimicrobial delivery on implantable materials. Few of the common methods to deposit polymeric coatings on metallic substrates are: radio-frequency glow discharge plasma deposition (RF-GDPD), dipping and drying, spray drying, layer-by-layer technique, sol-gel technology and self assembly monolayer (SAM) technique. However, the main drawbacks of the polymeric coatings include limited mechanical and chemical stability, local inflammatory reactions and uncontrolled drug-release kinetics. Alternatively, biodegradable polymeric coatings such as poly(lactic-co-glycolic acid) (PLGA), polylactic acid (PLA) and poly-DL-lactic

acid (PDLLA) may offer controlled release of antibacterial agents at a high rate [73-76]. Because the standard polymeric carriers are not bone-bioactive, attention has been focused on alternative osteoconductive materials. Thus, inorganic coatings such as biocompatible hydroxyapatite (HA) and calcium phosphates coatings can also be used as the carrier of antibacterial agents [77-80]. The problems of HA coatings loaded with antibiotics are that desorption of antibiotics is rapid and the concentration of antibiotics adsorbed on the surface is limited [78].

Other approaches use surface modification processes such as plasma vapor deposition, ion beam-assisted deposition and galvanic deposition to create hard metallic antibacterial coatings on the surface of orthopaedic implants. Few examples include silver (Ag) ion doped TiN coatings on Ti substrates [81, 82], electrodeposition of Ag on the Ti6Al4V megaprostheses [83, 84], Ag-doped functionally graded HA coatings on Ti surfaces [85] and ZrO_2-Ag/ZrO_2-Cu coatings on Ti implants [86]. The antibacterial properties of Ag have been attributed to its ionic form, a form of Ag that is not always present at a surface coated with metallic silver. Thus, the main disadvantage of metallic Ag coatings is that they do not continuously release ions.

Thermal spraying, especially the plasma spraying method appears to be the most commonly used technique for application of rough and porous coatings on orthopaedic implants. Plasma spraying requires high temperature flame or plasma jets and therefore, an interaction layer is formed at the substrate interface next to the deposition coating (Fig. 1.4). Recent research is focused on using plasma spraying process to create antibacterial coatings on titanium implants by using powdered Ag as a deposition material next to HA or Ti powders [87-90].

A new surface modification approach involves electrochemical conversion of the titanium surface into more desirable chemistries and topographies by using anodizing or plasma electrolytic oxidation (PEO) processes. Using this approach, titanium was anodically oxidized in chlorine solutions to produce Ti-Cl antibacterial surfaces [91, 92]. Furthermore, PEO of titanium in an electrolyte based on calcium phosphate, $AgNO_3$ and H_2PtCl_6 lead to the formation of an Ag (Pt) containing calcium phosphate coating [93]. In another work [94], zinc was incorporated into TiO_2 coatings on titanium by PEO and reported to have good bacterial inhibition ability and bone-formability.

Finally, the last surface modification strategy to create antibacterial coatings on titanium implants involves diffusion treatments like ion implantation. This surface modification method does not add any new material on top of the substrate, but mainly changes the composition of the outermost layer of the substrate material. Few examples include Ag plasma immersion ion implantation on commercial pure

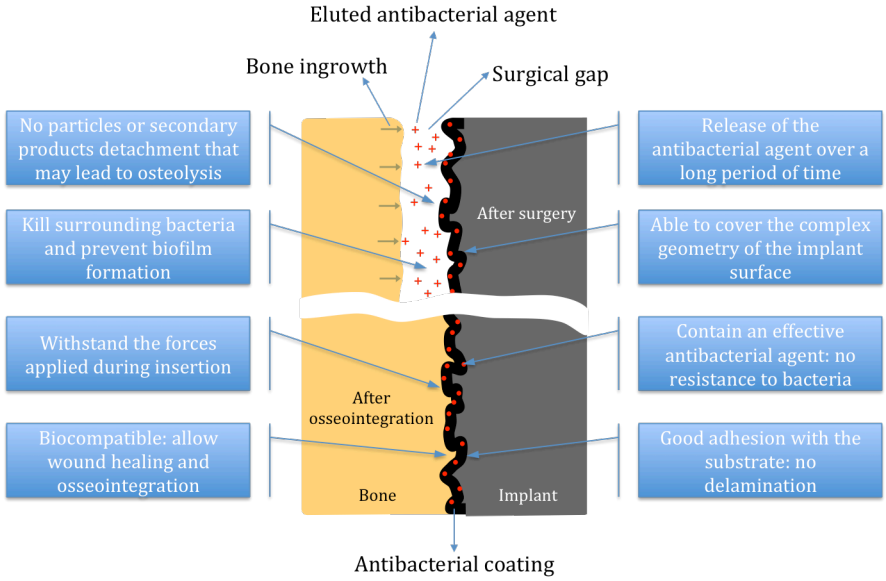

Fig. 1.5. Graphic representation of an ideal bone/antibacterial coating/implant interface for cementless implants.

titanium (cpTi) [95] and synthesis of a photocatalytic anatase TiO_2 film on a cpTi surface with bactericidal effect [96].

Until now, no antibacterial surface for cementless implants has become available for clinical practice. In Fig. 1.5 are indicated the most important properties that an antibacterial coating must have when applied on a cementless implant. One process suitable for creating antibacterial layers on metallic biomedical materials meeting these criteria within a single step process might be PEO.

1.4. Plasma electrolytic oxidation process

PEO, also known as micro-arc oxidation, anodic spark deposition or spark anodizing, is an electrochemical surface treatment process for generating porous oxide coatings on valve metals (*i.e.,* Ti, Ta, Mg, Al, Nb, W, Zr). The process is based on electrochemical conversion of the substrate metal into its oxide. The oxidation takes place in an aqueous electrolyte at voltages sufficient to determine dielectric breakdown of the oxide layers. The oxide coating grows both inwards and outwards from the original metal surface. The PEO process is usually carried out in an electrolytic bath, which

typically has a two-electrode configuration: the anode made by valve metal and the cathode made by stainless steel or platinum. The PEO can be performed by applying a constant current density (galvanostatic mode) or a constant voltage (potentiostatic mode) between the two electrodes. When a constant voltage or current is applied, electrode reactions (oxidation and reduction) in combination with field-driven ion diffusion and micro-arc discharges lead to the formation of an oxide layer on the anode surface [97].

The main stages during the growth of PEO coatings are: (a) formation of an anodic barrier layer in the first seconds of oxidation; (b) dielectric breakdown of the anodic film; (c) local thickening of the oxide at sparking locations; (d) the appearance of the pores; (e) sustained growth in the presence of sparking; (f) the appearance of larger sparks and breakdown channels, leading to large and protruding pores. The formation of oxide layers on titanium biomedical alloys is described in more detail in Chapter 3 of this thesis.

As a surface modification technique for biomedical applications, PEO on titanium alloys can provide:

a) Tailored chemistry of the oxide layers – the nanometer thick native TiO_2 layer, spontaneously formed on the surface of titanium, plays an important role in the biocompatibility of bone implants. PEO process enhances this native amorphous layer and further improves it by formation of anatase and rutile phases, known to induce apatite formation *in vitro* [98]. Furthermore, during PEO, the layers can also incorporate substantial amounts of electrolyte constituents, including anion and cation derivatives and, if present, particles from the electrolyte. For example, PEO performed in calcium and phosphorus-based electrolytes, such as calcium glycerophosphate and calcium acetate, results in formation of TiO_2 layers rich in both Ca and P and, hereby increasing bioactivity [99].

b) Multiscale interconnected porosity – the result of the PEO process is not only the thickening of the native oxide layer but also creation of interconnected micro- and/or nano-porosity. The oxidation process is rather complex and depending on various parameters such as current density, process time, applied voltage, type of alloy, electrolyte composition and concentration, layers with different porous architectures can be created (Fig. 1.6).

c) Enhanced adhesion of the oxide layer with the substrate (in-depth oxide growth) – because it is a conversion coating rather than a deposited coating (such as a coating formed by plasma spraying) it has excellent adhesion to the substrate metal (*e.g.,* 70 MPa for PEO coatings *vs.* 54.1 MPa for plasma spray coatings) [100, 101].

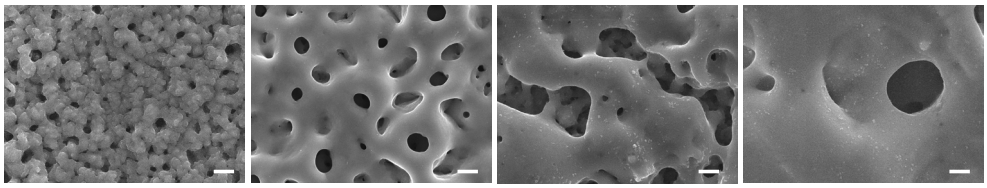

Fig. 1.6. Example of different porous surfaces created by PEO of titanium. Scale bar is 2 μm.

d) Possibility to cover complex geometries – compared with other processes for producing oxide films such as ion plating, sputtering, chemical vapor deposition (CVD), plasma spraying, sol–gel, and ion implantation, it is noteworthy that PEO can form oxide layers on metal surfaces with extremely complex geometries. Chapter 6 covers this aspect in more detail.

e) Possibility to embed particulate bioactive agents – as mentioned before, particle additions to the electrolyte (*e.g.,* antibacterial agents, drug nanocapsules, growth factors, peptides) can be incorporated within the oxide layer for extended biofunctionality.

f) Hard and corrosion resistant coatings – hardness values of 4.8 – 6.2 GPa were recorded for PEO layers grown on Ti6Al4V alloy, almost twice as hard as the substrate [102]. The oxide layer is considered to contribute also to the improvement of corrosion resistance. After PEO, the thickness of the protective oxide layer increases and it could lead to less ion release to the human body.

g) Low temperature process – although a higher temperature is believed to be developed in the discharge channels during PEO, the short discharge lifetime and high cooling rate reduce the effective temperature of layer synthesis, and hence the conditions of the PEO process may be considered to be close to room temperature.

1.5. Silver as an antibacterial agent

Because of the increasing problem of antibiotic resistant bacteria [103, 104], some antimicrobial agents outside the field of regular antibiotics have been investigated for their efficacy in the prevention of IAI as well, for *e.g.,* antimicrobial peptides (AMP), nitric oxide (NO), quaternary ammonium compounds (QAC), anti-quorum sensing molecules (AQSM) and Ag.

AMP present several advantages but also disadvantages as anti-infective drugs. Advantages include a broad-spectrum activity, a rapid killing, a low level of induced

resistance and concomitant anti-inflammatory activities. However, the potential local toxicity, the susceptibility to proteolysis, the pH sensitivity, the cost of synthesis and lack of stability constitute the main disadvantages [105].

NO is a highly reactive diatomic radical that is continually released by the endothelium at a flux of approximately 1–4 × 10^{-10} mol/cm^2/min [106], regulating vascular tone and inhibiting platelet adhesion and aggregation [107, 108]. It has been proven *in vitro* that NO is a potent antimicrobial agent, effective against a range of microorganisms, including both gram-negative and gram-positive bacteria [109]. NO possesses broad-spectrum antibacterial activity, primarily due to its reactive byproducts, such as peroxynitrite ($ONOO^-$), which is a reaction product of NO with superoxide, O^{2-} [28]. NO is an extremely reactive gas and difficult to administer as a therapeutic agent [107]. Currently, the only option to obtain NO-releasing biomaterials is to incorporate a NO donor into polymeric coatings [110-112].

QAC have also been shown to have antimicrobial activity. The generally accepted mechanism is that QAC destabilize the cytoplasmic membrane, which leads to leakage and eventually to bacteria cell death [113, 114]. However, a similar mechanism provokes cytotoxicity and further research is needed to optimize the balance between bactericidal activity and cytotoxicity by adapting the chemical structures [115].

Bacterial communication, also known as quorum sensing, is crucial for biofilm formation. Different strategies based on molecules interfering with the quorum sensing pathway (*e.g.,* furanones) were explored to influence the bacterial functions in order to inhibit the biofilm formation [116, 117]. However, some furanones have been shown to be cytotoxic and mutagenic, which is a limitation for medical applications [118, 119].

The antibacterial property of Ag has long been known and goes back to ancient Greece and Rome, where Ag coins were used to make water potable [120, 121]. Medical use of Ag goes back to the Middle Ages when Ag nitrate was first used to treat chronic wounds, ulcers and fistulas, as an alternative method to cauterizing iron. In 1700, Ag nitrate was used for the treatment of venereal diseases, fistulae from salivary glands, and bone and perianal abscesses. Another medical application of Ag ions was the use of a 2% Ag nitrate solution in the eyes of newborn children to prevent gonorrhea infections, introduced in 1880. In the 19th century granulation tissues were removed using Ag nitrate to allow epithelization and promote crust formation on the surface of wounds [122]. In the 1940s, after penicillin was introduced, the use of Ag for the treatment of bacterial infections minimized. Ag again came in picture in the 1960s when Moyer [123] introduced the use of 0.5% Ag nitrate for the treatment of burns. Recently, due to the emergence of antibiotic-resistant bacteria, research into the

medical applications of Ag has been extremely active. The advances in nanotechnology have enabled us to produce metallic Ag nanoparticles, which are more efficient in releasing Ag ions. Thus, Ag has recently started to be used in nanoparticulate form, with the advantage of a high specific surface area and a continuous release of Ag ions [124].

Today, a variety of commercial products containing Ag have emerged and are already being used in clinics (Table 1.1). Ag-coated catheters are used to prevent the formation of biofilms and resulting infections [125, 126]. Nanoparticulate Ag is used as an alternative antimicrobial agent in bone cement to replace the currently used antibiotics, in order to solve the problem of infections with antibiotic resistant bacteria [127]. Ag-coated megaprostheses proved to reduce the infection rate in a study performed on 51 patients with bone or soft-tissue tumors, with osseous infiltration and stage III giant cell tumors [84].

Besides medical applications, Ag products are being used as well in consumer products, such as household appliances (dishwashers, floors, refrigerators), clothes and cosmetic products.

Table 1.1. Examples of commercially available medical products containing Ag [83, 84, 128-131]

Product	Company	Description	Clinical uses
Acticoat™	Smith & Nephew	Nanocrystalline Ag wound dressing	Dressings for a range of wounds including burns and ulcers to prevent bacterial infection and improve wound healing.
Silverline™	Spiegelberg	Polyurethane ventricular catheter impregnated with Ag nanoparticles	Neurosurgical drain of cerebrospinal fluid for hydrocephalus. Ag nanoparticles in the coating prevents catheter-associated infections.
SilvaSorb™	Medline Industries and AcryMed	Antibacterial products: hand gels, wound dressings, cavity filler	Wound dressings and cavity filler prevent antibacterial infection. Hand gels used to disinfect skin in clinical and personal hygiene purposes.
ON-Q SilverSoaker™	I-Flow Corporation	Ag nanoparticles coated catheter for drug delivery	Local delivery of antibacterial agent per-, peri- or post-operatively.

Product	Company	Description	Clinical uses
Agento™	C. R. Bard, Inc.	Ag-coated endotracheal tube	Reduces risk of pneumonia for patients using ventilators.
Silvertouch™	Medline Industries	Antimicrobial urinary catheters	Catheter impregnated with Ag to prevent infection.
Mutars™	Implantcast	Ag-coated tumor endoprosthesis	Prevention of infection in the reconstruction of large bone defects caused by aseptic or septic loosening.

It is well known that Ag-based compounds are toxic to microorganisms, possessing strong antibacterial effects on at least 12 species of bacteria including multidrug-resistant strains like methicillin-resistant *S. aureus* (MRSA), multidrug-resistant *Pseudomonas aeruginosa*, ampicillin-resistant *Escherichia coli* O157:H7 and erythromycin-resistant *Streptococcus pyogenes* [132-135]. Among antibacterial activities, Ag exhibits activity against viruses, fungi and yeast as well [136-138].

The exact mechanism of action of Ag on the bacteria is still not known but a possible mechanism of action for Ag nanoparticles has been discussed in this thesis in Chapter 4.

Despite concerns, clinical development of antimicrobial resistance to Ag to date is rare [60, 139]. It has been shown that Ag has a lower susceptibility to induce microbial resistance than many other antimicrobial agents [140-143].

Based on the vast majority of *in vitro* and *in vivo* studies available, Ag is non-toxic to the human body at low concentrations [83, 144-148]. The concentration of Ag that can be safely consumed by humans (*i.e.,* the reference dose) is 5 μg/kg/day (approximately 350 μg), and the "critical" dose is estimated to be 14 μg/kg/day. Considering that in USA Ag is used as a disinfectant for drinking water, two liters of water a day would already provide around 200 μg of Ag. An additional 10-25 μg a day can be ingested with milk, which contains 27-54 μg/L. Ag is also found in variable quantities in a number of other foods as well, *e.g.,* mushrooms, which can contain hundreds of micrograms of Ag per gram [149]. Regardless of the route of administration, Ag is excreted in bile and, therefore, eliminated in urine (around 10 μg/day) and fecal matter (around 30-80 μg/day) [150]. Repeated exposure to Ag salts or colloidal Ag causes argyria, a deep blue-gray discoloration of the skin and gums caused by deposits of Ag sulfate or metallic Ag in the body [151-153]. Administration of 50 mg Ag or more is lethal, provoking pulmonary edema, hemorrhage, and necrosis of the bone marrow, liver, and kidneys [154].

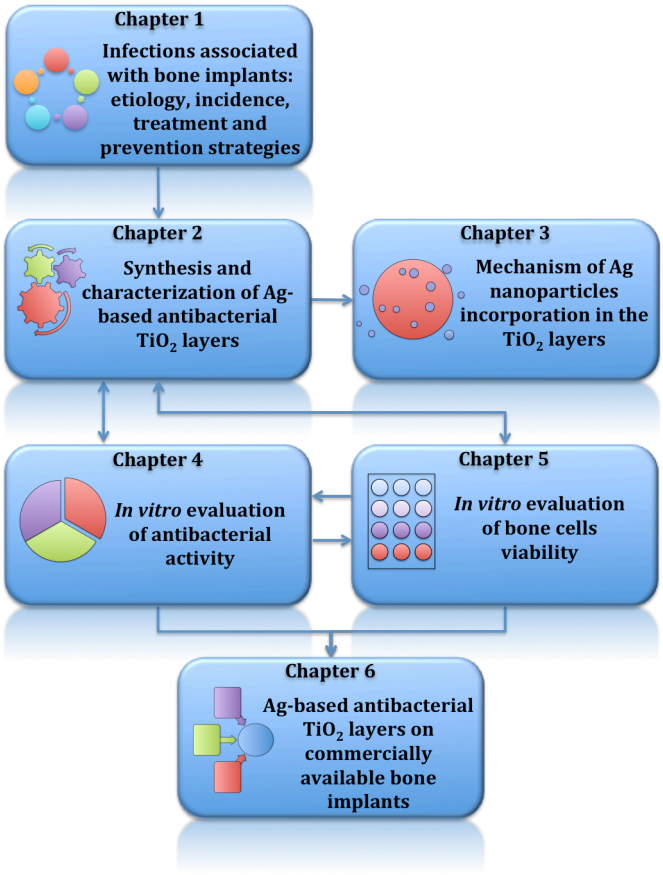

Fig. 1.7. Schematic representation of the thesis structure.

Delivered locally, in appropriate concentrations, Ag can be a suitable alternative to antibiotics. Its unique advantages to antibiotics include prolonged activity, the ability to kill a wide spectrum of bacteria without developing resistance and low *in vivo* toxicity.

1.6. Aim of the thesis

As cementless implants experience an increase in popularity because of good long-term survival, there is also an increasing interest in local antibacterial delivery for these types of implants. Currently, no such option is available for clinical practice. The aim of this thesis was to develop a novel antibacterial surface for cementless implants.

The research was focused on the synthesis, physicochemical characterization and biological evaluation of an Ag-based antibacterial surface on the Ti6Al7Nb biomedical alloy. The research layout is presented schematically in Fig. 1.7.

1.7. Research outline

The outline of the thesis is as follows. Chapter 1 covers a review on etiology, incidence, treatment and prevention of implant associated infections occurring after total joint replacement surgeries, dental implantation or bone trauma surgeries. Furthermore, the PEO as a possible process for generating antibacterial surfaces for bone implants and the motivation of using Ag nanoparticles as antibacterial agent are also presented. Chapter 2 reveals the experimental work that led to the synthesis of novel antibacterial layers on the Ti6Al7Nb alloy, comprising of a porous TiO_2 layer with embedded Ag nanoparticles. In addition, the main results of the physicochemical characterization of the antibacterial layers are presented. In Chapter 3 a possible mechanism of Ag nanoparticles incorporation in the TiO_2 layers was proposed. How and where are the Ag nanoparticles incorporated in the porous TiO_2 layer was the main research question addressed. Chapter 4 covers the aspects of antibacterial testing of solid surfaces against one of the most virulent pathogen for orthopaedic surgery *i.e.,* MRSA. Thus, new experimental assays have been proposed and used to test the antibacterial activity of Ag-bearing TiO_2 surfaces. A particular focus was on the antibacterial effect of different Ag nanoparticle concentrations in the TiO_2 layers. In addition, a mechanism of the antibacterial activity of these surfaces was proposed. Chapter 5 addresses another important aspect of antibacterial surfaces proposed for orthopaedic implants, namely the toxicity to human cells. Whether or not the Ag-bearing TiO_2 layers are toxic to osteoblast cells is descried in this chapter. Chapter 6 covers a feasibility study to see whether the PEO method, used to render the surface of titanium antibacterial, can be applied on commercially available bone implants such as plasma sprayed titanium hip components. Thus, the Ag-based antibacterial layers were created on a plasma sprayed titanium acetabular cup and characterized with respect to surface morphology and chemistry.

References

[1] R.B. Salter, The Biologic Concept of Continuous Passive Motion of Synovial Joints - the 1st 18 Years of Basic Research and Its Clinical-Application, Clinical Orthopaedics and Related Research, 242 (1989) 12-25.

[2] M. Solignac, [COART France 2003 report on new socioeconomic data on osteoarthritis in France], La Presse Médicale, 33 (2004) S4-6.

[3] R.C. Lawrence, D.T. Felson, C.G. Helmick, L.M. Arnold, H. Choi, R.A. Deyo, S. Gabriel, R. Hirsch, M.C. Hochberg, G.G. Hunder, J.M. Jordan, J.N. Katz, H.M. Kremers, F. Wolfe, W. National Arthritis Data, Estimates of the prevalence of arthritis and other rheumatic conditions in the United States. Part II, Arthritis & Rheumatism, 58 (2008) 26-35.

[4] C. Egloff, T. Hugle, V. Valderrabano, Biomechanics and pathomechanisms of osteoarthritis, Swiss Medical Weekly, 142 (2012).

[5] A.A. Guccione, D.T. Felson, J.J. Anderson, J.M. Anthony, Y.Q. Zhang, P.W.F. Wilson, M. Kellyhayes, P.A. Wolf, B.E. Kreger, W.B. Kannel, The Effects of Specific Medical Conditions on the Functional Limitations of Elders in the Framingham-Study, American Journal of Public Health, 84 (1994) 351-358.

[6] http://www.wecareforlife.com/total-knee-replacement.

[7] C.S. Moucha, R.M. Urban, T.M. Turner, J.J. Jacobs, Fixation of implants, in: A. Shanbhag, H.E. Rubash, J.J. Jacobs (Eds.) Joint replacement and bone resorption, Taylor & Francis Group, New York, 2006.

[8] S.H. Park, A. Llinas, V.K. Goel, J.C. Keller, Hard Tissue Replacements, in: J.B. Park, J.D. Bronzino (Eds.) Biomaterials - Principles and Applications, CRC Press, New York, 2003.

[9] http://www.wecareforlife.com/total-hip-replacement.

[10] J.R. Davis, Handbook of materials for medical devices, ASM International, USA, 2003.

[11] T.M. Wright, R.F. Closkey, Properties of biomaterials used in joint replacements, in: A. Shanbhag, H.E. Rubash, J.J. Jacobs (Eds.) Joint replacement and bone resorption, Taylor & Francis Group, New York, 2006.

[12] W. Zimmerli, Infection and musculoskeletal conditions: Prosthetic joint-associated infections, Best Practice & Research Clinical Rheumatology, 20 (2006) 1045-1063.

[13] I. Babiak, A. Gorecki, Treatment outcome in infections complicating total hip replacements, Orthopedic Traumatology Rehabilitation, 4 (Suppl 1) (2002) 49-52.

[14] B.A. Knobben, J.R. van Horn, H.C. van der Mei, H.J. Busscher, Evaluation of measures to decrease intra-operative bacterial contamination in orthopaedic implant surgery, The Journal of Hospital Infection, 62 (2006) 174-180.

[15] D. Pittet, G. Ducel, Infectious Risk-Factors Related to Operating-Rooms, Infection Control and Hospital Epidemiology, 15 (1994) 456-462.

[16] W. Whyte, R. Hodgson, J. Tinkler, The importance of airborne bacterial contamination of wounds, The Journal of Hospital Infection, 3 (1982) 123-135.

[17] B. Gottenbos, H.J. Busscher, H.C. van der Mei, Pathogenesis and prevention of biomaterial centered infections, Journal of Materials Science-Materials in Medicine, 13 (2002) 717-722.

[18] C.L. Wells, M.A. Maddaus, R.L. Simmons, Role of the Macrophage in the Translocation of Intestinal Bacteria, Archives of Surgery, 122 (1987) 48-53.

[19] M.T. Clarke, P.T.H. Lee, C.P. Roberts, J. Gray, G.S. Keene, N. Rushton, Contamination of primary total hip replacements in standard and ultra-clean operating theaters detected by the polymerase chain reaction, Acta Orthopaedica Scandinavica, 75 (2004) 544-548.

[20] G. Peersman, R. Laskin, J. Davis, M. Peterson, Infection in total knee replacement: a retrospective review of 6489 total knee replacements, Clinical Orthopaedics and Related Research, (2001) 15-23.

[21] S.D. Elek, P.E. Conen, The virulence of Staphylococcus pyogenes for man; a study of the problems of wound infection, British Journal of Experimental Pathology, 38 (1957) 573-586.

[22] G.D. Christensen, L.M. Baddour, D.L. Hasty, J.H. Lowrance, W.A. Simpson, in: A.L. Bisno, F.A. Waldvogel (Eds.) Infections associated with indwelling medical devices, American Society of Microbiology, Washington DC, 1989.

[23] S.P. Lyngstadaas, J.E. Ellingsen, A. Spahr, I. Slaby, Inducing Bone Growth Using Extracellular Matrix Proteins, in: J.E. Ellingsen, S.P. Lyngstadaas (Eds.) Bio-Implant Interface Improving Biomaterials and Tissue Reactions, CRC Press LLC, New York, 2003.

[24] M. Habash, G. Reid, Microbial biofilms: Their development and significance for medical device-related infections, Journal of Clinical Pharmacology, 39 (1999) 887-898.

[25] J. Palmer, S. Flint, J. Brooks, Bacterial cell attachment, the beginning of a biofilm, The Journal of Industrial Microbiology and Biotechnology, 34 (2007) 577-588.

[26] G. Herscu, S.E. Wilson, Prosthetic Infection: Lessons from Treatment of the Infected Vascular Graft, Surgical Clinics of North America, 89 (2009) 391-99.

[27] A. Trampuz, D.R. Osmon, A.D. Hanssen, J.M. Steckelberg, R. Patel, Molecular and antibiofilm approaches to prosthetic joint infection, Clinical Orthopaedics and Related Research, (2003) 69-88.

[28] E.M. Hetrick, M.H. Schoenfisch, Reducing implant-related infections: active release strategies, Chemical Society Reviews, 35 (2006) 780-789.

[29] A.W. Smith, Biofilms and antibiotic therapy: is there a role for combating bacterial resistance by the use of novel drug delivery systems?, Advanced Drug Delivery Reviews, 57 (2005) 1539-1550.

[30] F. Randelli, A. Aliprandi, L. Banci, L. Sconfienza, F. Sardanelli, Advantages of Two-Stage Revision Arthroplasty, in: H. Kienapfel, K.D. Kuhn (Eds.) The Infected Implant, Springer, Berlin, 2009.

[31] J.W. Costerton, P.S. Stewart, E.P. Greenberg, Bacterial biofilms: A common cause of persistent infections, Science, 284 (1999) 1318-1322.

[32] C.A.N. Broekhuizen, M.J. Schultz, A.C. van der Wal, L. Boszhard, L. de Boer, C.M.J.E. Vandenbroucke-Grauls, S.A.J. Zaat, Tissue around catheters is a niche for bacteria associated with medical device infection, Critical Care Medicine, 36 (2008) 2395-2402.

[33] E. Meani, P. Trezza, Revision One Stage Versus Two Stage - Introduction To Crossfire Session, in: H. Kienapfel, K.D. Kuhn (Eds.) The Infected Implant, Springer, Berlin, 2009.

[34] P. Gaston, Diagnosis and management of infected arthroplasty - the United Kingdom experience, in: Local antibiotics in arthroplasty, Thieme, Stuttgart New York, 2007.

[35] M.V. Loraas, I.G. Skrami, Addend hospital expenses following re-admissions due to postoperative orthopaedic wound infections, in: 23rd Annual meeting of the European Bone & Joint Infection Society, 27-29 May 2004, Milan.

[36] A.J. Mangram, T.C. Horan, M.L. Pearson, L.C. Silver, W.R. Jarvis, Guideline for Prevention of Surgical Site Infection, 1999, Infection Control and Hospital Epidemiology, 20 (1999) 250-278.

[37] B. AlBuhairan, D. Hind, A. Hutchinson, Antibiotic prophylaxis for wound infections in total joint arthroplasty - A systematic review, Journal of Bone and Joint Surgery-British Volume, 90B (2008) 915-919.

[38] J. Mannien, M.E. van Kasteren, N.J. Nagelkerke, I.C. Gyssens, B.J. Kullberg, J.C. Wille, A.S. de Boer, Effect of optimized antibiotic prophylaxis on the incidence of surgical site infection, Infection Control and Hospital Epidemiology, 27 (2006) 1340-1346.

[39] L. Lidgren, K. Knutson, A. Stefánsdóttir, Infection of prosthetic joints, Best Practice & Research Clinical Rheumatology, 17 (2003) 209-218.

[40] J. Mannien, S. van den Hof, J. Muilwijk, P.J. van den Broek, B. van Benthem, J.C. Wille, Trends in the Incidence of Surgical Site Infection in The Netherlands, Infection Control and Hospital Epidemiology, 29 (2008) 1132-1138.

[41] National Joint Registry England and Wales. Annual Report 2011. http://www.njrcentre.org.uk/NjrCentre/Portals/0/Documents/NJR 8th Annual Report 2011.pdf.

[42] K.L. Ong, S.M. Kurtz, E. Lau, K.J. Bozic, D.J. Berry, J. Parvizi, Prosthetic Joint Infection Risk After Total Hip Arthroplasty in the Medicare Population, Journal of Arthroplasty, 24 (2009) 105-109.

[43] S.M. Kurtz, K.L. Ong, E. Lau, K.J. Bozic, D. Berry, J. Parvizi, Prosthetic Joint Infection Risk after TKA in the Medicare Population, Clinical Orthopaedics and Related Research, 468 (2010) 52-56.

[44] R.O. Darouiche, Current concepts - Treatment of infections associated with surgical implants, New England Journal of Medicine, 350 (2004) 1422-1429.

[45] P. Kingshott, J. Wei, D. Bagge-Ravn, N. Gadegaard, L. Gram, Covalent attachment of poly(ethylene glycol) to surfaces, critical for reducing bacterial adhesion, Langmuir, 19 (2003) 6912-6921.

[46] J.A. Nagel, R.B. Dickinson, S.L. Cooper, Bacterial adhesion to polyurethane surfaces in the presence of pre-adsorbed high molecular weight kininogen, Journal of Biomaterials Science-Polymer Edition, 7 (1996) 769-780.

[47] A. Roosjen, W. Norde, H.C. van der Mei, H.J. Busscher, The use of positively charged or low surface free energy coatings versus polymer brushes in controlling biofilm formation, Characterization of Polymer Surfaces and Thin FIlms, 132 (2006) 138-144.

[48] M.R. Nejadnik, H.C. van der Mei, W. Norde, H.J. Busscher, Bacterial adhesion and growth on a polymer brush-coating, Biomaterials, 29 (2008) 4117-4121.

[49] X.J. Khoo, P. Hamilton, G.A. O'Toole, B.D. Snyder, D.J. Kenan, M.W. Grinstaff, Directed Assembly of PEGylated-Peptide Coatings for Infection-Resistant

Titanium Metal, Journal of the American Chemical Society, 131 (2009) 10992-10997.

[50] J.P. Celis, D. Drees, M.Z. Huq, P.Q. Wu, M. De Bonte, Hybrid processes - a versatile technique to match process requirements and coating needs, Surface & Coatings Technology, 113 (1999) 165-181.

[51] M. Gabriel, K. Nazmi, E.C. Veerman, A.V.N. Amerongen, A. Zentner, Preparation of LL-37-grafted titanium surfaces with bactericidal activity, Bioconjugate Chemistry, 17 (2006) 548-550.

[52] V. Humblot, J.F. Yala, P. Thebault, K. Boukerma, A. Hequet, J.M. Berjeaud, C.M. Pradier, The antibacterial activity of Magainin I immobilized onto mixed thiols Self-Assembled Monolayers, Biomaterials, 30 (2009) 3503-3512.

[53] M.C. Lawson, C.N. Bowman, K.S. Anseth, Vancomycin derivative photopolymerized to titanium kills S. epidermidis, Clinical Orthopaedics and Related Research, 461 (2007) 96-105.

[54] J. Parvizi, E. Wickstrom, A.R. Zeiger, C.S. Adams, I.M. Shapiro, J.J. Purtill, P.F. Sharkey, W.J. Hozack, R.H. Rothman, N.J. Hickok, Frank Stinchfield Award. Titanium surface with biologic activity against infection, Clinical Orthopaedics and Related Research, (2004) 33-38.

[55] B. Jose, V. Antoci, Jr., A.R. Zeiger, E. Wickstrom, N.J. Hickok, Vancomycin covalently bonded to titanium beads kills Staphylococcus aureus, Chemical Biology, 12 (2005) 1041-1048.

[56] C.P. Chen, E. Wickstrom, Self-protecting bactericidal titanium alloy surface formed by covalent bonding of daptomycin bisphosphonates, Bioconjugate Chemistry, 21 (2010) 1978-1986.

[57] V. Antoci, Jr., S.B. King, B. Jose, J. Parvizi, A.R. Zeiger, E. Wickstrom, T.A. Freeman, R.J. Composto, P. Ducheyne, I.M. Shapiro, N.J. Hickok, C.S. Adams, Vancomycin covalently bonded to titanium alloy prevents bacterial colonization, Journal of Orthopaedic Research, 25 (2007) 858-866.

[58] C. Ketonis, C.S. Adams, S. Barr, A. Aiyer, I.M. Shapiro, J. Parvizi, N.J. Hickok, Antibiotic modification of native grafts: improving upon nature's scaffolds, Tissue Engineering Part A, 16 (2010) 2041-2049.

[59] P. Basak, B. Adhikari, I. Banerjee, T.K. Maiti, Sustained release of antibiotic from polyurethane coated implant materials, Journal of Materials Science-Materials in Medicine, 20 Suppl 1 (2009) S213-221.

[60] I.A. Rojas, J.B. Slunt, D.W. Grainger, Polyurethane coatings release bioactive antibodies to reduce bacterial adhesion, Journal of Controlled Release, 63 (2000) 175-189.

[61] J.M. Schierholz, H. Steinhauser, A.F.E. Rump, R. Berkels, G. Pulverer, Controlled release of antibiotics from biomedical polyurethanes: Morphological and structural features, Biomaterials, 18 (1997) 839-844.

[62] P. Wu, D.W. Grainger, Drug/device combinations for local drug therapies and infection prophylaxis, Biomaterials, 27 (2006) 2450-2467.

[63] R. Kumar, H. Munstedt, Silver ion release from antimicrobial polyamide/silver composites, Biomaterials, 26 (2005) 2081-2088.

[64] V. Zaporojtchenko, R. Podschun, U. Schurmann, A. Kulkarni, F. Faupel, Physico-chemical and antimicrobial properties of co-sputtered Ag-Au/PTFE nanocomposite coatings, Nanotechnology, 17 (2006) 4904-4908.

[65] F. Furno, K.S. Morley, B. Wong, B.L. Sharp, P.L. Arnold, S.M. Howdle, R. Bayston, P.D. Brown, P.D. Winship, H.J. Reid, Silver nanoparticles and polymeric medical devices: a new approach to prevention of infection?, Journal of Antimicrobial Chemotherapy, 54 (2004) 1019-1024.

[66] B.J. Nablo, A.R. Rothrock, M.H. Schoenfisch, Nitric oxide-releasing sol-gels as antibacterial coatings for orthopedic implants, Biomaterials, 26 (2005) 917-924.

[67] B.J. Nablo, H.L. Prichard, R.D. Butler, B. Klitzman, M.H. Schoenfisch, Inhibition of implant-associated infections via nitric oxide release, Biomaterials, 26 (2005) 6984-6990.

[68] E.M. Hetrick, H.L. Prichard, B. Klitzman, M.H. Schoenfisch, Reduced foreign body response at nitric oxide-releasing subcutaneous implants, Biomaterials, 28 (2007) 4571-4580.

[69] Z.R. Zhou, M.E. Meyerhoff, Preparation and characterization of polymeric coatings with combined nitric oxide release and immobilized active heparin, Biomaterials, 26 (2005) 6506-6517.

[70] O. Etienne, C. Picart, C. Taddei, Y. Haikel, J.L. Dimarcq, P. Schaaf, J.C. Voegel, J.A. Ogier, C. Egles, Multilayer polyelectrolyte films functionalized by insertion of defensin: A new approach to protection of implants from bacterial colonization, Antimicrobial Agents and Chemotherapy, 48 (2004) 3662-3669.

[71] A. Shukla, K.E. Fleming, H.F. Chuang, T.M. Chau, C.R. Loose, G.N. Stephanopoulos, P.T. Hammond, Controlling the release of peptide antimicrobial agents from surfaces, Biomaterials, 31 (2010) 2348-2357.

[72] F. Costa, I.F. Carvalho, R.C. Montelaro, P. Gomes, M.C.L. Martins, Covalent immobilization of antimicrobial peptides (AMPs) onto biomaterial surfaces, Acta Biomaterialia, 7 (2011) 1431-1440.

[73] C. Teupe, R. Meffert, S. Winckler, W. Ritzerfeld, P. Tormala, E. Brug, Ciprofloxacin-Impregnated Poly-L-Lactic Acid Drug Carrier - New Aspects of a Resorbable Drug Delivery System in Local Antimicrobial Treatment of Bone-Infections, Archives of Orthopaedic and Trauma Surgery, 112 (1992) 33-35.

[74] J.S. Price, A.F. Tencer, D.M. Arm, G.A. Bohach, Controlled release of antibiotics from coated orthopedic implants, Journal of Biomedical Materials Research, 30 (1996) 281-286.

[75] M. Baro, E. Sanchez, A. Delgado, A. Perera, C. Evora, *In vitro - in vivo* characterization of gentamicin bone implants, Journal of Controlled Release, 83 (2002) 353-364.

[76] B. Wildemann, A. Sander, P. Schwabe, M. Lucke, U. Stockle, M. Raschke, N.P. Haas, G. Schmidmaier, Short term *in vivo* biocompatibility testing of biodegradable poly(D,L-lactide) - growth factor coating for orthopaedic implants, Biomaterials, 26 (2005) 4035-4040.

[77] M. Stigter, J. Bezemer, K. de Groot, P. Layrolle, Incorporation of different antibiotics into carbonated hydroxyapatite coatings on titanium implants, release and antibiotic efficacy, Journal of Controlled Release, 99 (2004) 127-137.

[78] M. Stigter, K. de Groot, P. Layrolle, Incorporation of tobramycin into biomimetic hydroxyapatite coating on titanium, Biomaterials, 23 (2002) 4143-4153.

[79] S. Radin, J.T. Campbell, P. Ducheyne, J.M. Cuckler, Calcium phosphate ceramic coatings as carriers of vancomycin, Biomaterials, 18 (1997) 777-782.

[80] V. Alt, A. Bitschnau, J. Osterling, A. Sewing, C. Meyer, R. Kraus, S.A. Meissner, S. Wenisch, E. Domann, R. Schnettler, The effects of combined gentamicin-hydroxyapatite coating for cementless joint prostheses on the reduction of infection rates in a rabbit infection prophylaxis model, Biomaterials, 27 (2006) 4627-4634.

[81] C. Moseke, U. Gbureck, P. Elter, P. Drechsler, A. Zoll, R. Thull, A. Ewald, Hard implant coatings with antimicrobial properties, Journal of Materials Science-Materials in Medicine, 22 (2011) 2711-2720.

[82] A. Ewald, S.K. Gluckermann, R. Thull, U. Gbureck, Antimicrobial titanium/silver PVD coatings on titanium, Biomedical Engineering Online, 5 (2006).

[83] J. Hardes, H. Ahrens, C. Gebert, A. Streitbuerger, H. Buerger, M. Erren, A. Gunsel, C. Wedemeyer, G. Saxler, W. Winkelmann, G. Gosheger, Lack of toxicological side-effects in silver-coated megaprostheses in humans, Biomaterials, 28 (2007) 2869-2875.

[84] J. Hardes, C. von Eiff, A. Streitbuerger, M. Balke, T. Budny, M.P. Henrichs, G. Hauschild, H. Ahrens, Reduction of periprosthetic infection with silver-coated megaprostheses in patients with bone sarcoma, Journal of Surgical Oncology, 101 (2010) 389-395.

[85] X. Bai, S. Sandukas, M. Appleford, J.L. Ong, A. Rabiei, Antibacterial effect and cytotoxicity of Ag-doped functionally graded hydroxyapatite coatings, Journal of Biomedical Materials Research Part B-Applied Biomaterials, 100B (2012) 553-561.

[86] H.L. Huang, Y.Y. Chang, J.C. Weng, Y.C. Chen, C.H. Lai, T.M. Shieh, Anti-bacterial performance of Zirconia coatings on Titanium implants, Thin Solid Films, 528 (2013) 151-156.

[87] H.J. Ruan, C.Y. Fan, X.B. Zheng, Y. Zhang, Y.K. Chen, *In vitro* antibacterial and osteogenic properties of plasma sprayed silver-containing hydroxyapatite coating, Chinese Science Bulletin, 54 (2009) 4438-4445.

[88] Y.K. Chen, X.B. Zheng, B.E. Li, Y.T. Xie, C.X. Ding, *In vitro* bioactivity, cytotoxicity and blood compatibility of anti-bacterial vacuum plasma sprayed titanium coatings, Eco-Materials Processing and Design Xi, 658 (2010) 511-514.

[89] B.E. Li, X.Y. Liu, F.H. Meng, J. Chang, C.X. Ding, Preparation and antibacterial properties of plasma sprayed nano-titania/silver coatings, Materials Chemistry and Physics, 118 (2009) 99-104.

[90] Y.K. Chen, X.B. Zheng, Y.T. Xie, C.X. Ding, H.J. Ruan, C.Y. Fan, Anti-bacterial and cytotoxic properties of plasma sprayed silver-containing HA coatings, Journal of Materials Science-Materials in Medicine, 19 (2008) 3603-3609.

[91] Y. Shibata, D. Suzuki, S. Omori, R. Tanaka, A. Murakami, Y. Kataoka, K. Baba, R. Kamijo, T. Miyazaki, The characteristics of *in vitro* biological activity of titanium

surfaces anodically oxidized in chloride solutions, Biomaterials, 31 (2010) 8546-8555.

[92] S. Omori, Y. Shibata, T. Arimoto, T. Igarashi, K. Baba, T. Miyazaki, Micro-organism and cell viability on antimicrobially modified titanium, Journal of Dental Research, 88 (2009) 957-962.

[93] W.H. Song, H.S. Ryu, S.H. Hong, Antibacterial properties of Ag (or Pt)-containing calcium phosphate coating formed by micro-arc oxidation, Journal of Biomedical Materials Research Part A, 88A (2009) 246-254.

[94] H. Hu, W. Zhang, Y. Qiao, X. Jiang, X. Liu, C. Ding, Antibacterial activity and increased bone marrow stem cell functions of Zn-incorporated TiO_2 coatings on titanium, Acta Biomaterialia, 8 (2012) 904-915.

[95] H.L. Cao, X.Y. Liu, F.H. Meng, P.K. Chu, Biological actions of silver nanoparticles embedded in titanium controlled by micro-galvanic effects, Biomaterials, 32 (2011) 693-705.

[96] N. Suketa, T. Sawase, H. Kitaura, M. Naito, K. Baba, K. Nakayama, A. Wennerberg, M. Atsuta, An antibacterial surface on dental implants, based on the photocatalytic bactericidal effect, Clinical Implant Dentistry and Related Research, 7 (2005) 105-111.

[97] A.L. Yerokhin, X. Nie, A. Leyland, A. Matthews, S.J. Dowey, Plasma electrolysis for surface engineering, Surface & Coatings Technology, 122 (1999) 73-93.

[98] W.H. Song, Y.K. Jun, Y. Han, S.H. Hong, Biomimetic apatite coatings on micro-arc oxidized titania, Biomaterials, 25 (2004) 3341-3349.

[99] X.L. Zhu, K.H. Kim, Y.S. Jeong, Anodic oxide films containing Ca and P of titanium biomaterial, Biomaterials, 22 (2001) 2199-2206.

[100] Y. Yang, N. Oh, Y. Liu, W. Chen, S. Oh, M. Appleford, S. Kim, K. Kim, S. Park, J. Bumgardner, W. Haggard, J. Ong, Enhancing osseointegration using surface-modified titanium implants, JOM Journal of the Minerals, Metals and Materials Society, 58 (2006) 71-76.

[101] Y.M. Wang, B.L. Jiang, T.Q. Lei, L.X. Guo, Microarc oxidation coatings formed on Ti6Al4V in Na_2SiO_3 system solution: Microstructure, mechanical and tribological properties, Surface & Coatings Technology, 201 (2006) 82-89.

[102] A.L. Yerokhin, X. Nie, A. Leyland, A. Matthews, Characterisation of oxide films produced by plasma electrolytic oxidation of a Ti-6Al-4V alloy, Surface & Coatings Technology, 130 (2000) 195-206.

[103] P.S. Stewart, J.W. Costerton, Antibiotic resistance of bacteria in biofilms, The Lancet, 358 (2001) 135-138.

[104] P.S. Stewart, Mechanisms of antibiotic resistance in bacterial biofilms, International Journal of Medical Microbiology, 292 (2002) 107-113.

[105] Y.J. Gordon, E.G. Romanowski, A.M. McDermott, A review of antimicrobial peptides and their therapeutic potential as anti-infective drugs, Current Eye Research, 30 (2005) 505-515.

[106] M.C. Frost, M.M. Batchelor, Y.M. Lee, H.P. Zhang, Y.J. Kang, B.K. Oh, G.S. Wilson, R. Gifford, S.M. Rudich, M.E. Meyerhoff, Preparation and characterization of implantable sensors with nitric oxide release coatings, Microchemical Journal, 74 (2003) 277-288.

[107] H. Xu, M.M. Reynolds, K.E. Cook, A.S. Evans, J.P. Toscano, 2-Hydroxy-5-nitrobenzyl as a Diazeniumdiolate Protecting Group: Application in NO-Releasing Polymers with Enhanced Biocompatibility, Organic Letters, 10 (2008) 4593-4596.

[108] A. Simchi, E. Tamjid, F. Pishbin, A.R. Boccaccini, Recent progress in inorganic and composite coatings with bactericidal capability for orthopaedic applications, Nanomedicine, 7 (2011) 22-39.

[109] S.M. Deupree, M.H. Schoenfisch, Morphological analysis of the antimicrobial action of nitric oxide on Gram-negative pathogens using atomic force microscopy, Acta Biomaterialia, 5 (2009) 1405-1415.

[110] M.C. Frost, M.M. Reynolds, M.E. Meyerhoff, Polymers incorporating nitric oxide releasing/generating substances for improved biocompatibility of blood-contactincy medical devices, Biomaterials, 26 (2005) 1685-1693.

[111] Y.D. Wu, Z.R. Zhou, M.E. Meyerhoff, *In vitro* platelet adhesion on polymeric surfaces with varying fluxes of continuous nitric oxide release, Journal of Biomedical Materials Research Part A, 81A (2007) 956-963.

[112] A.B. Seabra, M.G. de Oliveira, Poly(vinyl alcohol) and poly(vinyl pyrrolidone) blended films for local nitric oxide release, Biomaterials, 25 (2004) 3773-3782.

[113] C.J. Waschinski, V. Herdes, F. Schueler, J.C. Tiller, Influence of satellite groups on telechelic antimicrobial functions of polyoxazolines, Macromolecular Bioscience, 5 (2005) 149-156.

[114] Z. Jia, D. shen, W. Xu, Synthesis and antibacterial activities of quaternary ammonium salt of chitosan, Carbohydrate Research, 333 (2001) 1-6.

[115] E.F. Palermo, K. Kuroda, Chemical structure of cationic groups in amphiphilic polymethacrylates modulates the antimicrobial and hemolytic activities, Biomacromolecules, 10 (2009) 1416-1428.

[116] J.K. Baveja, M.D.P. Wilcox, E.B.H. Hume, N. Kumar, R. Odell, L.A. Poole-Warren, Furanones as potential anti-bacterial coatings on biomaterials, Biomaterials, 25 (2004) 5003-5012.

[117] E.B.H. Hume, J. Baveja, B.W. Muir, T.L. Schubert, N. Kumar, S. Kjelleberg, H.J. Griesser, H. Thissen, R. Read, L.A. Poole-Warren, K. Schindhelm, M.D.P. Willcox, The control of Staphylococcus epidermidis biofilm formation and *in vivo* infection rates by covalently bound furanones, Biomaterials, 25 (2004) 5023-5030.

[118] T. Janecki, E. Blaszczyk, K. Studzian, M. Rozalski, U. Krajewska, A. Janecka, New stereocontrolled synthesis and biological evaluation of 5-(1 '-hydroxyalkyl)-3-methylidenetetrahydro-2-furanones as potential cytotoxic agents, Journal of Medicinal Chemistry, 45 (2002) 1142-1145.

[119] K. Glinel, P. Thebault, V. Humblot, C.M. Pradier, T. Jouenne, Antibacterial surfaces developed from bio-inspired approaches, Acta Biomaterialia, 8 (2012) 1670-1684.

[120] D.W. Brett, A discussion of silver as an antimicrobial agent: Alleviating the confusion, Ostomy Wound Management, 52 (2006) 34-41.

[121] J.J. Castellano, S.M. Shafii, F. Ko, G. Donate, T.E. Wright, R.J. Mannari, W.G. Payne, D.J. Smith, M.C. Robson, Comparative evaluation of silver-containing antimicrobial dressings and drugs, International Wound Journal, 4 (2007) 114-122.

[122] H.J. Klasen, Historical review of the use of silver in the treatment of burns. I. Early uses, Burns, 26 (2000) 117-130.

[123] C.A. Moyer, L. Brentano, D.L. Gravens, H.W. Margraf, W.W. Monafo, Treatment of Large Human Burns with 0.5 % Silver Nitrate Solution, Archives of Surgery, 90 (1965) 812.

[124] D. Lee, R.E. Cohen, M.F. Rubner, Antibacterial properties of Ag nanoparticle loaded multilayers and formation of magnetically directed antibacterial microparticles, Langmuir, 21 (2005) 9651-9659.

[125] D. Kowalczuk, G. Ginalska, T. Piersiak, M. Miazga-Karska, Prevention of biofilm formation on urinary catheters: Comparison of the sparfloxacin-treated long-

term antimicrobial catheters with silver-coated ones, Journal of Biomedical Materials Research Part B-Applied Biomaterials, 100B (2012) 1874-1882.

[126] E.J. Tobin, R. Bambauer, Silver coating of dialysis catheters to reduce bacterial colonization and infection, Therapeutic Apheresis and Dialysis, 7 (2003) 504-509.

[127] M. Arora, E.K. Chan, S. Gupta, A.D. Diwan, Polymethylmethacrylate bone cements and additives: A review of the literature, World Journal of Orthopaedics, 4 (2013) 67-74.

[128] Y.S. Huang, X.L. Li, Z.J. Liao, G.A. Zhang, Q. Liu, J. Tang, Y.Z. Peng, X.S. Liu, Q.Z. Luo, A randomized comparative trial between Acticoat and SD-Ag in the treatment of residual burn wounds, including safety analysis, Burns, 33 (2007) 161-166.

[129] J.P. Guggenbichler, G. Juhl, G.G. Braun, M. Fraß, O.A. Künstle, J. Plötz, W. Saffartzik, M. Steinhäuser, C. Wenisch, Clinical Investigation of a new Central Venous Catheter Impregnated with Silver Nanoparticles, Hygiene & Medizin, 28 (2003) 228-234.

[130] P.M. Glat, W.D. Kubat, J.F. Hsu, T. Copty, B.A. Burkey, W. Davis, I. Goodwin, Randomized clinical study of SilvaSorb gel in comparison to Silvadene silver sulfadiazine cream in the management of partial-thickness burns, Journal of Burn Care & Research, 30 (2009) 262-267.

[131] K. Tarquinio, N. Rubien, T. Webster, Evaluation of pseudomonas aeruginosa and staphylococcus aureus growth on chemically etched endotracheal tubes and agento(R) *in vitro*, Critical Care Medicine, 38 (2010) U40-U40.

[132] H.H. Lara, N.V. Ayala-Nunez, L.D.I. Turrent, C.R. Padilla, Bactericidal effect of silver nanoparticles against multidrug-resistant bacteria, World Journal of Microbiology & Biotechnology, 26 (2010) 615-621.

[133] I. Sondi, B. Salopek-Sondi, Silver nanoparticles as antimicrobial agent: a case study on E-coli as a model for Gram-negative bacteria, Journal of Colloid and Interface Science, 275 (2004) 177-182.

[134] A.R. Shahverdi, A. Fakhimi, H.R. Shahverdi, S. Minaian, Synthesis and effect of silver nanoparticles on the antibacterial activity of different antibiotics against Staphylococcus aureus and Escherichia coli, Nanomedicine, 3 (2007) 168-171.

[135] W.R. Li, X.B. Xie, Q.S. Shi, S.S. Duan, Y.S. Ouyang, Y.B. Chen, Antibacterial effect of silver nanoparticles on Staphylococcus aureus, Biometals, 24 (2011) 135-141.

[136] H.H. Lara, N.V. Ayala-Nunez, L. Ixtepan-Turrent, C. Rodriguez-Padilla, Mode of antiviral action of Ag nanoparticles against HIV-1, J Nanobiotechnology, 8 (2010).

[137] K.J. Kim, W.S. Sung, S.K. Moon, J.S. Choi, J.G. Kim, D.G. Lee, Antifungal effect of silver nanoparticles on dermatophytes, Journal of Microbiology and Biotechnology, 18 (2008) 1482-1484.

[138] D. Baram-Pinto, S. Shukla, N. Perkas, A. Gedanken, R. Sarid, Inhibition of herpes simplex virus type 1 infection by silver nanoparticles capped with mercaptoethane sulfonate, Bioconjugate Chemistry, 20 (2009) 1497-1502.

[139] K. Chaloupka, Y. Malam, A.M. Seifalian, Nanosilver as a new generation of nanoproduct in biomedical applications, Trends in Biotechnology, 28 (2010) 580-588.

[140] J.S. Kim, E. Kuk, K.N. Yu, J.H. Kim, S.J. Park, H.J. Lee, S.H. Kim, Y.K. Park, Y.H. Park, C.Y. Hwang, Y.K. Kim, Y.S. Lee, D.H. Jeong, M.H. Cho, Antimicrobial effects of silver nanoparticles, Nanomedicine: Nanotechnology, Biology and Medicine, 3 (2007) 95-101.

[141] S. Silver, Bacterial silver resistance: molecular biology and uses and misuses of silver compounds, FEMS Microbiology Reviews, 27 (2003) 341-353.

[142] S. Silver, L.T. Phung, G. Silver, Silver as biocides in burn and wound dressings and bacterial resistance to silver compounds, Journal of Industrial Microbiology & Biotechnology, 33 (2006) 627-634.

[143] S. Franke, G. Grass, D.H. Nies, The product of the ybdE gene of the Escherichia coli chromosome is involved in detoxification of silver ions, Microbiology-Uk, 147 (2001) 965-972.

[144] C. Baker, A. Pradhan, L. Pakstis, D.J. Pochan, S.I. Shah, Synthesis and antibacterial properties of silver nanoparticles, Journal of Nanoscience and Nanotechnology, 5 (2005) 244-249.

[145] A. Agarwal, T.L. Weis, M.J. Schurr, N.G. Faith, C.J. Czuprynski, J.F. McAnulty, C.J. Murphy, N.L. Abbott, Surfaces modified with nanometer-thick silver-impregnated polymeric films that kill bacteria but support growth of mammalian cells, Biomaterials, 31 (2010) 680-690.

[146] D. Roe, B. Karandikar, N. Bonn-Savage, B. Gibbins, J.B. Roullet, Antimicrobial surface functionalization of plastic catheters by silver nanoparticles, Journal of Antimicrobial Chemotherapy, 61 (2008) 869-876.

[147] R. Foldbjerg, P. Olesen, M. Hougaard, D.A. Dang, H.J. Hoffmann, H. Autrup, PVP-coated silver nanoparticles and silver ions induce reactive oxygen species, apoptosis and necrosis in THP-1 monocytes, Toxicological Letters, 190 (2009) 156-162.

[148] P. Lackner, R. Beer, G. Broessner, R. Helbok, K. Galiano, C. Pleifer, B. Pfausler, C. Brenneis, C. Huck, K. Engelhardt, A.A. Obwegeser, E. Schmutzhard, Efficacy of Ag nanoparticles-impregnated external ventricular drain catheters in patients with acute occlusive hydrocephalus, Neurocritical Care, 8 (2008) 360-365.

[149] European Commision-Health and Consumer Protection Directorate, Toxicological Data on Colouring Agents for Medicinal Products: E 174 Silver, 2000.

[150] G.F. Nordberg, L. Gerhardsson, Silver, in: H.G. Seiler, H. Sigel (Eds.) Handbook on toxicity of inorganic compounds, Dekker, New York, 1988, pp. 619-624.

[151] N.S. Tomi, B. Kranke, W. Aberer, A Silver Man, The Lancet, 363 (2004) 532-532.

[152] C.M.E.R. Payne, C. Bladin, A.C.F. Colchester, J. Bland, R. Lapworth, D. Lane, Argyria from Excessive Use of Topical Silver Sulfadiazine, The Lancet, 340 (1992) 126-126.

[153] R.M. Greene, W.P.D. Su, Argyria, American Family Physician, 36 (1987) 151-154.

[154] B.A. Fowler, G.F. Nordberg, Silver, in: L. Friberg, G.F. Nordberg, V.B. Vouk (Eds.) Handbook on the toxicology of metals, Elsevier, 1986, pp. 521-531.


1cm

Chapter 2

Synthesis and characterization of Ag-based antibacterial TiO_2 layers*

Can Ag-based antibacterial layers be produced on Ti biomedical alloys using a single step process?

2.1. Introduction

Orthopaedic implant devices are intended to restore the function of load-bearing joints, which are subjected to high level of mechanical stresses, wear, and fatigue in the course of normal activity. The most commonly used materials for joint replacement applications include stainless steels, commercially pure titanium and titanium alloys, and cobalt-based alloys. So far, titanium and its alloys have been documented as most successful osseointegrated implants in long-term clinical studies due to their superior mechanical properties (tensile strength and fatigue strength), chemical stability (corrosion resistance), and biocompatibility under *in vivo* conditions [1, 2]. The contact zone with bone tissue at the bone/implant interface is not established by the bulk titanium but rather by the native TiO_2 layer that forms spontaneously in contact with air. Hence, the presence of this native TiO_2 is of crucial importance when speaking of osseointegration of titanium implants.

*Based on:
B.S. Necula, L.E. Fratila-Apachitei, S.A.J. Zaat, I. Apachitei, J. Duszczyk, *In vitro* antibacterial activity of porous TiO_2–Ag composite layers against methicillin-resistant Staphylococcus aureus, Acta Biomaterialia, 5 (2009) 3573–3580.

Plasma electrolytic oxidation (PEO) also called micro-arc oxidation, anodic spark deposition, or micro-arc discharge oxidation, is a surface modification technique that electrochemically enhances the native oxide layer present on the surface of titanium alloys as well as other several metals, such as aluminum, magnesium and tantalum [3-5]. The process combines electrochemical oxidation with a high-voltage spark treatment in an aqueous electrolytic bath, which also contains modifying elements in the form of dissolved salts or nanoparticles (*e.g.*, calcium, phosphate, hydroxyapatite, Ag) to be incorporated into the resulting coatings. The oxidation process on titanium can be performed at voltages either below the dielectric breakdown of the oxide layer, and in this case the process is called anodic oxidation, or above the breakdown limit, process known as PEO. Most research has been reported on anodic oxides produced below the breakdown limit, when relatively thin amorphous TiO_2 films are formed, mainly for oral implants [6-19]. When the oxidation is performed at potentials above the breakdown limit, oxide layers with increased roughness, interconnected porosity and anatase and/or rutile phases may be formed [20-26]. Currently, the PEO process is applied for biofunctionalization of titanium to create bioactive porous oxide coatings containing Ca and P species, using electrolytes based on calcium acetate and calcium glycerophosphate and specific oxidation conditions or post-treatment steps (*e.g.,* hydrothermal treatment) [27-35].

Incorporation of Ag nanoparticles into a PEO layer was performed for the first time on a magnesium alloy [36]. This has opened the possibility to incorporate Ag nanoparticles on titanium alloys used on total joint arthroplasties, such as Ti6Al7Nb.

The aim of this chapter was twofold (i) to produce an Ag-bearing TiO_2 layer on the surface of a Ti6Al7Nb biomedical alloy using the PEO process and (ii) to characterize the surface of the untreated Ti6Al7Nb biomedical alloy, Ag-free and Ag-bearing TiO_2 layers in detail with various analytical techniques, focusing on the surface appearance and morphology, pore configurations (pore size distribution, pore density, porosity), chemical and phase composition, surface roughness and surface free energy.

2.2. Experimental

2.2.1. Ti6Al7Nb substrate

2.2.1.1. General

The Ti6Al7Nb biomedical alloy was developed in 1977 by S.G. Steinemann and S.M. Perren at Gebruder Sulzer in Winterthur, Switzerland [37]. The objective was to create a titanium alloy for medical applications with properties nearly identical to

Ti6Al4V, substituting V with Nb as the beta-stabilizing element, due to toxicity of V. After six years of testing and evaluation, the alloy was introduced in 1985 by Sulzer-Protek as Protasul® 100 and has been used clinically since 1986 [38].

Ti6Al7Nb alloy starts to widen its use in the medical device industry, primarily for orthopaedic applications such as: total hip replacement systems, fracture fixation plates, intramedullary rods and nails, spinal devices, screws, and wires.

The work in the present thesis was conducted on the Ti6Al7Nb alloy unless otherwise specified. ACNIS International, France, supplied the Ti6Al7Nb alloy in the form of forged bars. The main mechanical properties of this alloy are listed in Table 2.1.

Table 2.1. Physical and mechanical properties of Ti6Al7Nb alloy.

Density	4.52 g/cm^3
Ultimate Tensile Strength	≥ 900 MPa
Yield Tensile Strength	≥ 800 MPa
Modulus of Elasticity	105 GPa
Elongation at Break	≥ 10 %
Fatigue Strength	500 MPa

2.2.1.2. Sample preparation

The as-received Ti6Al7Nb biomedical alloy was machined by turning to produce disks with a thickness of 8 mm and a diameter of 22 mm. All disks were then ground with successive 320, 800 and 1200 grit paper (Struers, Denmark) to a final roughness (R_a) of 0.1 μm, using water as lubricating liquid. After grinding, the samples were degreased in acetone and cleaned in an ultrasonic bath for five minutes in ethanol. Finally, the disks were thoroughly rinsed in deionized water, dried and stored in sample bags until use.

2.2.1.3. Chemical and phase composition

Prior to PEO process, the chemical composition of the Ti6Al7Nb substrate was determined by X-ray fluorescence (XRF) analysis using a Philips PW2400 X-ray fluorescence spectrometer. The data was processed using a Uniquant v. 5.49 software. The phase composition of the Ti6Al7Nb disks was analyzed by X-ray diffraction (XRD). The measurements were carried out on a Bruker-AXS type DX Advance Series 2 diffractometer using CoKα radiation.

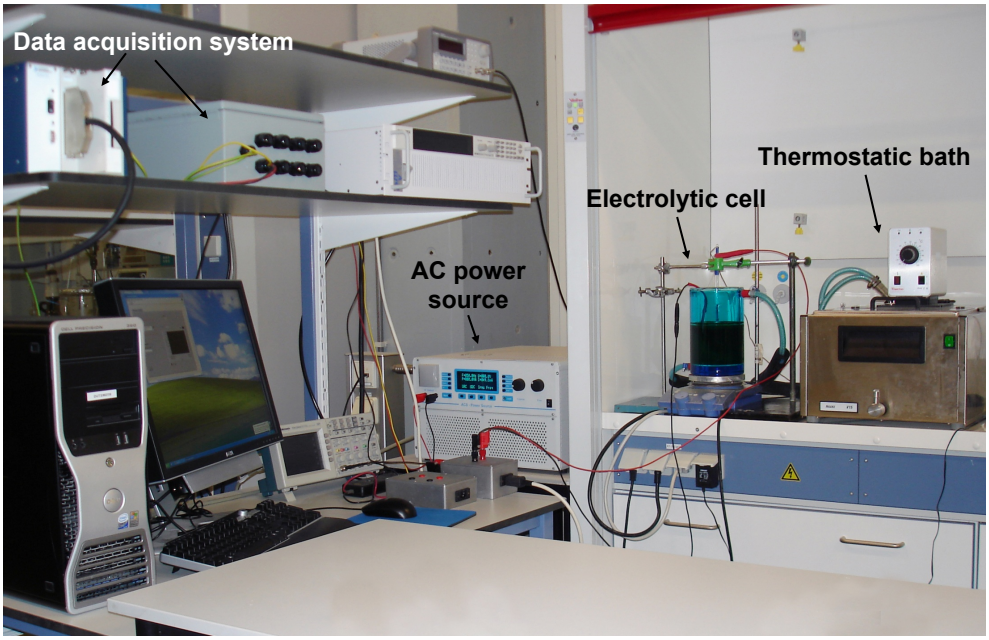

Fig. 2.1. Picture representation of the custom made set-up used for PEO process.

2.2.2. Synthesis of Ag-based TiO_2 layers on Ti6Al7Nb alloy

2.2.2.1. Equipment

The PEO process was performed on a custom made laboratory scale set-up showed in Fig. 2.1. The main constituents are: an AC power supply, type ACS 1500 (ET Power Systems Ltd., UK), a Haake V15 thermostatic bath, a computer interfaced with the AC power supply through a data acquisition board (National Instruments SCXI), a double wall glass electrolytic cell with a two electrodes configuration (the Ti6Al7Nb disk as the anode the and a stainless steel counter electrode) and a thermocouple that continuously monitors the temperature during the process.

2.2.2.2. Experimental conditions

The TiO_2 layers were produced in the double wall glass electrolytic cell having the main constituents depicted in Fig. 2.2. The cell was filled with 800 mL of electrolyte prepared by dissolving 4.2 g/L calcium glycerophosphate (Ca-GP) and 24 g/L calcium acetate (CA) salts in double distilled water and adding different concentrations of Ag nanoparticles *i.e.,* 0 g/L, 0.3 g/L and 3.0 g/L. The electrolyte was cooled at 10°C by

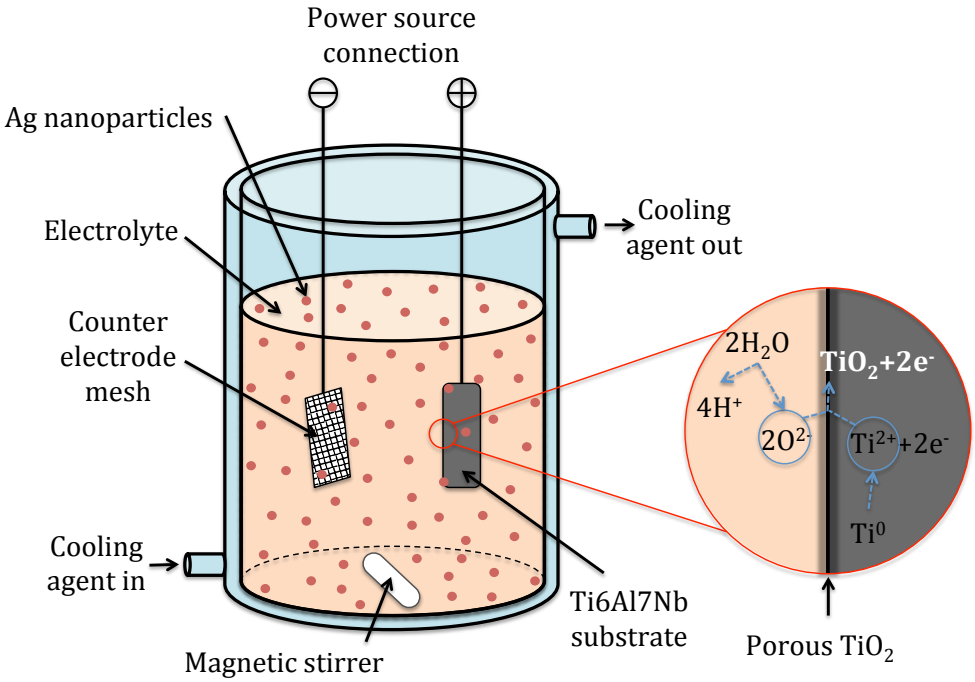

Fig. 2.2. Schematic representation of the electrolytic cell used in the PEO set-up.

circulating a mixture of water and glycerol through the double wall jacket of the cell using the Haake V15 thermostatic bath. The conductivity of the electrolyte was 8.06 mS/cm. The pH of the electrolyte was 9.

To maintain particle dispersion in the electrolyte, this was constantly stirred at 500 r.p.m. using a magnetic stirrer. The PEO process was performed under galvanostatic mode using current densities of 10 to 20 A/dm^2 for 1 to 10 minutes. The current was supplied by means of the AC (50 Hz) power supply. During this time, the voltage–time transients were recorded at 1-second intervals using a computer interfaced with the AC power supply through a National Instruments SCXI data acquisition system.

After the layer synthesis, the samples were washed in running tap water for 5 minutes, ultrasonically cleaned in ethanol, rinsed for a further 5 minutes in deionized water and dried for 1 h at 110°C using a Nabertherm TR60 oven. This process allows the removal of the unattached Ag nanoparticles from the surfaces.

The sample codes, electrolyte components and process parameters are listed in Table 2.2.

Table 2.2. Sample code, electrolyte components and process parameters used

Sample code	Electrolyte components			Process parameters				
	Calcium acetate, g/L	Calcium glycero-phosphate, g/L	Ag nano-particles, g/L	Current density, A/dm^2	Final voltage, V	Duration, minutes	Temperature, °C	
							start	end
0Ag	24	4.2	0	20	239 ± 2	5	11 ± 1	34±0.3
0.3Ag	24	4.2	0.3	20	234 ± 3	5	11 ± 1	33±0.9
3.0Ag	24	4.2	3.0	20	237 ± 2	5	11 ± 1	32±1.0

2.2.3. Characterization of Ag-based TiO_2 layers

2.2.3.1. Visual observation

After the PEO process the Ag-free and Ag-bearing TiO_2 layers on the Ti6Al7Nb disks were photographed with a digital camera for visual assessment of the coating appearance.

2.2.3.2. Surface morphology

The surface morphology of the TiO_2 layers was characterized on a JEOL JSM-6500F Scanning Electron Microscope (SEM) using an electron energy beam of 5 to 15 keV and both secondary and backscattered electron (BSE) signals. Prior to SEM investigation the titanium samples were coated with a uniform carbon layer for good electrical conductivity.

2.2.3.3. Chemical and phase composition

The SEM, equipped with an energy dispersive X-ray (EDX) detector, was used to determine the chemical composition of the TiO_2 layers.

The phase composition of the Ag nanoparticles, Ag-bearing coatings and Ag-free coatings was analyzed by X-ray diffraction (XRD). The measurements were carried out on a Bruker-AXS type DX Advance Series 2 diffractometer using CoKα radiation.

2.2.3.4. Surface roughness

Surface roughness (R_a) was evaluated with a surface texture meter type Surtronic 3+ (Taylor Hobson Limited, England). The R_a value indicates the arithmetic mean of the

departures of the surface profile from the mean line (*i.e.,* the line that bisects the profile such that the area below and above is equal). Ten measurements were performed for each sample using an evaluation length of 4 mm and a sampling length of 0.8 mm.

The evaluation length is the length over which the values of R_a are assessed. It may contain one or more sampling lengths. The sampling length is the length of the reference line used for identifying the irregularities characterizing the surface.

2.2.3.5. Porosity and pore size distribution

A series of parameters, such as: porosity, pore size distribution, pore density, mean pore size and maximum pore size were used to describe the Ag-free and Ag-bearing TiO_2 porous surfaces, in more details. SEM imaging method was used to gather negatives of X1000 magnification from randomly selected areas of the porous surfaces. Scanned areas were 90 µm x 120 µm. The SEM negatives were then loaded in the Adobe Photoshop CS5 image analysis software and the pores were individually selected by means of Photoshop selection tools. Adobe Photoshop CS5 software automatically calculates the size and area of each pore. The selection data was used in Microsoft Excel to calculate the pore size distribution (as percentages of pores within a certain size range), the porosity (represented as the area covered by pores per total scanned area), pore density (number of pores per scanned area) and the mean and maximum pore size. This method is restricted to the "opened pores" on the surface not including the hidden pores.

2.2.3.6. Contact angle and surface free energy

The wettability of TiO_2 layers was determined by measuring the advancing contact angle using a Drop Shape Analyzer DSA 100 (Kruss, Germany). Drops of ultrapure deionized water and diiodomethane (suitable for calculation of surface free energy (SFE)) were delivered onto the testing surfaces by a syringe and forced to wet the neighboring position by the increase in deposition volume. Immediately after contact, images of the droplet were recorded at 1-second intervals for 30 seconds. The total deposition volume was 20 µL with a deposition time of 90 seconds. The right and left contact angles between the drop and the substrate were measured from the magnified images. Minimum three measurements were performed on each sample, using both of the testing liquids, to assure accuracy.

Calculation of SFE was based on Fowkes theory, which is mathematically equivalent to that of Owens and Wendt:

$$\frac{\sigma_L\,(cos\theta+1)}{2} = (\sigma_L^D)^{1/2}\,(\sigma_S^D)^{1/2} + (\sigma_L^P)^{1/2}\,(\sigma_S^P)^{1/2} \quad (1)$$

where:

σ_L = overall surface tension of the wetting liquid

θ = the contact angle between the liquid and the solid

σ_L^D = dispersive component of the surface tension of the wetting liquid

σ_S^D = dispersive component of the surface energy of the solid

σ_L^P = polar component of the surface tension of the wetting liquid

σ_S^P = polar component of the surface energy of the solid

Two main steps are involved in determining a SFE using the Fowkes theory. First is the determination of contact angle using diiodomethane as a testing liquid. Diiodomethane, because of its molecular symmetry, has no polar component to its overall surface tension, so that $\sigma_L^D = \sigma_L$ = 50.8 mN/m. In this case, the equation (1) reduces to:

$$\sigma_S^D = \frac{\sigma_L\,(cos\theta+1)^2}{2} \quad (2)$$

and σ_S^D can be calculated directly from the contact angle data obtained. The second step is the determination of contact angle using ultrapure deionised water that has both a dispersive and a polar component to its surface tension. Knowing that σ_L^P = 46.4 mN/m, σ_L^D = 26.4 mN/m and the contact angle that the water has on the solid, the only unknown in the equation (1) is σ_S^P. The final surface energy of the solid σ_S was then calculated as:

$$\sigma_S = \sigma_S^P + \sigma_S^D \quad (3)$$

2.3. Results and discussion

2.3.1. Chemical composition of Ti6Al7Nb substrate

The XRF analysis was performed to check the chemical composition of the Ti6Al7Nb substrate. The result, presented in Table 2.3, confirms the elemental composition corresponding to the Ti6Al7Nb biomedical alloy.

Table 2.3. Chemical composition (wt. %) of the Ti6Al7Nb substrate

Substrate	Ti	Al	Nb	O	Fe	Ta	N	C
Ti6Al7Nb	86.639	6.010	6.950	0.185	0.160	0.05	0.004	0.002

2.3.2. Synthesis of Ag-based TiO_2 layers

The PEO of Ti6Al7Nb was first performed in Ag nanoparticles-free electrolyte in order to find the optimum process parameters (*i.e.,* current density and oxidation time). The anode, made by the Ti6Al7Nb disk, was immersed in the calcium acetate/calcium glycerophosphate electrolyte, and a constant current was applied between the anode and the cathode for a defined period of time. The Ti6Al7Nb alloy is natively protected by a 3-7 nm thick amorphous TiO_2 film, which is resistant to current flow. Electrode reactions (oxidation and reduction) in combination with field-driven ion diffusion lead to the formation of a TiO_2 layer on the Ti6Al7Nb surface. In order to maintain the constant current density throughout the PEO process, the voltage value has to increase with the increasing self-resistance in the growing oxide coating. The voltage between titanium substrate and electrolyte rapidly rises as the native oxide thickens. When the voltage exceeds a certain critical value dielectric breakdown through the oxide layer occurs which is accompanied by micro-arc discharges. Fresh portions of the electrolyte are injected into the bare metal surface during the breakdowns, and the process continues as long as the voltage is sufficient for new breakdowns, which constantly perforate the growing oxide layer.

When a current density of 10 A/dm^2 was applied between the anode and cathode, the generated voltage was not enough to produce dielectric breakdown of the native oxide and sustain the growth of TiO_2 layer in the presence of spark discharges. The breakdown potential for Ti6Al7Nb in the calcium acetate/calcium glycerophosphate was found to be at 111 V when using a current density of 20 A/dm^2 (Chapter 3 [39]).

The overall reactions leading to oxide layer formation and incorporation of Ag nanoparticles in the layer can be written as follows:

At anode (Ti/TiO_2 interface):

- $Ti \rightarrow Ti^{2+} + 2e^-$

At anode (TiO_2/electrolyte interface):

- $2H_2O \rightarrow 2O^{2-} + 4H^+$
- $2H_2O \rightarrow O_2 \uparrow + 4H^+ + 4e^-$

At anode (both interfaces):

- $Ti^{2+} + 2O^{2-} \rightarrow TiO_2 + 2e^-$
- Electrophoretic mobility of negatively charged Ag nanoparticles and their deposition in the newly formed TiO_2 layer

At cathode (counter electrode/electrolyte interface):

- $2H_2O \rightarrow 2O^{2-} + 4H^+ \rightarrow H_2 \uparrow$

The growth of TiO_2 layers in electrolytes bearing Ag nanoparticles was discussed in detail in Chapter 3.

2.3.3. Characterization of Ag-based TiO_2 layers

2.3.3.1. Visual observation

Following PEO, the Ti6Al7Nb disks changed their appearance from reflective metallic to a matt ceramic-like finish. Fig. 2.3 shows the visual appearance of the uncoated Ti6Al7Nb disks together with the coated 0Ag, 0.3Ag and 3.0Ag surfaces. It can be seen that Ag-bearing coatings have a brown color as compared with the grey Ag-free coatings. The brown color is attributed to the Ag content and increases in intensity with increasing the concentration of Ag nanoparticles in the electrolyte.

2.3.3.2. Surface morphology

The specimens were examined, in plan, prior to PEO and following PEO using SEM. As can be seen in Fig. 2.4, the PEO process changed significantly the morphology of the Ti6Al7Nb surfaces. Groves due to grinding were observed on the untreated Ti6Al7Nb disks. After the PEO treatment a porous oxide layer was formed throughout the surface. The pores are well separated, ranging from a few nanometers up to 10 μm in size, and homogeneously distributed over the coating surface. No obvious differences in the surface morphology between the Ag-bearing and Ag-free coatings were observed.

This porous morphology of the TiO_2 coating can enhance the anchorage of the implant to the bone tissue considering that the presence of micro-pores can make the surface osteoinductive.

The high magnification SEM-BSE micrographs are presented in Fig. 2.5. High atomic-number elements, such as Ag, backscatter electrons more strongly than elements with lower atomic numbers such as Ti, O, Ca or P and, thus appear brighter in the SEM-BSE micrographs. Ag-free specimens showed a smooth surface without any bright spots to

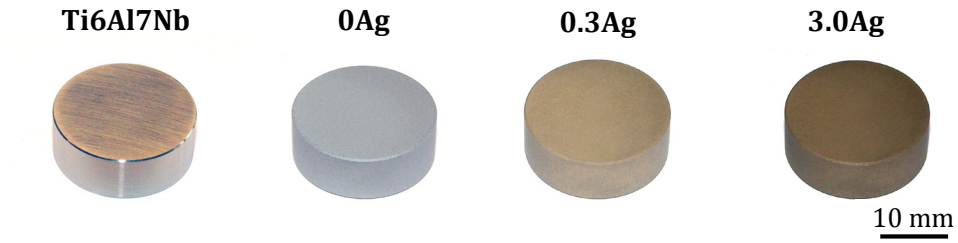

Fig. 2.3. General sample appearance before and after the synthesis of Ag-free and Ag-bearing TiO_2 layers.

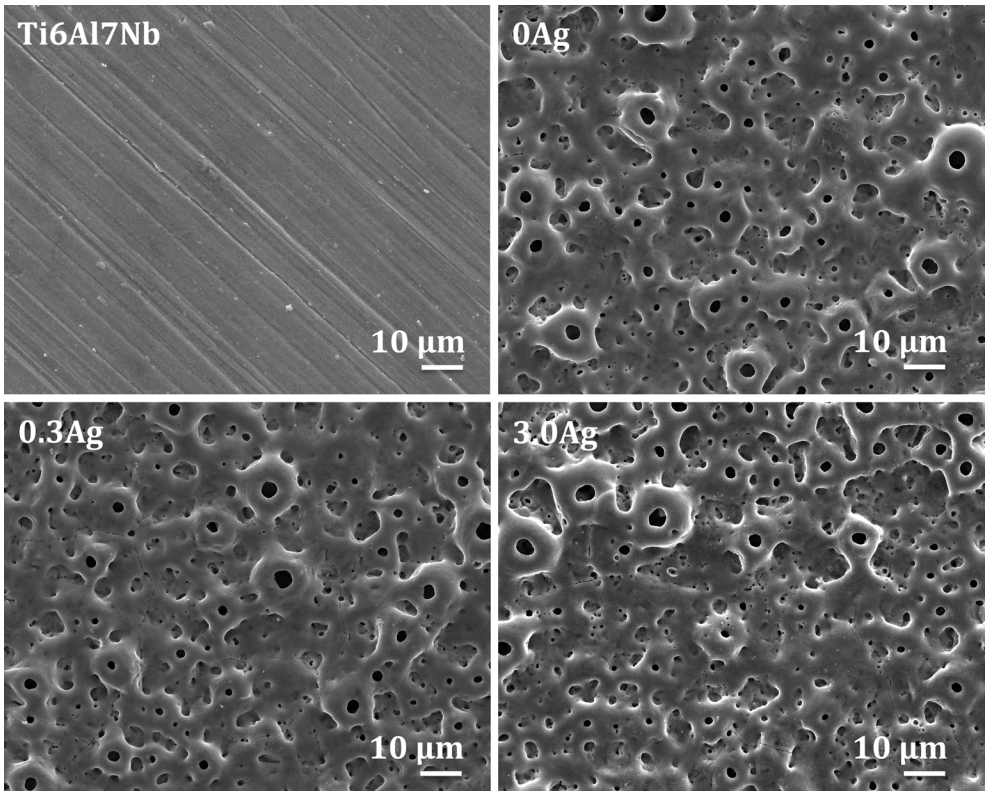

Fig. 2.4. Surface morphology of Ti6Al7Nb prior to PEO process, Ag-free (0Ag) and Ag-bearing layers (0.3Ag; 3.0Ag), as revealed by SEM.

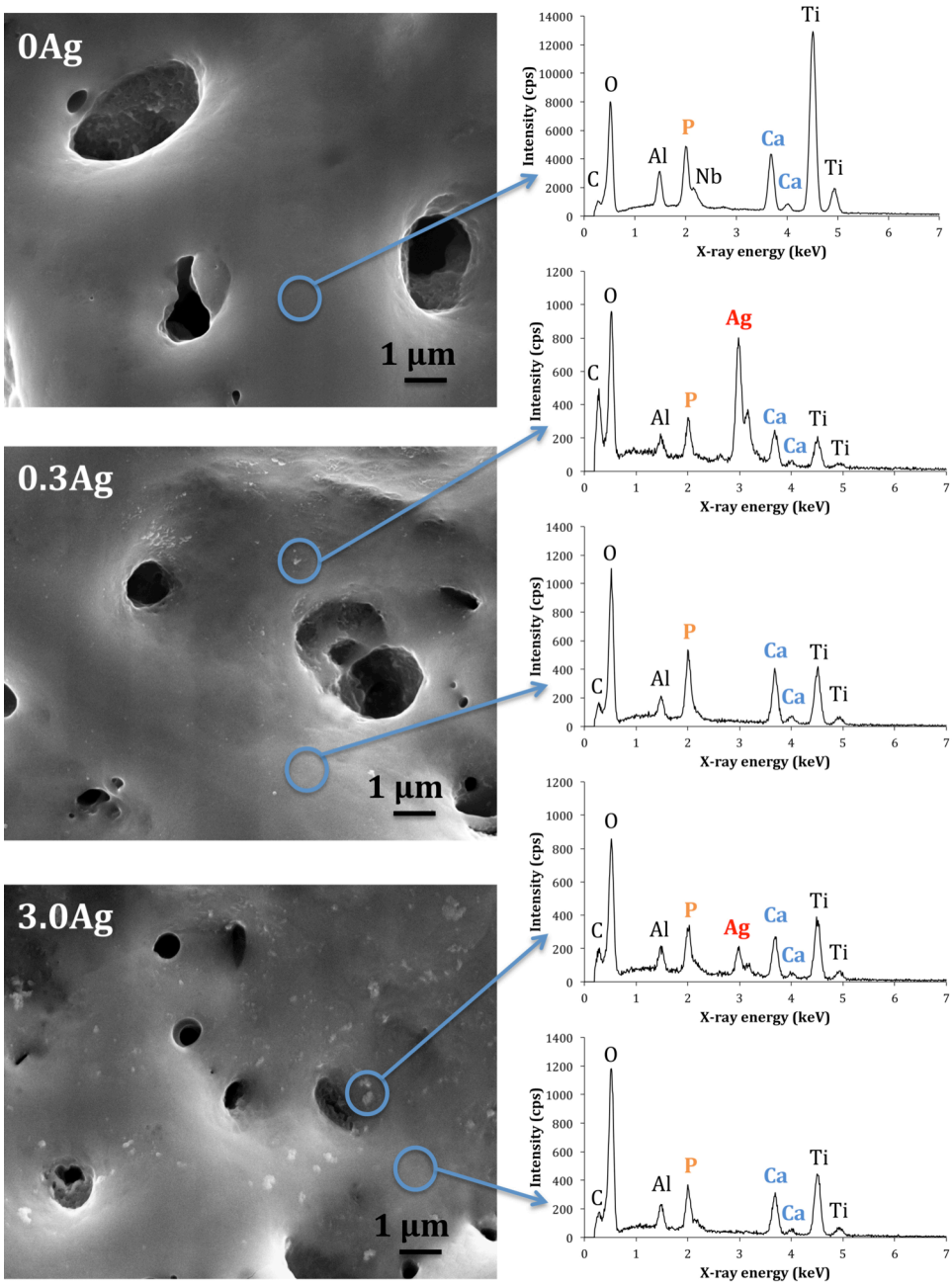

Fig. 2.5. High-resolution SEM-BSE images of Ag-free and Ag-bearing TiO_2 layers with the corresponding EDX patterns.

indicate the presence of Ag nanoparticles. SEM-BSE images of the 0.3Ag and 3.0Ag surfaces indicated the presence of Ag nanoparticles fused on the TiO_2 surface and inside the pores. Increasing the concentration of Ag nanoparticles in the electrolyte lead to an increase of particle incorporation in the TiO_2 layers, as it can be seen in Fig. 2.5.

2.3.3.3. Chemical composition

Spot analyses of the chemical composition were performed on the Ag-free and Ag-bearing layers using the SEM equipped with an EDX detector. The SEM-BSE images with the location of the spots where chemical analyses was performed (circled areas) together with the corresponding EDX patterns are showed in Fig. 2.5. For the Ag-bearing samples two measurements are presented: first on one of the bright particles, presumed to be Ag and second on a particle-free area. As expected, the EDX spot analyses of the identified bright spots confirmed the presence of Ag nanoparticles next to Ti, Al and Nb from the metallic substrate and Ca and P species from the electrolyte. Ca and P were detected in the oxidation layer, which indicated that Ca and P species from the electrolyte were involved in the physicochemical reactions of the PEO process.

2.3.3.4. Phase composition

Fig. 2.6 shows the XRD patterns of the surfaces prepared in the calcium acetate/calcium glycerophosphate electrolyte bearing different concentrations of Ag nanoparticles. The main TiO_2 phases present within the structure of the oxidized specimens were rutile and anatase, regardless of the Ag concentration in the electrolyte. Titanium peaks still appeared in the XRD patterns of the PEO treated samples and it is assumed that they belong to the Ti6Al7Nb alloy. Unoxidized Ti6Al7Nb alloy is expected to consist of a mixture of alpha and beta phases. The XRD patterns of Ag-bearing surfaces did not reveal any Ag or Ag-containing phases. This may be due to the low concentration of Ag incorporated in the porous layers, possibly below the detection limit of the XRD analysis.

2.3.3.5. Surface roughness

The average roughness values for the ground Ti6Al7Nb alloy, Ag-free and Ag-bearing TiO_2 surfaces are presented in Fig. 2.7. PEO is a process that increases the surface

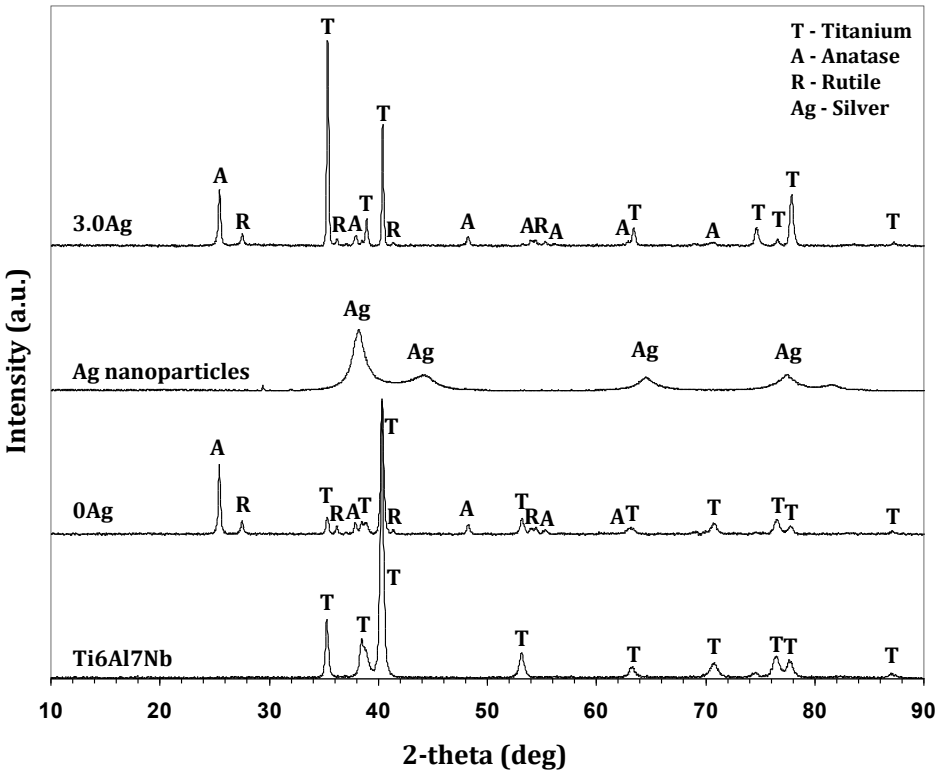

Fig. 2.6. XRD patterns for Ti6Al7Nb alloy, 0Ag, 3.0Ag and Ag nanoparticles.

roughness of the titanium due to the in-depth growing of a porous TiO_2 oxide layer, deposition of electrolytic components and generation of large protruding pores as the layer thickens. Thus, the roughness increased from 0.10 ± 0.017 μm on the ground Ti6Al7Nb surface to 1.53 ± 0.13 μm on the Ag-free TiO_2 surface (0Ag). When Ag nanoparticles were incorporated into the porous oxide layers, the average roughness was not changed as compared with the Ag-free specimens. Thus, the 0.3Ag surfaces had an average surface roughness of 1.56 ± 0.19 μm while the 3.0Ag surfaces 1.43 ± 0.14 μm. Addition of Ag nanoparticles in the electrolyte did not influence the final surface roughness of the grown oxides.

It is well established that morphological features such as surface roughness and its topography can strongly influence the protein adsorption, cell attachment, cell proliferation, contact guidance, and cells differentiation [40]. Hence, they control the rate and quality of new tissue formation at the bone/implant interface.

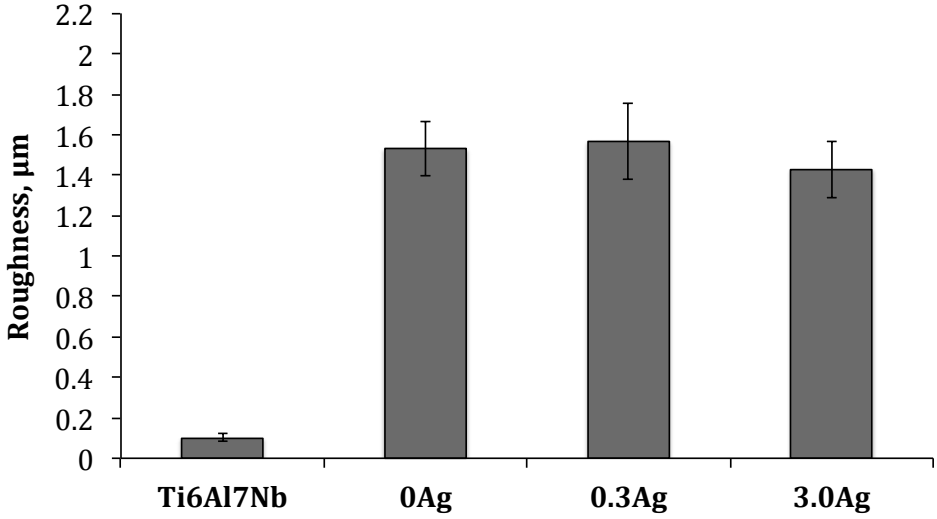

Fig. 2.7. Average surface roughness values for Ti6Al7Nb, 0Ag, 0.3Ag and 3.0Ag surfaces.

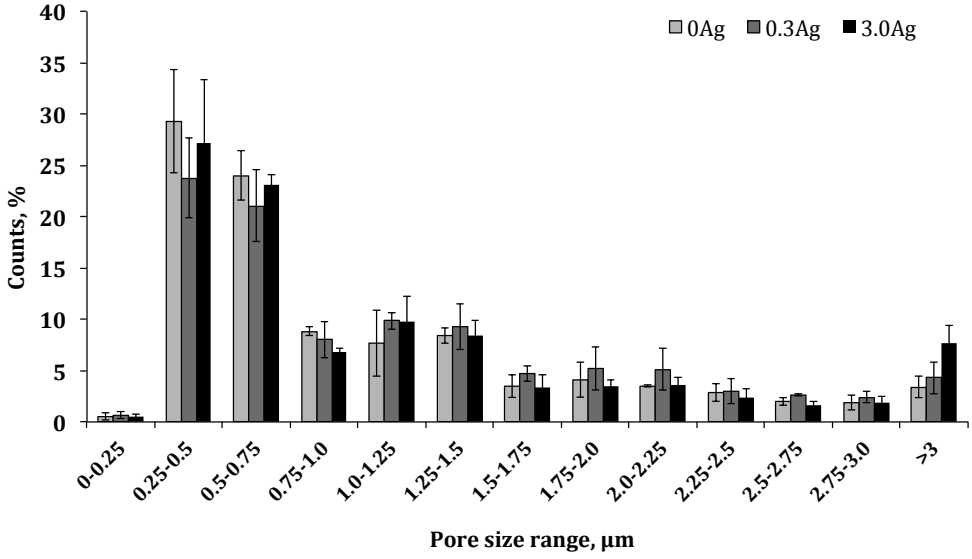

Fig. 2.8. Pore size distribution results for Ag-free and Ag-bearing TiO_2 surfaces.

2.3.3.6. Porosity and pore size distribution

The pore size distribution on the PEO treated samples is presented in Fig. 2.8 as percentages of pores within a certain size range. It can be noticed that approximately 50% of the pores are within the 0.25 - 0.75 μm range, followed by 30% in the range of 0.75 - 1.5 μm and the rest larger than 1.5 μm.

Table 2.4. Pore characteristics for Ag-free and Ag-bearing TiO_2 surfaces.

	Porosity, %	**Pore density, pores/mm^2**	**Mean pore size, μm**	**Max pore size, μm**
0Ag	4.03 ± 0.43	38289 ± 5826	0.71 ± 0.05	6.17 ± 0.81
0.3Ag	6.3 ± 1.07	32927 ± 2447	1.06 ± 0.19	9.63 ± 1.11
3.0Ag	5.14 ±0.64	30956 ± 2328	0.82 ± 0.25	9.06 ± 0.65

Table 2.4 shows the porosity, pore density, mean pore size and maximum pore size for the Ag free and Ag-bearing TiO_2 surfaces. The porosity of PEO layers was found to be 4.03 ± 0.43 % for the Ag-free TiO_2 layers, 6.3 ± 1.07 % for the 0.3 Ag and 5.14 ± 0.64 % for the 3.0Ag. A pore density of 3.8 x 10^4, 3.2 x 10^4 and 3.1 x 10^4 pores/mm^2 was found for the 0Ag, 0.3Ag and 3.0Ag, respectively. The mean pore size for the samples oxidized in the Ag-free electrolyte was 0.71 ± 0.05 μm as compared with 1.06 ± 0.19 μm and 0.82 ± 0.25 μm in the case of 0.3Ag and 3.0Ag, respectively. The maximum size of the pores found on the 0Ag, 0.3Ag and 3.0Ag surfaces was 6.17 ± 0.81 μm, 9.63 ± 1.11 μm and 9.06 ± 0.65 μm, respectively. Statistical analyses of the data showed no significantly difference between the Ag-free surfaces and Ag-bearing ones.

2.3.3.7. Contact angle and surface free energy

When an implant material is placed inside a human body, the first and the foremost event that takes place is the wetting of the implant surface by the physiological fluids. This further controls the adsorption of proteins followed by attachment of cells to the implant surface. Hence surface wettability is considered an important criterion that can dictate the biocompatibility of the implant material. The three most important factors that affect the wettability of a surface are its chemical composition, microstructural topography, and surface charge. Contact angle measurements are probably the most adopted technique to measure the average wettability of a surface. If the contact angle is high (>90°) the surface is considered to be nonwetting or hydrophobic. If the contact angle is small (<90°) the surface is considered to be hydrophilic or easily wetted [41].

SFE values, calculated from the contact angle measurements are presented in Fig. 2.9.

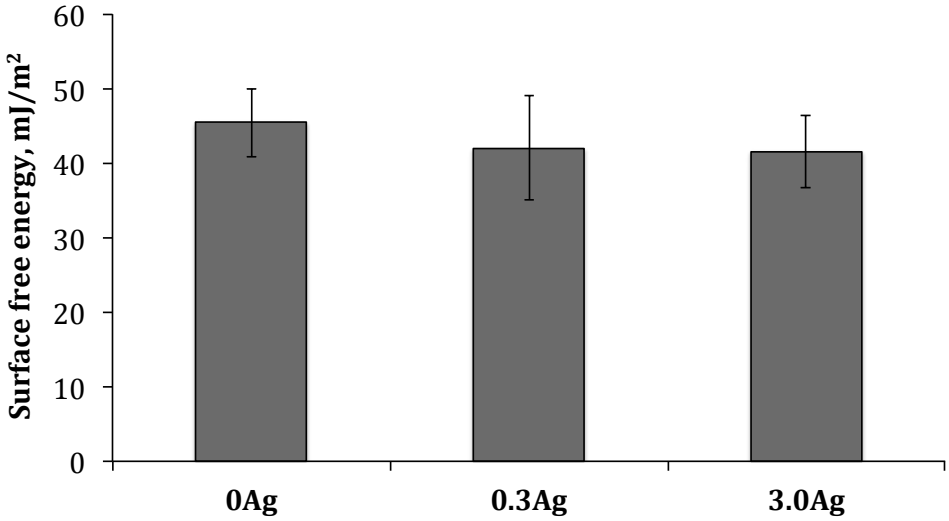

Fig. 2.9. Surface free energy results for Ag-free and Ag-bearing TiO_2 surfaces.

It can be seen that the SFE for the Ag-free (*i.e.,* 0Ag) and Ag-bearing (*i.e.,* 0.3Ag and 3.0Ag) was 45.46 ± 4.49 mJ/m², 42.01 ± 6.96 mJ/m² and 41.62 ± 4.90 mJ/m², respectively. Again, addition of Ag did not change the SFE of the Ag-bearing TiO_2 layers as compared with the Ag-free layers.

2.4. Conclusions

Ag-bearing TiO_2 layers were successfully produced on a Ti6Al7Nb biomedical alloy using the PEO process performed in a calcium acetate/calcium glycerophosphate-based electrolyte bearing two different concentrations of Ag nanoparticles (*i.e,* 0.3 g/L and 3.0 g/L).

The resultant coatings were characterized thoroughly with respect to surface morphology, chemical and phase composition, surface roughness, porosity, pore density, pore size distribution and surface free energy.

All layers presented a porous morphology, with pore sizes ranging from a few nanometers up to 10 μm and a 15 times increase in surface roughness compared with the untreated Ti6Al7Nb surface. TiO_2 layers contained anatase and rutile phases, as well as Ca and P species from the electrolyte. In addition, Ag associated with particles distributed in the porous oxide surface was identified by SEM-BSE and SEM-EDX

analyses. The porosity of the layers was between 4.03 % and 6.3 % and 50 % of the surface pores were no larger that 0.75 μm.

Except the presence of Ag nanoparticles (in different concentrations) in the TiO_2 layers, the main surface characteristics (*e.g.,* surface morphology, surface roughness, porosity, pore density, pore size distribution, SFE) remained unchanged as compared with the Ag-free coatings.

References

[1] M. Semlitsch, Titanium alloys for hip joint replacements, Clinical Materials, 2 (1987) 1-13.

[2] D.M. Brunette, P. Tengvall, M. Textor, P. Thomsen, Titanium in Medicine, Springer, 2001.

[3] A.L. Yerokhin, X. Nie, A. Leyland, A. Matthews, S.J. Dowey, Plasma electrolysis for surface engineering, Surface & Coatings Technology, 122 (1999) 73-93.

[4] E. Matykina, M. Montuori, J. Gough, F. Monfort, A. Berkani, P. Skeldon, G.E. Thompson, H. Habazaki, Spark anodising of titanium for biomedical applications, Transactions of the Institute of Metal Finishing, 84 (2006) 125-133.

[5] Q. Dong, C.Z. Chen, D.G. Wang, Q.M. Ji, Research status about surface modification of biomedical Ti and its alloys by micro-arc oxidation, Surface Review and Letters, 13 (2006) 35-43.

[6] Y.T. Sul, C. Johansson, E. Byon, T. Albrektsson, The bone response of oxidized bioactive and non-bioactive titanium implants, Biomaterials, 26 (2005) 6720-6730.

[7] C. Yao, T.J. Webster, Anodization: a promising nano-modification technique of titanium implants for orthopedic applications, Journal of Nanoscience and Nanotechnology, 6 (2006) 2682-2692.

[8] C.Y. Chiang, S.H. Chiou, W.E. Yang, M.L. Hsu, M.C. Yung, M.L. Tsai, L.K. Chen, H.H. Huang, Formation of TiO_2 nano-network on titanium surface increases the human cell growth, Dental Materials, 25 (2009) 1022-1029.

[9] Z.X. Chen, Y. Takao, W.X. Wang, T. Matsubara, L.M. Ren, Surface characteristics and *in vitro* biocompatibility of titanium anodized in a phosphoric acid solution at different voltages, Biomedical Materials, 4 (2009) 65003.

[10] R.D. Franco, R. Chiesa, M.M. Beloti, P.T. de Oliveira, A.L. Rosa, Human osteoblastic cell response to a Ca- and P-enriched titanium surface obtained by anodization, Journal of Biomedical Materials Research Part A, 88A (2009) 841-848.

[11] Y.M. Lee, E.J. Lee, S.T. Yee, B.I. Kim, E.S. Choe, H.W. Cho, *In vivo* and *in vitro* response to electrochemically anodized Ti-6Al-4V alloy, Journal of Materials Science-Materials in Medicine, 19 (2008) 1851-1859.

[12] R. Jimbo, T. Sawase, K. Baba, T. Kurogi, Y. Shibata, M. Atsuta, Enhanced initial cell responses to chemically modified anodized titanium, Clinical Implant Dentistry and Related Research, 10 (2008) 55-61.

[13] I.S. Park, T.G. Woo, W.Y. Jeon, H.H. Park, M.H. Lee, T.S. Bae, K.W. Seol, Surface characteristics of titanium anodized in the four different types of electrolyte, Electrochimica Acta, 53 (2007) 863-870.

[14] P. Kern, O. Zinger, Purified titanium oxide with novel morphologies upon spark anodization of Ti alloys in mixed H_2SO_4/H_3PO_4 electrolytes, Journal of Biomedical Materials Research Part A, 80A (2007) 283-296.

[15] E. Matykina, F. Monfort, A. Berkani, P. Skeldon, G.E. Thompson, J. Gough, Characterization of spark-anodized titanium for biomedical applications, Journal of the Electrochemical Society, 154 (2007) C279-C285.

[16] H.J. Song, M.K. Kim, G.C. Jung, M.S. Vang, Y.J. Park, The effects of spark anodizing treatment of pure titanium metals and titanium alloys on corrosion characteristics, Surface & Coatings Technology, 201 (2007) 8738-8745.

[17] K. Das, S. Bose, A. Bandyopadhyay, Surface modifications and cell-materials interactions with anodized Ti, Acta Biomaterialia, 3 (2007) 573-585.

[18] I.S. Park, T.G. Woo, M.H. Lee, S.G. Ahn, M.S. Park, T.S. Bae, K.W. Seol, Effects of anodizing voltage on the anodized and hydrothermally treated titanium surface, Metals and Materials International, 12 (2006) 505-511.

[19] S.H. Sohn, H.K. Jun, C.S. Kim, K.N. Kim, S.M. Chung, S.W. Shin, J.J. Ryu, M.K. Kim, Biological responses in osteoblast-like cell line according to thin layer hydroxyapatite coatings on anodized titanium, Journal of Oral Rehabilitation, 33 (2006) 898-911.

[20] Y. Han, S.H. Hong, K.W. Xu, Porous nanocrystalline titania films by plasma electrolytic oxidation, Surface & Coatings Technology, 154 (2002) 314-318.

[21] Y. Zhang, E. Matykina, P. Skeldon, G.E. Thompson, Calcium and titanium release in simulated body fluid from plasma electrolytically oxidized titanium, Journal of Materials Science-Materials in Medicine, 21 (2010) 81-88.

[22] P. Whiteside, E. Matykina, J.E. Gough, P. Skeldon, G.E. Thompson, *In vitro* evaluation of cell proliferation and collagen synthesis on titanium following plasma electrolytic oxidation, Journal of Biomedical Materials Research Part A, 94 (2010) 38-46.

[23] H.J. Hu, X.Y. Liu, C.X. Ding, Preparation and *in vitro* evaluation of nanostructured TiO_2/TCP composite coating by plasma electrolytic oxidation, Journal of Alloys and Compounds, 498 (2010) 172-178.

[24] E. Matykina, R. Arrabal, P. Skeldon, G.E. Thompson, Transmission electron microscopy of coatings formed by plasma electrolytic oxidation of titanium, Acta Biomaterialia, 5 (2009) 1356-1366.

[25] D.Q. Wei, Y. Zhou, D.C. Jia, Y.M. Wang, Chemical treatment of TiO2-based coatings formed by plasma electrolytic oxidation in electrolyte containing nano-HA, calcium salts and phosphates for biomedical applications, Applied Surface Science, 254 (2008) 1775-1782.

[26] Z.P. Yao, Y.L. Jiang, F.Z. Jia, Z.H. Jiang, F.P. Wang, Growth characteristics of plasma electrolytic oxidation ceramic coatings on Ti-6Al-4V alloy, Applied Surface Science, 254 (2008) 4084-4091.

[27] X.L. Zhu, K.H. Kim, Y.S. Jeong, Anodic oxide films containing Ca and P of titanium biomaterial, Biomaterials, 22 (2001) 2199-2206.

[28] X.H. Zhu, C.Z. Wang, B.D. Kou, X.K. Su, W.Q. Zhang, Influence of electrolyte composition on the calcium-phosphorus compound coating on titanium substrate by micro-arc oxidation, 14th Congress of International Federation for Heat Treatment and Surface Engineering, Vols 1 and 2, Proceedings, (2004) 1064-1067.

[29] Y. Zhang, P. Huang, K.W. Xu, Y. Han, Influence of Ca concentration in electrolyte and hydrothermal conditions on the morphology and composition of the TiO_2/hydroxyapatite composite layer by microarc oxidation, Rare Metal Materials and Engineering, 32 (2003) 1007-1010.

[30] Y.J. Wang, L. Wang, H.D. Zheng, C. Du, C.Y. Ning, Z.F. Shi, C.X. Xu, Effect of frequency on the structure and cell response of Ca- and P-containing MAO films, Applied Surface Science, 256 (2010) 2018-2024.

[31] W.H. Song, Y.K. Jun, Y. Han, S.H. Hong, Biomimetic apatite coatings on micro-arc oxidized titania, Biomaterials, 25 (2004) 3341-3349.

[32] S.R. Paital, N.B. Dahotre, Calcium phosphate coatings for bio-implant applications: Materials, performance factors, and methodologies, Materials Science & Engineering - Reports, 66 (2009) 1-70.

[33] C.F. Ma, D.M. Li, H.J. Li, B.L. Jiang, L.J. Zhang, Modification of titanium surface with calcium and phosphorus ions using micro-arc oxidation and its effect on osteoblast attachment, Di Yi Jun Yi Da Xue Xue Bao, 25 (2005) 62-65.

[34] F. Liu, F.P. Wang, T. Shimizu, K. Igarashi, L.C. Zhao, Structure and characteristics of oxide films containing Ca and P on Ti substrate, Journal of Materials Science & Technology, 21 (2005) 285-288.

[35] Y. Huang, Y.J. Wang, C.Y. Ning, K.H. Nan, Y. Han, Hydroxyapatite coatings produced on commercially pure titanium by micro-arc oxidation, Biomedical Materials, 2 (2007) 196-201.

[36] B.S. Necula, L.E. Fratila-Apachitei, A. Berkani, I. Apachitei, J. Duszczyk, Enrichment of anodic MgO layers with Ag nanoparticles for biomedical applications, Journal of Materials Science-Materials in Medicine, 20 (2009) 339-345.

[37] S.G. Steinemann, S.M. Perren, Surgical implant and alloy for use in making an implant, US Patent 4040129, 9 Aug 1977.

[38] J. Disegi, Titanium-6% Aluminum-7% Niobium Implant Material, Synthes (USA), Paoli PA USA, (1993).

[39] B.S. Necula, I. Apachitei, F.D. Tichelaar, L.E. Fratila-Apachitei, J. Duszczyk, An electron microscopical study on the growth of TiO_2-Ag antibacterial coatings on Ti6Al7Nb biomedical alloy, Acta Biomaterialia, 7 (2011) 2751-2757.

[40] F. Gentile, L. Tirinato, E. Battista, F. Causa, C. Liberale, E.M. di Fabrizio, P. Decuzzi, Cells preferentially grow on rough substrates, Biomaterials, 31 (2010) 7205-7212.

[41] M.J. Jaycock , G.D. Parfitt, Chemistry of Interfaces, Chichester, Great Britain: John Wiley & Sons, Ltd (1981), pp. 234–47.

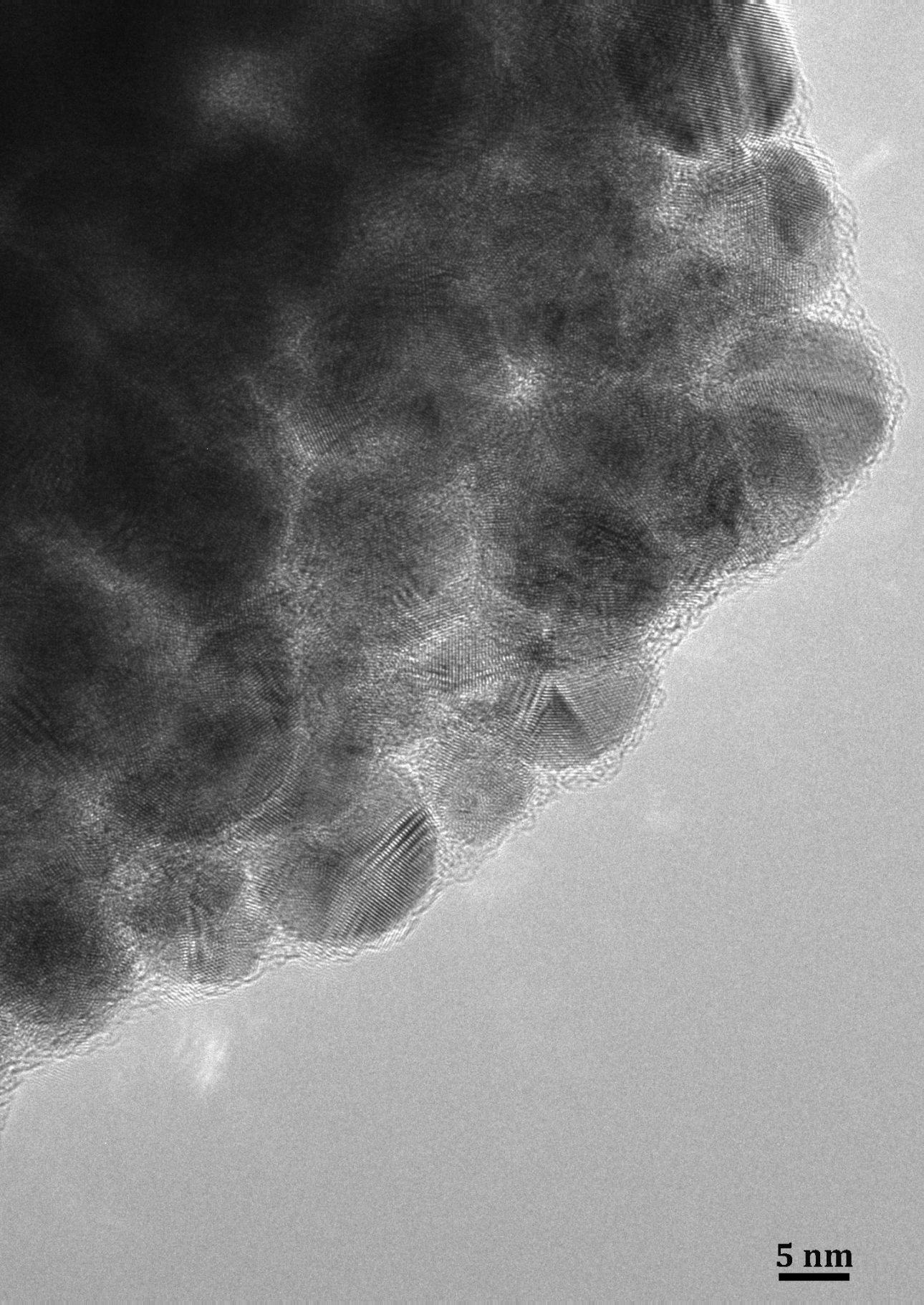
5 nm

Chapter 3

Mechanism of Ag nanoparticles incorporation in the TiO_2 layers*

How and where are the Ag nanoparticles incorporated in the TiO_2 layers?

3.1. Introduction

Plasma electrolytic oxidation (PEO) of titanium and its alloys performed in Ca and P based electrolytes has been studied extensively and represents a versatile surface modification technology for biomedical applications [1-4]. However, PEO performed in electrolytes bearing nanoparticles (*i.e.,* Ag, hydroxyapatite, *etc*.) is relatively new and allows the synthesis of biocomposite layers on titanium with definite advantages. A comprehensive electron-microscopical study on the growth of PEO coatings in the presence of nanoparticles in the electrolyte has not been performed on titanium and its alloys. Several authors [5-9] have studied the incorporation of zirconia nanoparticles by PEO process on Mg and Al substrates. Furthermore, few studies on PEO of titanium using hydroxyapatite nanoparticles in the electrolyte were also reported [10, 11] but without a close look at the mechanism of coating growth and distribution of particles within the coatings.

The aim of this chapter was to investigate the mechanism of Ag nanoparticles incorporation in the TiO_2 layers during PEO of Ti6Al7Nb biomedical alloy in an

*Based on:
B.S. Necula, I. Apachitei, F.D. Tichelaar, L.E. Fratila-Apachitei, J. Duszczyk, An electron-microscopical study on the growth of TiO_2-Ag antibacterial coatings on Ti6Al7Nb biomedical alloy, Acta Biomaterialia, 7 (2011) 2751-2757.

electrolyte based on calcium acetate/calcium glycerophosphate bearing Ag nanoparticles. To understand the layer growth in the presence of Ag nanoparticles and the mechanism of Ag incorporation and its distribution, the Ag-bearing layers were grown at different PEO times (*i.e.,* 10, 30, 60, 90, 120, 180, 240 and 300 seconds) and comprehensively studied. The experimental study includes plan view and cross-sectional investigations of the layers using high-resolution transmission electron microscopy (HRTEM) and scanning electron microscopy (SEM) imaging techniques combined with energy dispersive X-ray spectroscopy (EDX) for chemical analyses.

3.2. Experimental

3.2.1. TiO_2 layers synthesis

Cylinder-shape samples (22 mm diameter, 8 mm height) were machined from forged bars of Ti6Al7Nb biomedical alloy (ACNIS International, France). The disks were ground with successive 320, 800 and 1200 grit paper (Struers, Denmark) and thoroughly cleaned in acetone, ethanol and deionised water using an ultrasonic bath. The electrolyte comprised of 24 g/L calcium acetate and 4.2 g/L calcium glycerophosphate solutions to which 3.0 g/L Ag nanoparticles (Sigma Aldrich) were added. The PEO process was performed under galvanostatic mode using a current density of 20 A/dm^2 for 10, 30, 60, 90, 120, 180, 240 and 300 seconds. After each time-point, the samples were kept in running tap water for 5 minutes, ultrasonically cleaned for 30 seconds in 70% ethanol, rinsed for further 5 minutes in deionised water and dried for 1 hour at 110°C using a Nabertherm TR60 oven. A description of the equipments used and more experimental details on PEO coatings synthesis are included in Chaper 2 of this thesis.

3.2.2. Ag nanoparticles and TiO_2 layers characterization

Ag nanoparticles were characterized with respect to particle size and morphology using a Tecnai 20ST/STEM transmission electron microscope (TEM) operated at 200 keV. For this, a suspension of Ag nanoparticles was prepared in ethanol and placed on a carbon foil on a Cu support grid. After drying the specimen was analyzed by TEM.

Plan view and cross-sectional analyses of the Ag-bearing layers were performed with a JEOL JSM-6500F SEM using both secondary and backscattered electron (BSE)

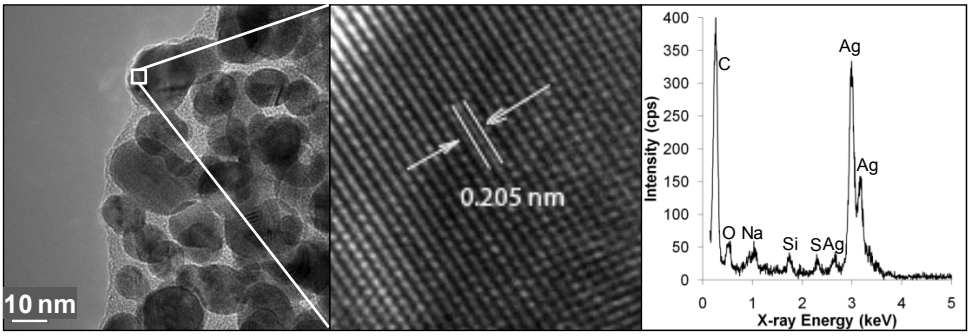

Fig. 3.1. TEM representation of a cluster of Ag nanoparticles (left) with corresponding lattice spacing of a single particle as revealed by HRTEM (center) and EDX pattern (right).

signals. Prior to imaging the samples were coated with a uniform carbon layer, for good electrical conductivity. HRTEM images of several thin sections of the coatings were taken using the Tecnai 20ST/STEM instrument. For this a silicon plate was glued on the coated part of the specimen and a cross-section with a thickness of 0.5-1 mm was cut with a diamond saw. The cross-section was ground and polished to a thickness of ~10 μm and mounted on a Cu slot grid. This was further thinned to electron transparency using a Gatan PIPS 691 ion mill in the presence of Ar.

Both the scanning and transmission electron microscopes were equipped with EDX analyses facilities for determination of the chemical composition. The coating thickness was measured using a Elcometer 456 Coating Thickness Gauge (Elcometer Instruments GmbH, Germany).

3.3. Results

3.3.1. Ag nanoparticles characterization

As-received Ag nanoparticles were analyzed by TEM prior to the PEO process. From the HRTEM images the particle size of Ag was determined to be 7 – 25 nm (Fig. 3.1). The particles appear to be spherical in shape. The middle image of Fig. 3.1 is the high magnification of the corresponding left nanoparticles.

The lattice spacings were measured to be approximately 0.204 ± 0.05 nm and 2.32 ± 0.05 nm which is matched with the fcc Ag (2 0 0) and (1 1 1) planes, respectively. Occasionally deviating lattice spacings were also measured.

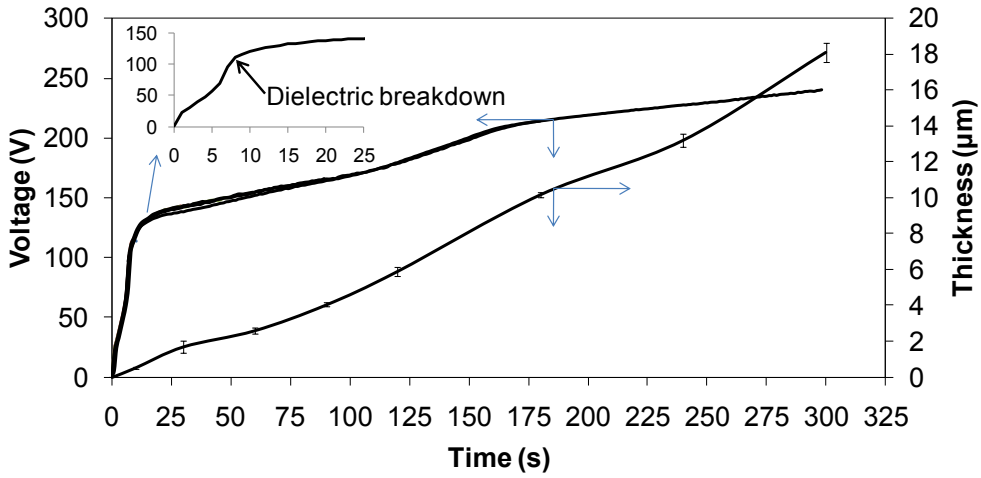

Fig. 3.2. Voltage-time transients and thickness evolution during the growth of Ag-based TiO_2 layers at different oxidation times.

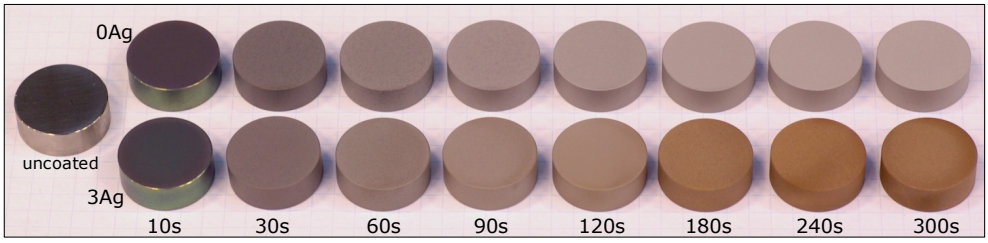

Fig. 3.3. Visual observation of the coated samples at different PEO times with or without Ag nanoparticles incorporation. Disk diameter is 22 mm.

EDX analyses of the carbon foil with Ag nanoparticles showed the presence of Ag, S, O, C, Na and Si. The C, O, Si and Na elements are always detected on the carbon foil. The presence of S is probably because of the amorphous binding in between the particles.

3.3.2. Kinetics of coating growth

Voltage-time transients (Fig. 3.2) recorded during oxidation of Ti6Al7Nb alloy for 10 to 300 seconds revealed two main regions: (i) a sharp increase in voltage (13.5 V/s) up to 111 V corresponding with the growth of an amorphous anodic TiO_2 film,

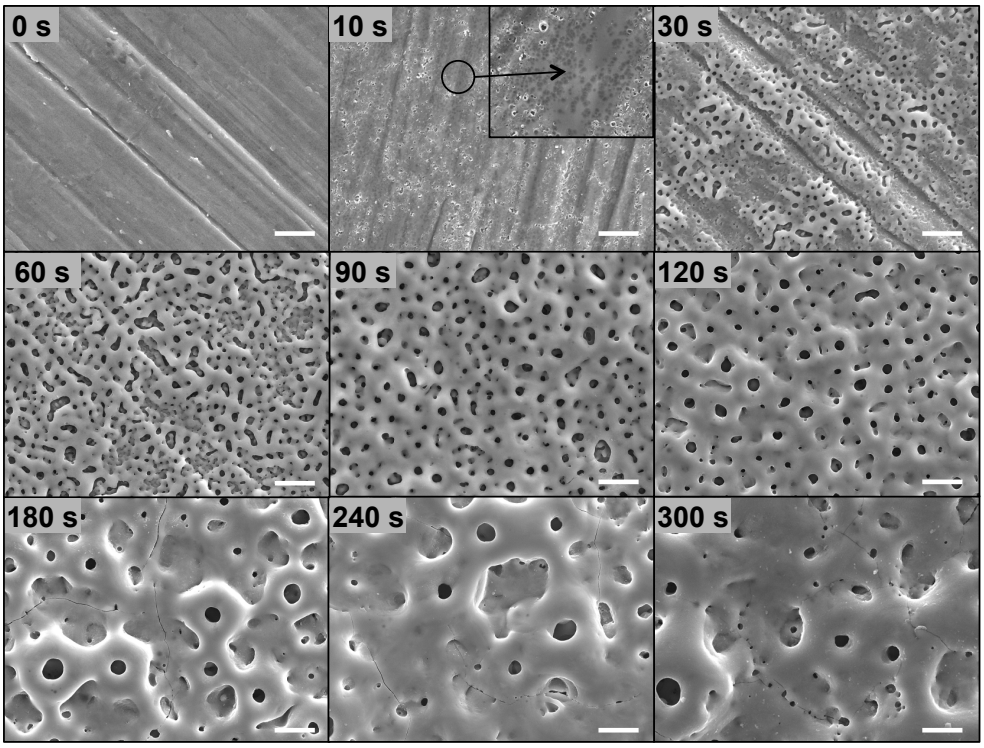

Fig. 3.4. SEM micrographs showing the evolution of TiO_2 layer growth during PEO at 20A/dm^2 and different treatment times (scale bar - 5 μm).

followed by (ii) an inflection in the curve determined by a reduced rise of voltage (0.2 V/s) associated with the moment of dielectric breakdown of the barrier film and sustained growth of TiO_2 layer in the presence of spark discharges.

After the initiation of sparking, there is a linear increase in coating thickness with the oxidation time. The thickest point of the coating was approximately 18.1 ± 1.85 μm corresponding to a rate of coating growth of 60 ± 6.2 nm/s. The formation ratio of the barrier layer produced below the sparking mode is 4.52 nm/V, while the porous layer is formed at a rate of 74.18 nm/V after 300 seconds. No differences in voltage-time transients were observed when the layers were produced in the absence of Ag nanoparticles in the electrolyte.

The coatings produced at 10, 30, 60 and 90 seconds were of uniform matt dark grey appearance while the coatings produced at 120, 180, 240 and 300 seconds were matt brown due to the Ag nanoparticles incorporation in higher concentrations (Fig. 3.3).

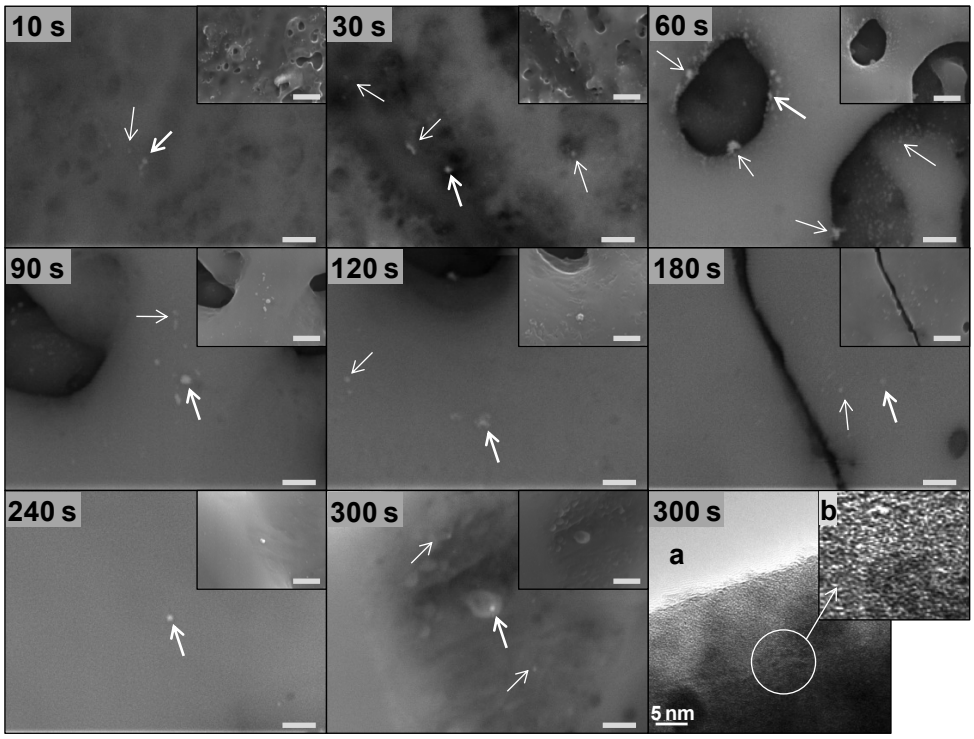

Fig. 3.5. High magnification SEM-BSE images of the surface of antibacterial coatings showing the presence of Ag nanoparticles at all oxidation times (scale bar - 250 nm). Small images depict the same image but in secondary electron mode (scale bar - 500 nm). The HRTEM images (a,b) show the incorporation of Ag nanoparticles close to the surface of the TiO_2 layer.

3.3.3. TiO_2 layer morphology and distribution of Ag nanoparticles

3.3.3.1. Surface investigation

Fig. 3.4 shows the SEM micrographs of the surface morphology of antibacterial coatings produced at different oxidation times. Nano-sized pores (50 – 250 nm) are visible starting with very early stages of coating growth (*i.e.,* 10 seconds) surrounded by non-porous areas with visible dark features (Fig. 3.4, 10 seconds).

This is in accordance with the voltage-time transients indicating an inflection in the curve at 8 seconds determined by starting of dielectric breakdown events. As the oxidation process is run for longer durations, large pores start to appear mainly on top of the grinding lines suggesting higher current flow through these regions being

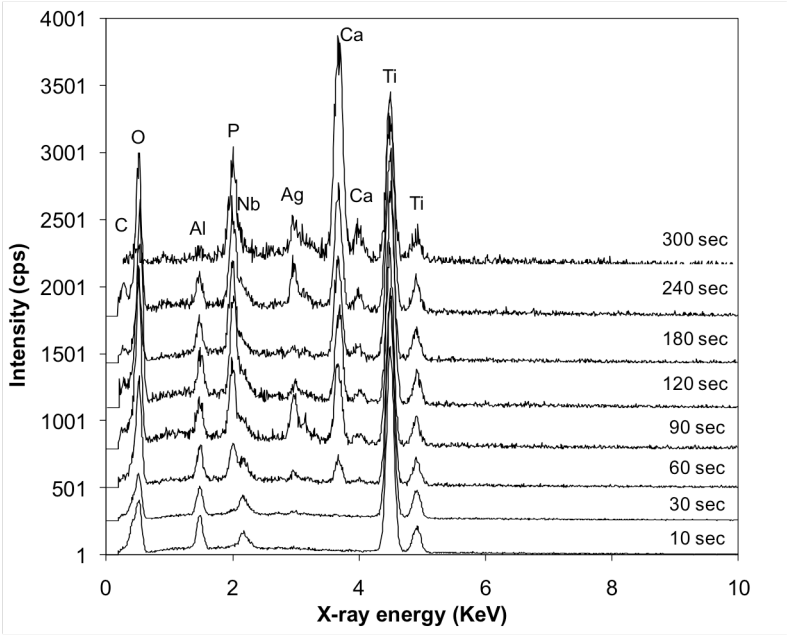

Fig. 3.6. SEM EDX patterns of different spots (Fig. 3.5 bold arrows) showing the presence of Ag on the surface of the oxide coatings.

more prone to breakdown (Fig. 3.4, 30 seconds). After 60 seconds, the surface is completely covered with elongated pores having a maximum size of 5 μm. Further oxidation determines the formation of an oxide containing fewer pores, with a round morphology, that is being maintained also at 120 seconds. As the oxidation process reaches 180 seconds, appearance of big protruding pores among the smaller pores suggests local bigger and stronger spark discharges. This morphology is being maintained for longer oxidation times *i.e.,* 300 seconds.

High-resolution SEM micrographs (BSE mode) of the surface of the bactericidal coatings are presented in Fig. 3.5. High atomic number elements such as Ag back-scatter electrons more strongly than elements with lower atomic numbers and thus appear brighter in BSE micrographs. Ag nanoparticles were found encroached on the surface of oxide coatings and fused inside the open pores at all oxidation times. EDX spot analyses on the detected nanoparticles further confirmed the presence of Ag next to the Ti, Al, and Nb from the metallic substrate and Ca and P from the electrolyte (Fig. 3.6).

EDX signals of Ca and P were first detected starting with 60 seconds of PEO and seem to increase with increasing the oxidation time.

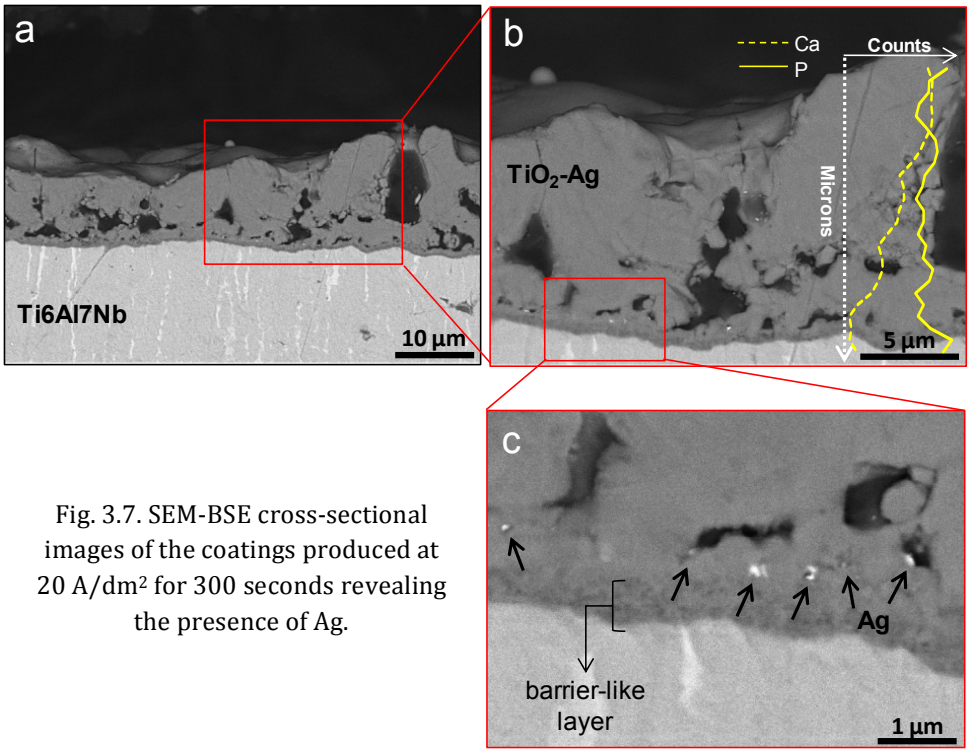

Fig. 3.7. SEM-BSE cross-sectional images of the coatings produced at 20 A/dm² for 300 seconds revealing the presence of Ag.

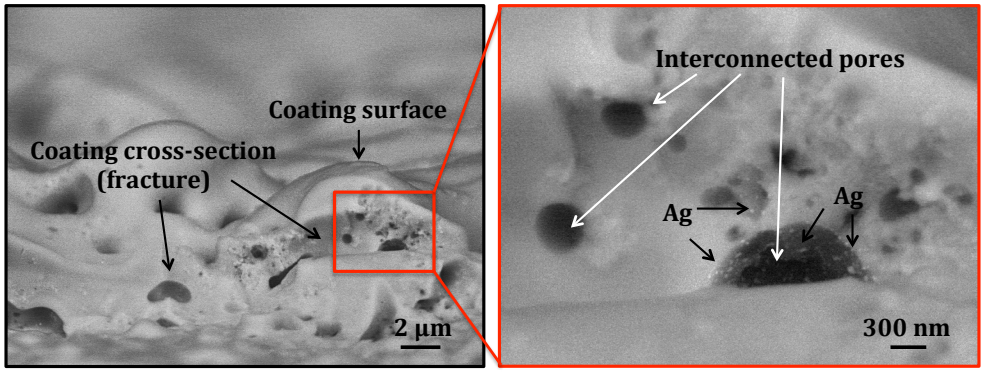

Fig. 3.8. SEM-BSE image of a fractured cross-section of TiO_2 layer depicting the presence of Ag nanoparticles fused inside the interconnected pores.

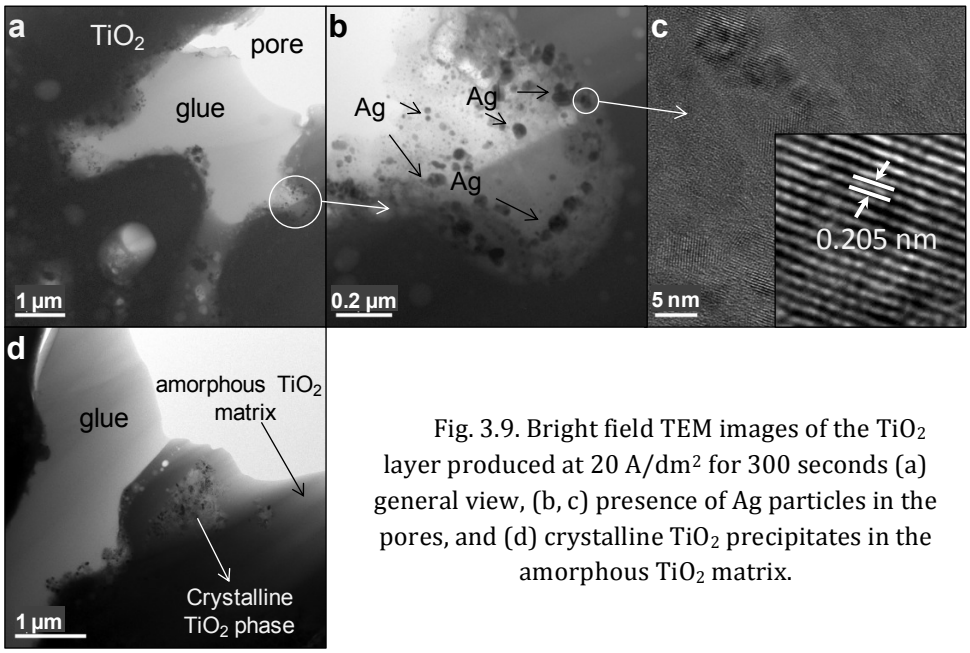

Fig. 3.9. Bright field TEM images of the TiO_2 layer produced at 20 A/dm^2 for 300 seconds (a) general view, (b, c) presence of Ag particles in the pores, and (d) crystalline TiO_2 precipitates in the amorphous TiO_2 matrix.

HRTEM images (Fig. 3.5 a,b) of the lattice spacings corresponding to fcc Ag, and also the EDX signal obtained with the electron beam on a particle, indicated the presence of Ag nanoparticles on the surface of the coating. The nanoparticles seem to be embedded in an amorphous TiO_2 matrix.

3.3.3.2. Cross-sectional investigation

SEM cross-sectional investigation (Fig. 3.7) of the coatings produced at 20 A/dm^2 for 300 seconds revealed a rough, porous layer with Ag nanoparticles distributed throughout the thickness. At the metal interface there is a thin TiO_2 barrier-like layer of approximately 0.5 µm. Ag nanoparticles were found across the layer thickness fused into the pores wall (Fig. 3.8) and embedded inside the dense TiO_2 matrix starting just above the barrier-like layer (Fig. 3.7 b,c). This finding was also confirmed by EDX analyses.

TEM investigation of the thin sections of the bactericidal coating produced at 20 A/dm^2 for 300 seconds revealed a very porous layer with glue from the preparation process in many of the pores (Fig. 3.9a). Ag nanoparticles were found mainly inside the pores (Fig. 3.9b and c) but also embedded in the oxide matrix (Fig. 3.5a). The

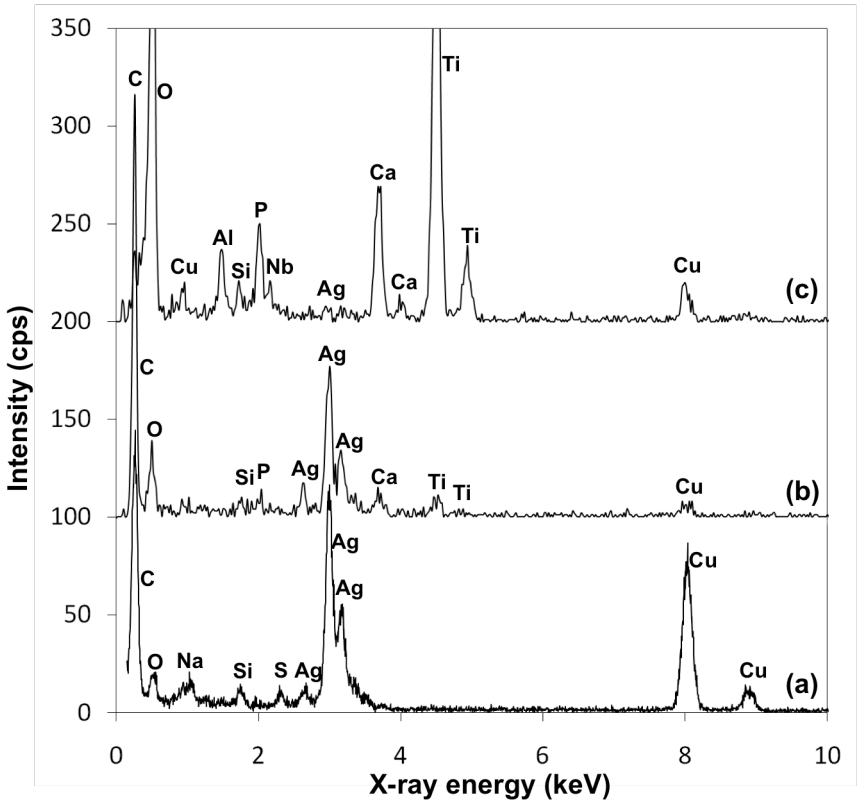

Fig. 3.10. TEM EDX analyses of (a) original Ag nanoparticles used in the PEO process, (b) Ag nanoparticle inside the pores, and (c) amorphous TiO_2 and crystalline TiO_2 showing the same EDX pattern.

morphology of the Ag found in the coatings matches the one of the particles used in the electrolyte. HRTEM images of the nanoparticles revealed lattice spacings corresponding to fcc metallic Ag. Fig. 3.10b shows a typical EDX pattern when the electron beam is focused on one Ag nanoparticle (spot depicted in Fig. 3.9b). The matrix comprised of amorphous TiO_2 with embedded crystalline precipitates (Fig. 3.9d) determined by X-ray diffraction analysis to be anatase and rutile, as revealed in Chapter 2 in Fig. 2.6. EDX analyses of the amorphous matrix and crystalline precipitates (Fig. 3.10c) showed the same composition in atomic percents: 55% O, 27% Ti, 6% Ca, 4% P, 4% Al, 2% Nb and 1% Si.

3.4. Discussion

3.4.1. TiO_2 layer growth

PEO of Ti6Al7Nb biomedical alloy has been performed in a calcium acetate/calcium glycerophosphate electrolyte bearing Ag nanoparticles, using a current density of 20 A/dm^2 and oxidation times varying from 10 to 300 seconds.

Few main stages were identified during the growth of the antibacterial layers on titanium under the selected conditions: (a) formation of the anodic barrier layer in the first 8 seconds of oxidation, (b) dielectric breakdown of the anodic film (8 – 10 seconds), (c) local thickening of the oxide at sparking locations, (d) appearance of the pores, (e) sustained growth in the presence of sparking, and (f) appearance of bigger sparks and breakdown channels leading to large and protruding pores.

The anodic barrier layer is mainly formed at the metal/oxide interface by migration of O^{2-} ions inwards and migration of Ti^{4+} outwards, with only 35-38% of the film formed at the oxide/electrolyte interface [12]. The high slope in the voltage-time transients corresponding with the formation of the barrier layer (Fig. 3.2) indicates the high efficiency of the process, as no species from the film are lost to the electrolyte. Close inspection of the BSE micrographs of the layers formed at 20 A/dm^2 for 10 seconds indicates the presence of dark depressions that might be oxygen filled voids similar with the finding of Matykina *et al.* [13]. These regions are associated with the formation of TiO_2 nanocrystals at a depth of 35-38% of the amorphous anodic film [12] and can be precursors of the dielectric breakdown and beginning of sparking at higher potentials. A barrier layer is constantly being formed and destroyed during PEO. Cross-sectional investigation of the layer formed for 300 seconds (Fig. 3.7c) reveals the existence of a barrier-like layer close to metal/film interface probably created in the later stages of the dielectric breakdown just before the process was terminated. This finding is in line with the work of Matykina *et al.* [2]. The barrier layer acts like a resistor to current flow. Thus, on locations with less resistance dielectric breakdown of the layer occurs, leading to thickening of the oxide, as observed in Fig. 3.4. These locations appear to be on top of the grinding lines formed during preparation of titanium specimens. Breakdown is accompanied by spark discharges, high local temperatures and release of oxygen with enough pressure to break through the soft material forming the pores [14]. Formation of new layer material restores the resistance to current flow and other spot, relatively less resistant, is prone to breakdown. The sparks continually initiate and extinguish at locations of dielectric breakdown *i.e.,* at the TiO_2 layer/metal interface, within the coating bulk and at the coating surface. At these sites new material is formed by

destruction of the original/previous layer due to the intense local heating at the sites of breakdown that accelerate chemical dissolution and/or melting and evaporation of the TiO_2 material [15]. Breakdown events allow the access of electrolyte species to the inner part of the layer through short-circuit paths [7, 15]. As the oxidation time increases, large breakdown channels accompanied by intense sparking and gas bubbles, lead to the formation of protruding pores. The layer formed at 300 seconds consists of amorphous TiO_2 rich in Ca and P species, as well as anatase and rutile phases. The crystalline phases are formed by local high temperatures and pressures associated with spark discharges. EDX analyses (Fig. 3.7b) of the chemical composition of the layer across its thickness showed an increased concentration of Ca towards the oxide surface, suggesting incorporation during growth of oxide at the film/electrolyte interface and transport of Ca ions outward in the layer [16].

3.4.2. Incorporation of Ag nanoparticles

Ag as clusters or stand-alone nanoparticles was evidenced both by SEM and TEM within the TiO_2 matrix. Close investigation of the coatings for evidence of particles revealed three different locations of Ag within the oxide: encroached on the surface of the oxide (with some particles protruding from the film), fused into the pores wall and embedded across the entire thickness of the dense oxide matrix, starting just above the barrier-like layer. The morphology of Ag nanoparticles appears to be similar to that of the original particles used in the electrolyte indicating temperatures at the sites of incorporation below the melting point of Ag (961°C [17]).

The incorporation mechanism of Ag nanoparticles within the porous TiO_2 matrix comprises of four main steps:

- Transport of Ag nanoparticles towards the TiO_2 surface;
- Attachment/adsorption of Ag nanoparticles to the sites of layer growth;
- Entrapment of Ag nanoparticles at the sites of coating growth;
- Preservation of the already embedded particles during the layer growth.

The nanoparticles are moving in the electrolytic bath following the unidirectional stirring of the electrolyte via mechanical agitation. Nanoparticles can be transported to the sites of coating growth (where dielectric breakdown occurs) through different transport pathways (*e.g.,* open pores, cracks and short-circuit channels) while other particles might be deflected back by the shock-waves, heat-waves and by the generation of gas bubbles during spark discharges. Electrophoresis might help in delivery of nanoparticles into the inner parts of the coating considering that they are negatively charged in the calcium acetate/calcium glycerophosphate electrolyte and

were found to easily move towards the positive electrode under the influence of the applied electric field.

At the locations of coating growth, with the local heating generated by sparking events, the newly formed coating can be relatively soft and Ag nanoparticles may become entrapped and fused into it once the spark extinguishes and the site is cooled by the electrolyte. Thus, Ag nanoparticles are embedded into the oxide layer as it grows. The new coating material formed close to the metal interface might be extruded through breakdown channels and molten material may fill the pores and cracks, moving the Ag particles that were fused in a previous discharge event.

The antibacterial activity of Ag bearing coatings may involve close contact of bacteria with the nanoparticles and/or release of ions, detachment of nanoparticles or release of free radicals in contact with a liquid media [18]. Considering the distribution of Ag within the oxide coating, it can be underlined that only two locations are important for conferring the material with the antibacterial activity, *i.e.,* nanoparticles fused in the wall of the open pores and those encroached on the surface of the coatings, respectively.

3.5. Conclusions

In this chapter, an electron microscopy research on the growth of Ag-bearing TiO_2 antibacterial layers on Ti6Al7Nb biomedical alloy was conducted.

TEM of Ag nanoparticles used in the electrolyte showed a round morphology, a particle size of 7 - 25 nm and lattice spacings corresponding to fcc Ag. The layers comprised of amorphous TiO_2 with anatase and rutile precipitates and randomly distributed Ag nanoparticles. Ag nanoparticles were found embedded into the dense oxide layer, fused into the pores wall and encroached on the surface of the oxide with some particles protruding outside the film.

As far as the mechanism of Ag nanoparticles incorporation is concern, it was found that Ag nanoparticles might be delivered to the sites of layer growth through short-circuit channels, open pores and cracks, probably assisted by electrophoresis, where are incorporated into relatively soft material and fused into it once this is cooled and solidified. The morphology of Ag nanoparticles in the layers seems to match the one of the particles used in the electrolyte, indicating temperatures at the sites of incorporation below 961°C, the melting point of Ag.

References

[1] J.Z. Shi, C.Z. Chen, S.J. Zhang, Y.J. Wu, Application of surface modification in biomedical materials research, Surface Review and Letters, 14 (2007) 361-369.

[2] E. Matykina, F. Monfort, A. Berkani, P. Skeldon, G.E. Thompson, J. Gough, Characterization of spark-anodized titanium for biomedical applications, Journal of the Electrochemical Society, 154 (2007) C279-C285.

[3] S.R. Paital, N.B. Dahotre, Calcium phosphate coatings for bio-implant applications: Materials, performance factors, and methodologies, Materials Science & Engineering R-Reports, 66 (2009) 1-70.

[4] Q. Dong, C.Z. Chen, D.G. Wang, Q.M. Ji, Research status about surface modification of biomedical Ti and its alloys by micro-arc oxidation, Surface Review and Letters, 13 (2006) 35-43.

[5] E. Matykina, R. Arrabal, P. Skeldon, G.E. Thompson, Investigation of the growth processes of coatings formed by AC plasma electrolytic oxidation of aluminium, Electrochimica Acta, 54 (2009) 6767-6778.

[6] R. Arrabal, E. Matykina, P. Skeldon, G.E. Thompson, Incorporation of zirconia particles into coatings formed on magnesium by plasma electrolytic oxidation, Journal of Materials Science, 43 (2008) 1532-1538.

[7] R. Arrabal, E. Matykina, F. Viejo, P. Skeldon, G.E. Thompson, M.C. Merino, AC plasma electrolytic oxidation of magnesium with zirconia nanoparticles, Applied Surface Science, 254 (2008) 6937-6942.

[8] E. Matykina, R. Arrabal, F. Monfort, P. Skeldon, G.E. Thompson, Incorporation of zirconia into coatings formed by DC plasma electrolytic oxidation of aluminium in nanoparticle suspensions, Applied Surface Science, 255 (2008) 2830-2839.

[9] E. Matykina, R. Arrabal, P. Skeldon, G.E. Thompson, Incorporation of zirconia nanoparticles into coatings formed on aluminium by AC plasma electrolytic oxidation, Journal of Applied Electrochemistry, 38 (2008) 1375-1383.

[10] D.Y. Kim, M. Kim, H.E. Kim, Y.H. Koh, H.W. Kim, J.H. Jang, Formation of hydroxyapatite within porous TiO_2 layer by micro-arc oxidation coupled with electrophoretic deposition, Acta Biomaterialia, 5 (2009) 2196-2205.

[11] J.H. Lee, H.E. Kim, Y.H. Koh, Highly porous titanium (Ti) scaffolds with bioactive microporous hydroxyapatite/TiO_2 hybrid coating layer, Materials Letters, 63 (2009) 1995-1998.

[12] H. Habazaki, M. Uozumi, H. Konno, K. Shimizu, P. Skeldon, G.E. Thompson, Crystallization of anodic titania on titanium and its alloys, Corrosion Science, 45 (2003) 2063-2073.

[13] E. Matykina, R. Arrabal, P. Skeldon, G.E. Thompson, H. Habazaki, Influence of grain orientation on oxygen generation in anodic titania, Thin Solid Films, 516 (2008) 2296-2305.

[14] E. Matykina, A. Berkani, P. Skeldon, G.E. Thompson, Real-time imaging of coating growth during plasma electrolytic oxidation of titanium, Electrochimica Acta, 53 (2007) 1987-1994.

[15] E. Matykina, G. Doucet, E. Monfort, A. Berkani, P. Skeldon, G.E. Thompson, Destruction of coating material during spark anodizing of titanium, Electrochimica Acta, 51 (2006) 4709-4715.

[16] E. Matykina, R. Arrabal, P. Skeldon, G.E. Thompson, Transmission electron microscopy of coatings formed by plasma electrolytic oxidation of titanium, Acta Biomaterialia, 5 (2009) 1356-1366.

[17] C. Brown, Dictionary of metalurgy, John Wiley and Sons, New York, 1998.

[18] J.S. Kim, E. Kuk, K.N. Yu, J.H. Kim, S.J. Park, H.J. Lee, S.H. Kim, Y.K. Park, Y.H. Park, C.Y. Hwang, Y.K. Kim, Y.S. Lee, D.H. Jeong, M.H. Cho, Antimicrobial effects of silver nanoparticles, Nanomedicine: Nanotechnology, Biology and Medicine, 3 (2007) 95-101.


1 cm

Chapter 4

In vitro evaluation of antibacterial activity*

Are Ag-bearing TiO_2 layers antibacterial?

4.1. Introduction

Joint replacement surgery is the current procedure to alleviate pain and restore mobility in patients with osteoarthritic joints [1]. One of the limitations associated with total joint arthroplasties is represented by the implant associated infections (IAI)[2-4]. For instance, in the United States the number of infections associated with orthopaedic implants approaches one million cases per year [5, 6]. Such infections may lead to implant failure, revision surgery and even member amputation, all associated with extremely high medical costs in addition to the pain and suffering of the patients. The average cost for a total hip arthroplasty procedure is about $40,000 while if an infection develops the estimated cost for the treatment, surgery and new implant will easily go beyond $75,000 [7].

*Based on:
B.S. Necula, L.E. Fratila-Apachitei, S.A.J. Zaat, I. Apachitei, J. Duszczyk, *In vitro* antibacterial activity of porous TiO_2-Ag composite layers against methicillin-resistant Staphylococcus aureus, Acta Biomaterialia, 5 (2009) 3573–3580.

B.S. Necula, L.E. Fratila-Apachitei, J.P.T.M. van Leeuwen, S.A.J. Zaat, I. Apachitei, J. Duszczyk, *In vitro* cytotoxicity evaluation of porous TiO_2-Ag antibacterial coatings on human fetal osteoblasts, Acta Biomaterialia, 8 (2012) 4191–4197.

One of the most promising approaches in preventing IAI is to provide an antibacterial activity to the implant itself. It is desired that the implant should have the ability to elute locally controlled and sustained amounts of antibacterial agents. This will prevent bacteria colonization and biofilm formation. As presented in Chapters 2 and 3, plasma electrolytic oxidation (PEO) is a surface modification technique, which has the ability to produce porous TiO_2 coatings on Ti and its alloys. Therefore, incorporation of Ag nanoparticles into TiO_2 porous surfaces represents an important route of making titanium implants with antibacterial function [8, 9]. The primary role of these antibacterial coatings is the release of the bactericidal agent directly at the site of implantation, minimizing the risk of reaching concentrations that can cause harmful side reactions to the other parts of the body.

From a number of assays available for measuring antibacterial activity of solid surfaces [10, 11], few reflect the actual conditions under which the bacteria will come in close contact with a potentially bactericidal surface (*i.e.,* implant). The testing conditions should mimic the scenario of an infection during primary total joint replacement (TJR) surgery or of a revision surgery performed after infection occurred when bacteria in the form of a biofilm will surround the new implant. An accurate assay should always consider the number of bacteria initially adhering onto the testing surface and quantify their decrease or increase in numbers over time under conditions resembling as much as possible the tissue environment. In addition, a quantitative assessment of the numbers of surviving colony forming units (CFU) on a bactericidal surface compared with a non-bactericidal surface should be performed.

In this chapter, new assays to test the antibacterial activity of solid surfaces have been proposed. In addition, using the new assays, the antibacterial activity of Ag-based TiO_2 layers against methicillin-resistant *Staphylococcus aureus* (MRSA) was evaluated. A particular focus was on the effects of different Ag nanoparticle concentrations in the TiO_2 layers. Furthermore, the total Ag content from the layers and the Ag ions release were measured. Corroborating the results from antibacterial testing and Ag content and release from the layers a mechanism of antibacterial activity for these particular Ag-based layers was proposed.

4.2. Experimental

4.2.1. Synthesis of antibacterial layers

The Ti6Al7Nb disks were plasma electrolytically oxidized in an electrolyte based on calcium acetate/calcium glycerophosphate salts bearing different concentrations of

Ag nanoparticles. The oxidation process was performed under galvanostatic mode using a current density of 20 A/dm^2 for 5 minutes. A description of the equipment used and more experimental details on the Ag-bearing TiO_2 layers synthesis are presented in Chapter 2. To remove the unattached Ag nanoparticles, all modified disks were washed in running tap water for 5 minutes, ultrasonically cleaned in 70% ethanol and deionized water for 30 seconds each, then rinsed again for 5 minutes in deionized water.

Four different types of specimens were prepared for investigation of antibacterial activity *i.e.,* uncoated Ti6Al7Nb disks (TG), Ag-free TiO_2 layers (0Ag) and Ag-bearing TiO_2 layers in two different concentrations (0.3Ag and 3.0Ag).

Before antibacterial testing, all samples were sterilized for 1 hour at 110°C using a Nabertherm TR60 oven and kept in sterile sample bags.

4.2.2. Assays for evaluation of antibacterial activity

4.2.2.1. Direct contact assay - surface antibacterial activity

A modified version of the Japanese Industrial Standard, JIS Z 2801:2000 [10] was used to evaluate the bactericidal activity of the Ag-bearing TiO_2 layers against MRSA. The Japanese assay was modified to better simulate the situation of an infection occurring during primary TJR surgery. Considering the porous morphology of the Ag-based TiO_2 layers, sonication and vortexing were used to detach any adherent bacteria. Furthermore, the modified assay allowed testing in the presence of host biomatrices, such as human serum.

A fresh liquid culture of MRSA strain AMC201 was prepared by adding 1-5 colonies from a streak plate into 5 mL of Bacto Tryptic Soy Broth (TSB) (Brunschwig Chemie, The Netherlands). The suspension was incubated at 37°C under rotation for approximately 2 hours and subsequently diluted with TSB to an optical density (OD620) of 0.03, corresponding to 10^7 CFU/mL. Round sterilized nitrocellulose filters (Optitran BA-S 85, Whatman Nederland BV) cut to a diameter of 18 mm, thus slightly smaller than that of the titanium disks, were placed on a blood agar plate. Twenty µL of the diluted MRSA culture, containing 2 x 10^5 CFU, was pipetted onto the filters. The medium was absorbed by the agar while the MRSA bacteria were retained on the filter (Fig. 4.1a). Twenty µL of 1% TSB in 10mM phosphate, with and without the addition of 10% and 50% of pooled human serum, was pipetted centrally on the surface of each titanium disk, and an inoculated filter disk was carefully placed, with the bacteria contacting the metal surface (Fig. 4.1b). All titanium disks were then

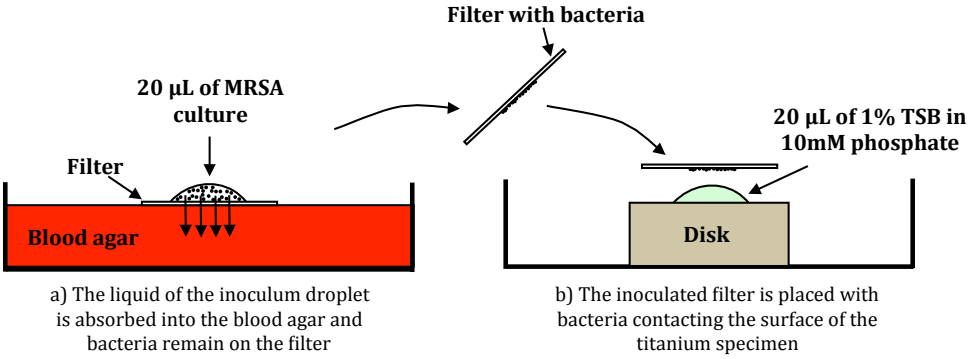

a) The liquid of the inoculum droplet is absorbed into the blood agar and bacteria remain on the filter

b) The inoculated filter is placed with bacteria contacting the surface of the titanium specimen

Fig. 4.1. Schematic representation of the assay used to investigate the antibacterial activity of the Ag-bearing layers. As the filter diameter is smaller than that of the disk, all bacteria will be in contact with the disc surface and/or the liquid interface.

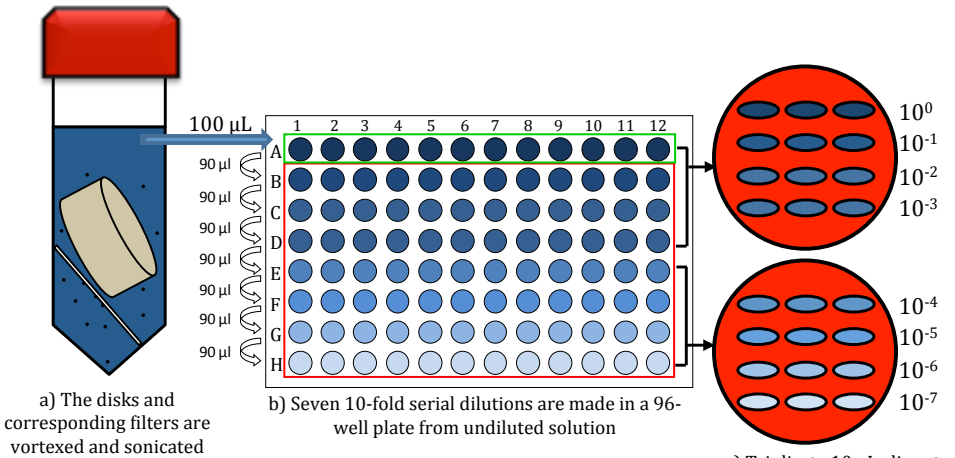

a) The disks and corresponding filters are vortexed and sonicated in 5 mL TSB

b) Seven 10-fold serial dilutions are made in a 96-well plate from undiluted solution

c) Triplicate 10 µL aliquots of the undiluted suspension and of the 7 dilutions is pipetted onto blood agar plates

Fig. 4.2. Experimental procedure for quantitative determination of antibacterial activity.

placed individually in Petri dishes and incubated at 37°C for 24 hours in a humid atmosphere. After incubation, each disk together with the corresponding filter was placed in 5 mL TSB, sonicated for 30 seconds and vortexed for one minute to dislodge adherent bacteria. This procedure does not affect bacterial viability. Seven 10-fold serial dilutions were made in a 96 well ELISA microtiter plate (*i.e.,* 10^{-1} to 10^{-7}). Subsequently, triplicate 10 µL aliquots of the undiluted suspension and of the 7 dilutions were pipetted onto blood agar plates (Fig. 4.2). The blood agar plates were incubated overnight at 37°C and the number of colonies was counted the next day. The sample size for this experiment is $n \geq 3$. The immediate recovery of the inoculum from the titanium disks was performed to check the correctitudeness of the assay.

4.2.2.2. 3M Petrifilm assay - leachable antibacterial activity

The leachable antibacterial activity of the Ag-bearing PEO coatings was tested using a modified version of the 3M petrifilm plate assay. This assay was designed specifically to evaluate the activity of leachables, specifically Ag ions and Ag free radicals, from the Ag-based PEO layers.

A typical petrifilm plate (Fig. 4.3a) has a bottom film (10 cm length by 7.5 cm width) which contains a foam barrier that accommodates the plating surface (a circular area of about 20 cm^2) and a top film that encloses the sample within the petrifilm. The central plating surface generally comprises of a cold-water-soluble gelling agent, nutrients, and indicators for activity and enumeration.

To inoculate, the top layer was lifted to expose the plating surface, and with a pipette, 1 mL of medium, containing 2×10^7 MRSA CFU, was added. The top film was then slowly rolled down and gently pressed to ensure even distribution of the MRSA. After approximately one minute gelling occurred and the top film was lifted together with the gel. The titanium disks to be tested (0Ag, 0.3Ag and 3.0Ag) were placed in the middle of the plating area and the top film was carefully placed on top of the disks (Fig. 4.3 a-d). The petrifilm was then incubated for 24 hours at 37°C in a humid atmosphere.

After the incubation period the gel becomes darker due to bacterial activity. In the case of bacterial inhibition the gel should retain its original state (Fig. 4.3 e-f).

In the modified assay the bacterial inoculum was added to the plating surface together with the medium. The bacteria might also end up inside the agar of the petrifilm and therefore the activity of the surface will not be distinguished.

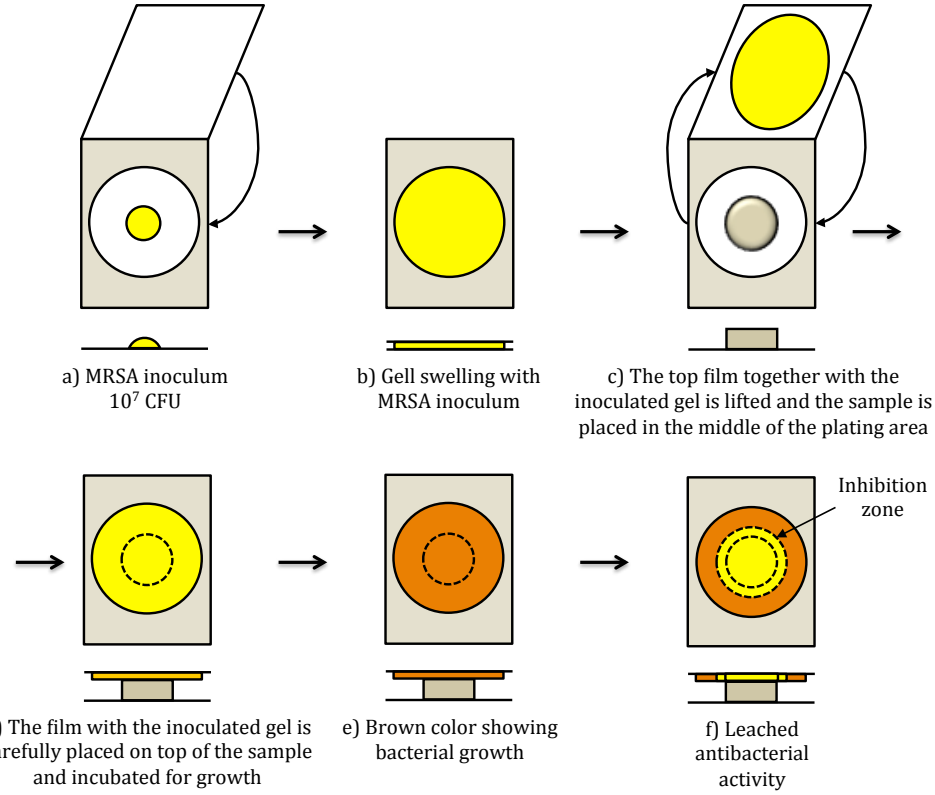

Fig. 4.3. 3M Petrifilm assay for determination of leachable antibacterial activity of Ag-bearing layers.

4.2.3. Total Ag content in the layers and Ag ions release

4.2.3.1. Total Ag content in the layers

The total concentration of Ag incorporated in the TiO_2 layers was determined for the 0.3Ag and 3.0Ag samples, in triplicates. The TiO_2 layer, bearing the Ag nanoparticles, was dissolved in concentrated sulfuric acid (98%) at a temperature of 90°C in an ultrasonic bath for 2 hours. The hot sulfuric acid is able to completely dissolve the TiO_2 layer leaving the Ti6Al7Nb substrate unaffected. After cooling, the disks were removed and concentrated nitric acid (69%) was added to completely dissolve the loose Ag nanoparticles. The liquid samples were then tested for Ag content with Flame - Atomic Absorption Spectroscopy (Flame-AAS) technique using the PerkinElmer AAnalyst 100 instrument.

To determine the total concentration of Ag available for release, the Ag-bearing specimens were treated with concentrated nitric acid that selectively dissolves only the Ag nanoparticles present on the surface and inside the open interconnected porosity. The TiO_2 layer is not soluble in nitric acid. Thus, the Ag-bearing disks were immersed in 15 mL concentrated nitric acid (69%) and kept under gentle stirring conditions. The immersion liquid was collected after 24 hours and analyzed by Flame-AAS.

4.2.3.2. Ag ions release

Ag release experiments were performed in triplicates for the 0.3Ag and 3.0Ag samples. The titanium disks were placed in dark Wheaton bottles containing 30 mL of double distilled water and kept at 37°C under gentle stirring conditions up to 7 days. The liquid was collected at day 1, 2, 5 and 7 and replaced with fresh double distilled water. All collected samples were acidified with nitric acid to a final concentration of 0.5M and were analyzed with the Graphite Furnace Atomic Absorption Spectrometry (GFAAS) technique using the PerkinElmer 4100ZL instrument. The time points were selected according to the cytotoxicity tests described in Chapter 5.

4.3. Results

4.3.1. Direct contact assay - surface antibacterial activity

The surface antibacterial activity of the TG, 0Ag, 0.3Ag and 3.0Ag disks was assessed using the direct contact assay. Fig. 4.4 shows the percentage killing or growth of MRSA CFU on 0Ag, 0.3Ag and 3.0Ag coatings, calculated based on the quantitative cultures (shown in Fig. 4.5) of the solutions resulted after sonication of the disks, inoculated and incubated for 24 hours. The percent of MRSA killing was found to be 98.0 ± 2% in the case of 0.3Ag and 99.75 ± 0% for the 3.0Ag. The TG and Ag-free coatings (0Ag) showed no bactericidal nor bacteriostatic properties as evidenced by the 1000-fold increase in MRSA CFU. The bactericidal activity of the Ag-bearing coatings was not affected by the addition of 10% and 50% human serum to the culture medium as shown in Fig. 4.6. A complete killing of the inoculum was observed regardless the presence of 10% or 50% human pooled serum in the culture medium. The immediate recovery of the MRSA from the titanium disks revealed a number of 200,000 CFU, similar with the inoculum.

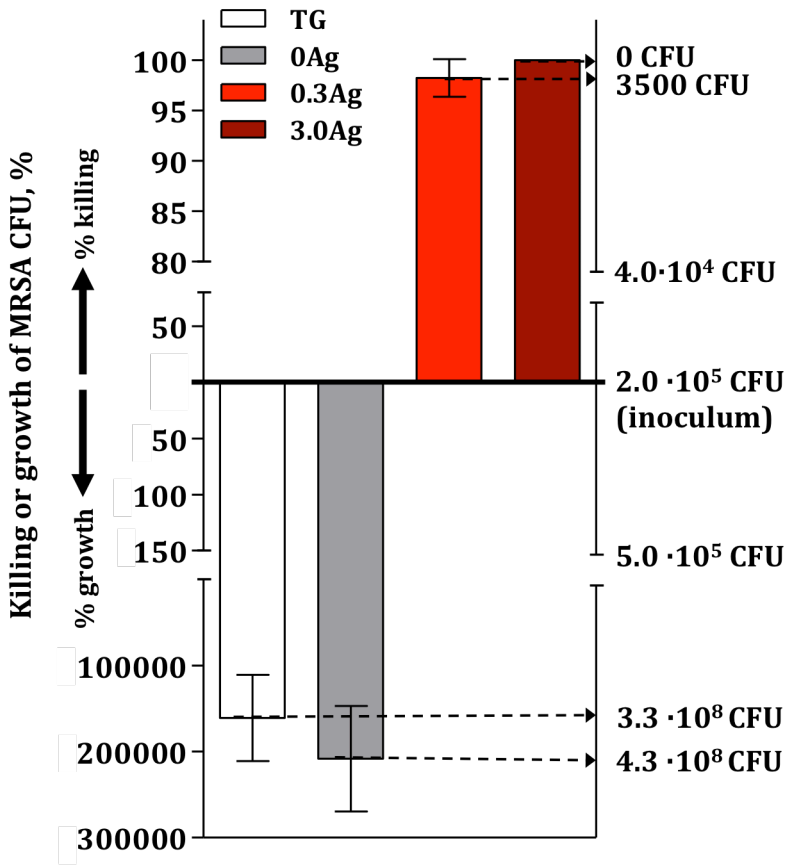

Fig. 4.4. Percentage of killing/growth of MRSA inoculum (with the corresponding CFU numbers) tested on uncoated disks, Ag-free and Ag-bearing TiO_2 layers using the direct contact assay.

4.3.2. 3M Petrifilm assay - leachable antibacterial activity

With the 3M Petrifilm assay the antibacterial activity of Ag ions released from Ag-bearing layers can be observed. As seen in Fig. 4.7, both 0.3Ag and 3.0Ag surfaces have a circular growth inhibition zone of approximately 2 mm (depicted with black arrows) as a result of Ag ions release from the surface. The Ag-free surface shows no sign of bacterial inhibition, as the gel remains darker.

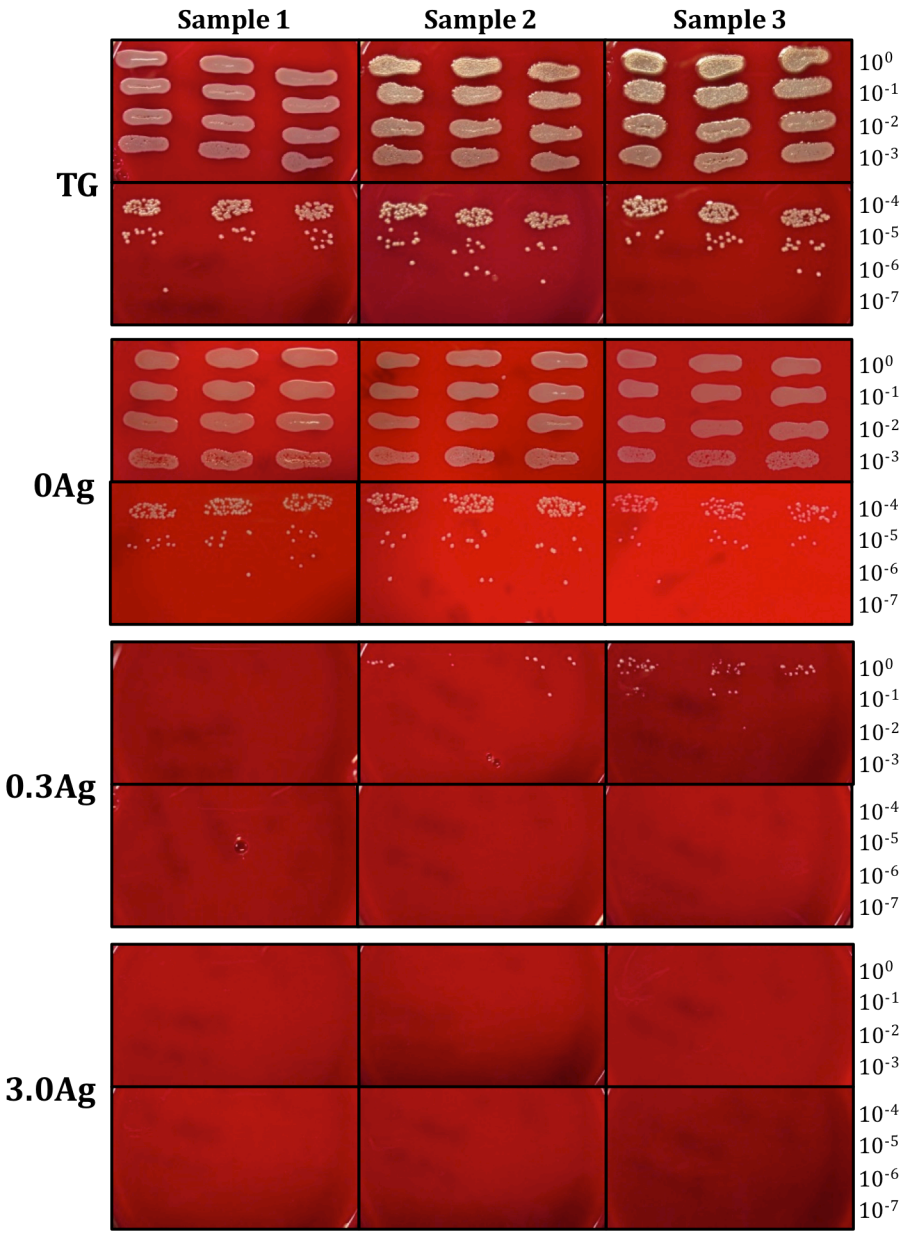

Fig. 4.5. Quantitative cultures after 24 hours of incubation for TG, 0Ag, 0.3Ag and 3.0Ag samples.

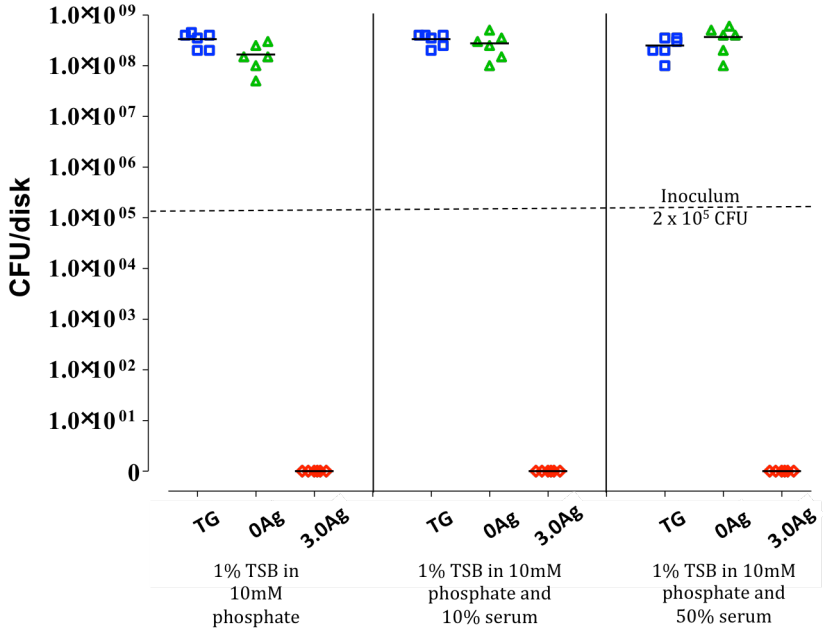

Fig. 4.6. Antibacterial activity of Ag-bearing TiO_2 layers in the presence of human pooled serum.

4.3.3. Total Ag content in the layers and Ag ions release

The total concentration of Ag incorporated in the 0.3Ag and 3.0Ag coatings was determined by Flame-AAS after total dissolution of the porous layers in hot sulfuric acid and nitric acid. The results showed that the total concentration of Ag embedded in the 0.3Ag and 3.0Ag coatings was 27.53 ± 0.82 and 213.9 ± 3.13 µg/disk, respectively.

However, only the Ag nanoparticles fused into the open interconnected pore walls and on the surface of the coatings can actually contribute to the antibacterial activity of the coatings, and this concentration was determined to be 20.82 ± 0.88 and 127.75 ± 5.28 µg/disk for the 0.3Ag and 3.0Ag, respectively.

The concentration of Ag ions released from the 0.3Ag and 3.0Ag coatings was measured by GFAAS and the results are shown in Fig. 4.8. The cumulative release of Ag from 0.3Ag and 3.0Ag surfaces after 2, 5 and 7 days is 0.0077, 0.0096 and 0.012 µg/mL and 0.05, 0.063 and 0.09 µg/mL, respectively.

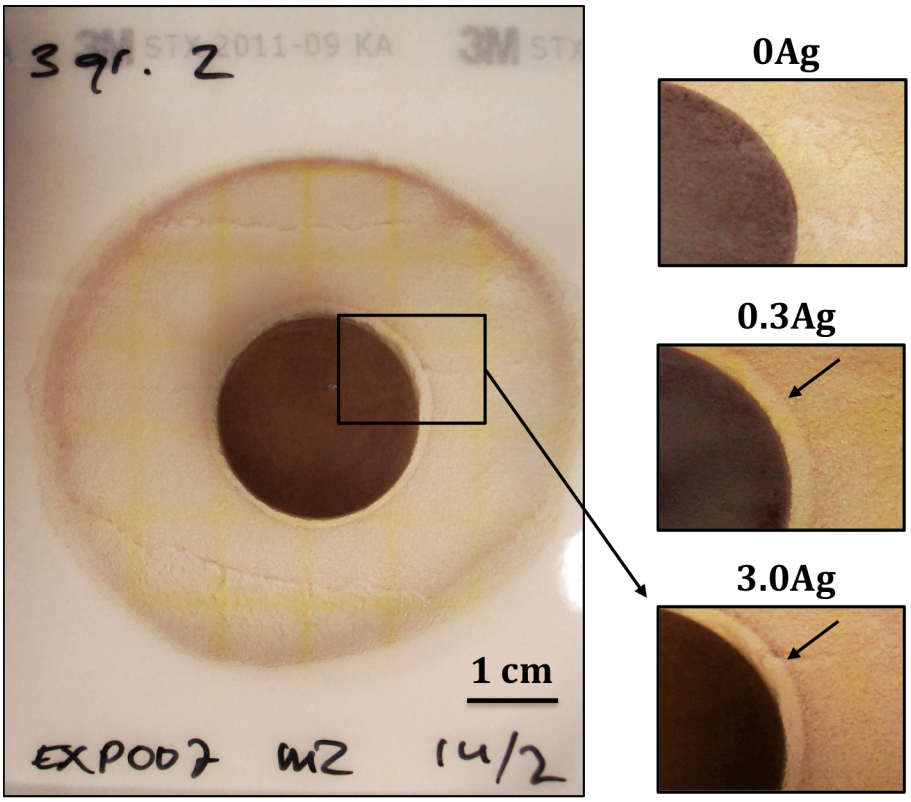

Fig. 4.7. Leachable antibacterial activity after 24 hours of incubation of Ag-bearing layers having different concentrations of Ag nanoparticles. The arrow shows the inhibition zone formed after leaching of Ag ions from the layers.

4.4. Discussion

The surface bactericidal activity of 0Ag, 0.3Ag and 3.0Ag layers was assessed using one of the most prevalent and virulent pathogen responsible for IAI (*i.e.,* MRSA) through a direct contact assay. The direct contact assay allows a quantitative interpretation of bactericidal activity based on killing of a defined inoculum. The percentage killing of MRSA seeded on 0.3Ag coatings was 98.0 ± 2% (Fig. 4.4), indicating that incorporation of a small concentration of Ag nanoparticles (*i.e.,* 1.6 μg/cm^2) into the TiO_2 layers can provide enough antibacterial activity to kill 98% of 2 x 10^5 CFU of MRSA in 24 hours. As expected, this activity is enhanced with increasing the concentration of Ag nanoparticles in the layers. Incorporation of 9.8 μg/cm^2 Ag

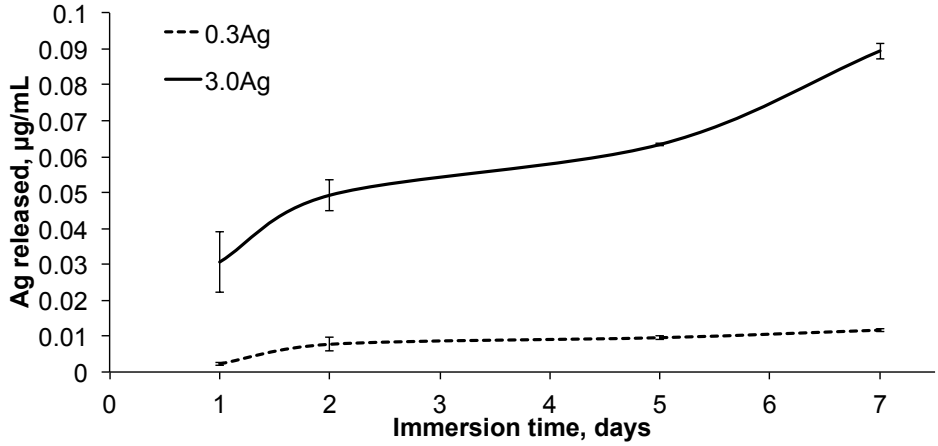

Fig. 4.8. Cumulative release of Ag from Ag-bearing TiO_2 layers immersed in deionized water at 37°C for up to 7 days.

nanoparticles in the 3.0Ag layers showed a complete killing of the MRSA inoculum (>99.75%) after 24 hours, while Ag-free samples (0Ag) allowed bacteria growth up to 1000-fold. The 3.0Ag layers showed no MRSA CFU after the quantitative cultures (Fig. 4.5) of the corresponding sonicated solutions. However, the detection limit of the method is 500 CFU. This means that 500 CFU in 5 mL (total volume of the sonicated solution) will not be culturable in 10 µL. Therefore, the percent killing for the 3.0Ag is reported to be 99.75% and not 100%.

The 3M Petrifilm assay demonstrates that Ag-bearing layers have not only surface antibacterial activity (close contact with bacteria is needed to kill) but also leachable antibacterial activity (Ag ions are being released from the surface of the layers and exhibit antibacterial properties).

The antibacterial activity of Ag-bearing TiO_2 layers should be attributed to the Ag nanoparticles incorporated in these layers since the TG and Ag-free layers showed no bactericidal activity. As it was found out in Chapter 3 [8], the Ag nanoparticles are embedded into the dense TiO_2 layer, fused into the pores wall and encroached on the surface of the oxide with some particles protruding outside the film. Based on these, some hypotheses can be made as a stating point for understanding the bactericidal mechanism of Ag-bearing TiO_2 layers.

As both ionic silver and the nanoparticles *per se* contribute to the bactericidal activity of Ag-bearing TiO_2 surfaces, a dual antibacterial mechanism is proposed. Using the direct contact assay the Ag nanoparticles embedded in the TiO_2 matrix were in close

contact with the MRSA. Thus, Ag nanoparticles could directly interact with the microbial cells causing degradation of the lipopolysaccharide molecules and forming ''pits'' leading to large increases in membrane permeability [12]. Ag may also produce secondary products (such as reactive oxygen species) that can penetrate the bacterial cell envelope and cause DNA damage and protein oxidation [13]. Furthermore, Ag ions released from Ag nanoparticles had an additional contribution to the bactericidal effect of the Ag-bearing TiO_2 layers by interacting with the thiol group proteins, turning the DNA into condensed form and disabling its replication ability [14].

4.5. Conclusions

The *in vitro* antibacterial activity of the TiO_2 surfaces bearing two different Ag concentrations against MRSA was investigated using the direct contact assay and the 3M Petrifilm assay for surface antibacterial activity and leachable antibacterial activity, respectively. The assays were modified to better simulate the scenario of IAI during primary surgery.

The direct contact of MRSA with the Ag-bearing surfaces may have strongly contributed to the 98% and 99.75% reduction in CFU for 0.3Ag and 3.0Ag surfaces, respectively. The TG surfaces and Ag-free samples showed a 1000-fold increase in bacterial CFU.

The 3M Petrifilm assay demonstrated the leaching antibacterial capability of the both 0.3Ag and 3.0Ag layers. Within 24h a clear growth inhibition zone was observed around Ag-bearing samples due to the release of Ag ions.

The antibacterial assays together with the experiments performed to determine the Ag ions release and the total Ag content in the layers helped hypothesizing the potential bactericidal mechanism of Ag-bearing layers. A dual antibacterial mechanism was proposed, as both direct contact of Ag nanoparticles *per se* as well as the release of Ag ions contribute to the bactericidal activity of the TiO_2 layers.

References

[1] C.S. Moucha, R.M. Urban, T.M. Turner, J.J. Jacobs, Fixation of implants, in: A. Shanbhag, H.E. Rubash, J.J. Jacobs (Eds.) Joint replacement and bone resorption, Taylor & Francis Group, New York, 2006.

[2] K.L. Ong, S.M. Kurtz, E. Lau, K.J. Bozic, D.J. Berry, J. Parvizi, Prosthetic Joint Infection Risk After Total Hip Arthroplasty in the Medicare Population, Journal of Arthroplasty, 24 (2009) 105-109.

[3] W. Zimmerli, A. Trampuz, P.E. Ochsner, Current concepts: Prosthetic-joint infections, New England Journal of Medicine, 351 (2004) 1645-1654.

[4] W. Zimmerli, Infection and musculoskeletal conditions: Prosthetic-joint-associated infections, Best Practice and Research Clinical Rheumatology, 20 (2006) 1045-1063.

[5] Y. Qiu, N. Zhang, Y.H. An, X. Wen, Biomaterial strategies to reduce implant-associated infections, International Journal of Artificial Organs, 30 (2007) 828-841.

[6] E.M. Hetrick, M.H. Schoenfisch, Reducing implant-related infections: active release strategies, Chemical Society Reviews, 35 (2006) 780-789.

[7] S.M. Kurtz, E. Lau, J. Schmier, K.L. Ong, K. Zhao, J. Parvizi, Infection Burden for Hip and Knee Arthroplasty in the United States, The Journal of Arthroplasty, 23 (2008) 984-991.

[8] B.S. Necula, I. Apachitei, F.D. Tichelaar, L.E. Fratila-Apachitei, J. Duszczyk, An electron microscopical study on the growth of TiO_2-Ag antibacterial coatings on Ti6Al7Nb biomedical alloy, Acta Biomaterialia, 7 (2011) 2751-2757.

[9] B.S. Necula, L.E. Fratila-Apachitei, S.A. Zaat, I. Apachitei, J. Duszczyk, In vitro antibacterial activity of porous TiO_2-Ag composite layers against methicillin-resistant Staphylococcus aureus, Acta Biomaterialia, 5 (2009) 3573-3580.

[10] JIS Z 2801:2000 Antimicrobial Products – Test for antimicrobial activity and efficacy.

[11] ASTM E 2149 - 01: 2001 Standard Test Method for Determining the Antimicrobial Activity of Immobilized Antimicrobial Agents Under Dynamic Contact Conditions.

[12] I. Sondi, B. Salopek-Sondi, Silver nanoparticles as antimicrobial agent: a case study on E-coli as a model for Gram-negative bacteria, Journal of Colloid and Interface Science, 275 (2004) 177-182.

[13] J.R. Morones, J.L. Elechiguerra, A. Camacho, K. Holt, J.B. Kouri, J.T. Ramirez, M.J. Yacaman, The bactericidal effect of silver nanoparticles, Nanotechnology, 16 (2005) 2346-2353.

[14] Q.L. Feng, J. Wu, G.Q. Chen, F.Z. Cui, T.N. Kim, J.O. Kim, A mechanistic study of the antibacterial effect of silver ions on Escherichia coli and Staphylococcus aureus, Journal of Biomedical Materials Research, 52 (2000) 662-668.

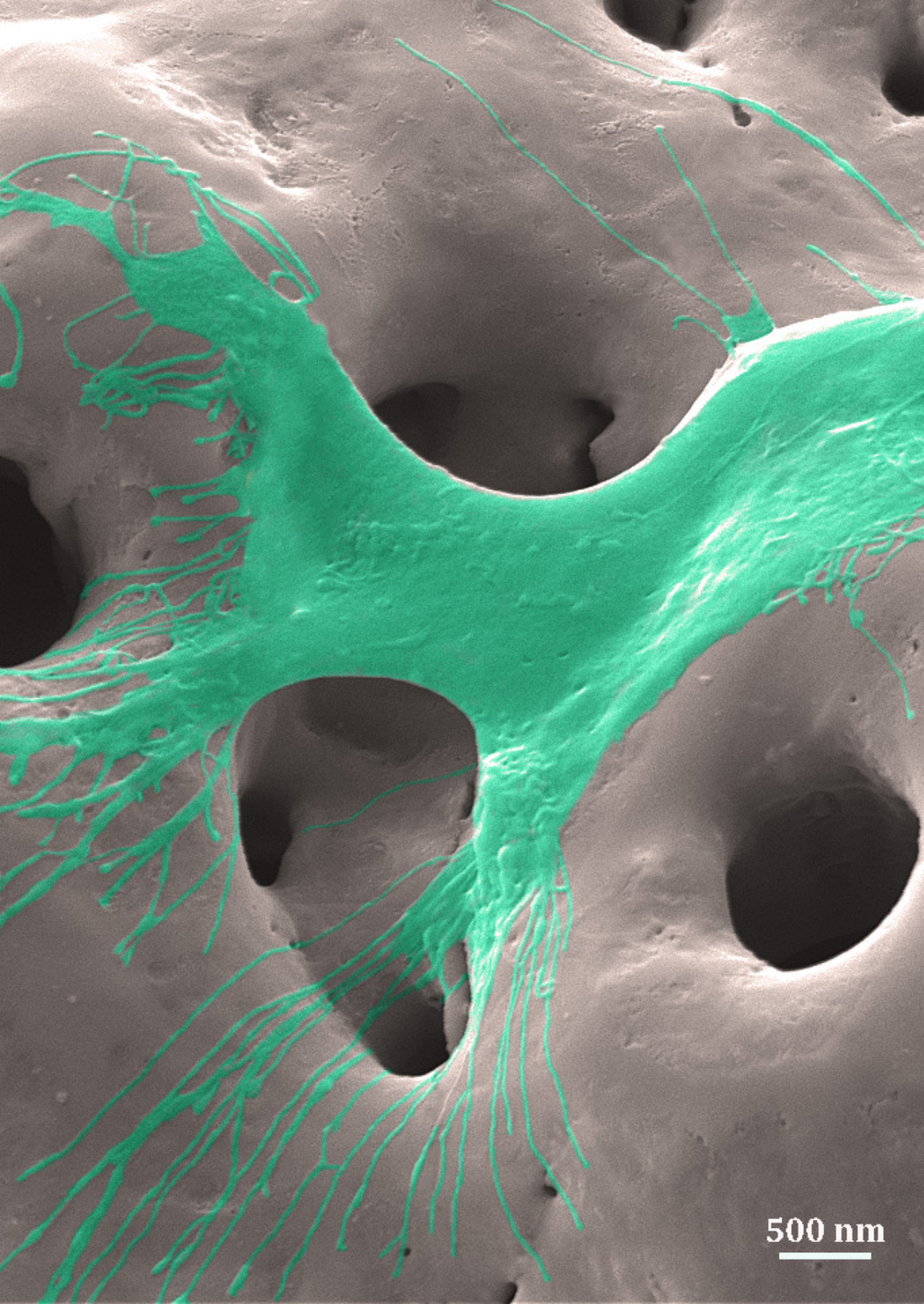
500 nm

Chapter 5

In vitro evaluation of bone cells viability*

Are Ag-bearing TiO_2 layers toxic to human bone cells?

5.1. Introduction

Biomedical devices (*e.g.,* artificial joints, dental implants and fracture fixation plates) are commonly used in total joint arthroplasties, dental implantation or bone trauma surgeries, improving the quality of life by relieving pain and restoring mobility and function [1].

Despite advanced sterilization techniques, strict surgery rules and systemic antibiotic prophylaxis, implant associated infections (IAI) remain a great risk in such surgeries [2-5]. IAI is a result of bacteria adhesion to the implant, colonization of its surface and subsequent biofilm formation at the implantation site. The biofilm has an extraordinary resistance to antibiotics and, furthermore, it can promote detachment of individual bacteria into the surrounding tissue and circulatory system, leading to further complications [6].

Once the IAI occurs, it is often impossible to heal without revision surgery, which most of the time requires the replacement of the implant. This devastating complication may lead to large skeletal defects, member amputation and even death.

*Based on:
B.S. Necula, L.E. Fratila-Apachitei, J.P.T.M. van Leeuwen, S.A.J. Zaat, I. Apachitei, J. Duszczyk, *In vitro* cytotoxicity evaluation of porous TiO_2-Ag antibacterial coatings on human fetal osteoblasts, Acta Biomaterialia, 8 (2012) 4191–4197.

Besides patient trauma, the treatment of such infections incurs huge costs for the healthcare system [2, 7, 8].

Preventing bacterial adhesion on the biomedical devices or providing bactericidal activity to the biomedical device itself can be essential strategies to prevent IAI [9]. Therefore, research on surface modification of biomedical alloys to apply/form coatings/layers that kill any adherent and/or surrounding bacteria has garnered significant interest [10]. The unique advantage of these coatings is the ability to provide locally, at the site of implantation, a controlled concentration of the antibacterial agent that will prevent bacteria colonization. Furthermore, the local delivery of the antibacterial agents will reduce the risk of toxicity caused by conventional systemic delivery of antibiotics. Ideally, these layers should not change the structural integrity of the device and maintain the surface biocompatibility with the host tissue.

Previous studies demonstrated the potential of the plasma electrolytic oxidation (PEO) process to produce Ag-bearing porous TiO_2 coatings on Mg and Ti biomedical alloys using electrolytes bearing Ag nanoparticles [11, 12]. The coatings showed excellent *in vitro* antibacterial activity against methicillin-resistant *Staphylococcus aureus* (MRSA) (Chapter 4, [13]).

As presented in Chapter 3, the mechanism of incorporation of the Ag nanoparticles, their distribution throughout the coatings and their chemical composition in the layer were assessed using high resolution transmission electron microscopy (HRTEM) and scanning electron microscopy (SEM), combined with energy dispersive X-ray spectroscopy (EDX)[12]. However, the toxicity of Ag-bearing TiO_2 layers for osteoblast cells still remains an open question.

The simian virus 40 (SV40)-immortalized human fetal osteoblast (SV-HFO) cell line is valuable for studying bone metabolism via osteoblast differentiation [14-16]. Proliferating osteoblasts (days 2–7) differentiate to extracellular matrix producing cells (days 7–14), which will mineralize after 14–21 days. In this chapter, the human osteoblast cells were used to assess the potential toxicity of TiO_2 layers bearing various concentrations of Ag nanoparticles during the proliferation stage (days 2–7).

The aim of this *in vitro* study was to investigate and compare the effects of TiO_2 surfaces bearing different concentrations of Ag nanoparticles (*i.e.,* 0.3Ag, 0.8Ag, 1.6Ag and 3.0Ag) on the viability of SV-HFO cells in order to provide an indication of the biocompatibility of these materials specifically if used as antibacterial implants when these cells will be likely to contact the surfaces.

5.2. Experimental

5.2.1. Preparation of Ag-bearing TiO_2 layers

Ti6Al7Nb biomedical alloy disks (22 mm diameter, 8 mm height) were ground with 320, 800 and 1200# abrasive papers and then ultrasonically cleaned with acetone, ethanol and distilled water in an ultrasonic bath.

The PEO process was performed on a custom-made laboratory scale set-up consisting of an AC power supply, type ACS 1500 (ET Power Systems Ltd., UK) and a double wall glass electrolytic cell cooled by a mixture of water and glycerol using a Haake V15 thermostatic bath. The electrolytic cell was filled with the electrolyte, which comprised of 24 g/L calcium acetate (99%, Sigma–Aldrich) and 4.2 g/L calcium glycerophosphate (Dr. Paul Lohmann, Germany) solutions to which 0, 0.3, 0.6, 0.8, 1.6 and 3.0 g/L Ag nanoparticles (99.5%, Sigma–Aldrich) were added. To maintain particle homogeneity, the electrolyte was stirred at 500 r.p.m. during the PEO process. The PEO process was performed under galvanostatic conditions using a current density of 20 A/dm^2 for 5 minutes.

After the PEO process, the Ag-bearing layers were kept in running tap water for 5 minutes, ultrasonically cleaned in 70% ethanol and rinsed for 5 minutes in deionized water. All samples were sterilized for 1 hour at 110°C using a Nabertherm TR60 oven and kept in sterile conditions until the biological evaluation. All experimental procedures on coating synthesis together with the details on equipment used are presented in Chapter 2 of this thesis.

5.2.2. Evaluation of bone cells viability

5.2.2.1. SV-HFO cells culture

SV-HFO cells were precultured for 1 week in α-minimum essential medium (α MEM) (GIBCO, Paisley, UK) supplemented with 20 mM 4-(2-hydroxyethyl)piperazine-1-ethanesulfonic acid (HEPES) (Sigma–Aldrich), 2% streptomycin/penicillin, 1.8 mM $CaCl_2$ (Sigma–Aldrich) and 10% heat-inactivated fetal calf serum (HI-FCS) (GIBCO) at pH 7.5, 37 °C and 5% CO_2 in a humidified atmosphere [17]. During this preculture, the SV-HFO cells remained in an undifferentiated stage. After preculturing, the cells were washed with a phosphate buffered saline solution (PBS), detached with trypsin, counted with a hemocytometer and seeded on the samples in a density of 3.5 x 10^4 cells per disk. Osteogenic medium (αMEM supplemented with fresh β-glycerophosphate (Sigma–Aldrich) (10 mM) and dexamethasone (Sigma–Aldrich)

(100 nM)) was added, starting 2 days after seeding and replaced every 2–3 days. The coated titanium disks fit precisely in the 12-well plates, avoiding the growth of cells on the polystyrene.

5.2.2.2. Cell viability assay by Alamar Blue

Alamar Blue assay (Invitrogen) was used to assess SV-HFO cell viability on the Ag-free and Ag-bearing TiO_2 layers. At day 2, 5 and 7 of culture, Alamar Blue reagent was added to each well, in an amount equal to 10% of the well volume. The plates were incubated for further 3 hours at 37°C to allow the resazurin, a blue non-fluorescent indicator dye, to be converted to highly red fluorescent resorufin via reduction reactions of metabolically active cells. Fluorescence measurements were made on a Wallac microplate fluorometer using an excitation length of 535 nm and emission of 590 nm. The assay was performed at least in triplicate.

5.2.2.3. Cell morphology and spreading assay by SEM

The SV-HFO cell morphology and spreading was observed using scanning electron microscopy (SEM). After 2, 5 and 7 days of SV-HFO culture on the coated disks, the cells were fixed with 4% formaldehyde and 2% glutaraldehyde in 0.1 M sodium cacodylate solution for 1 hour at 4°C. The samples were then rinsed in 0.1 M sodium cacodylate solution and dehydrated in a series of graded ethanol and then 100% tetramethylsilane. All samples were gold coated and examined on a Jeol 6500F-D scanning electron microscope operated at 5 - 10 keV.

5.2.2.4. Fluorescence microscopy of actin cytoskeletal organization and nucleus

After culturing for 48 hours, the cells seeded on the titanium disks were washed with PBS and fixed for 15 minutes at room temperature using 4% paraformaldehyde in PBS. After three rinses with PBS the cells were permeabilized with PBS/Triton X-100 for 10 minutes and stained with rhodamine-phalloidin (Invitrogen) (1:100 in PBS) for 20 minutes at room temperature and in the dark. The disks were further rinsed 3 times with PBS and stained with a 4',6-diamidino-2-phenylindole (DAPI) solution (Invitrogen) (1:50000 in PBS) for 5 minutes. The actin cytoskeleton and cell nuclei were examined using an epifluorescence microscope (Nikon Eclipse LV 100D-U, Japan).

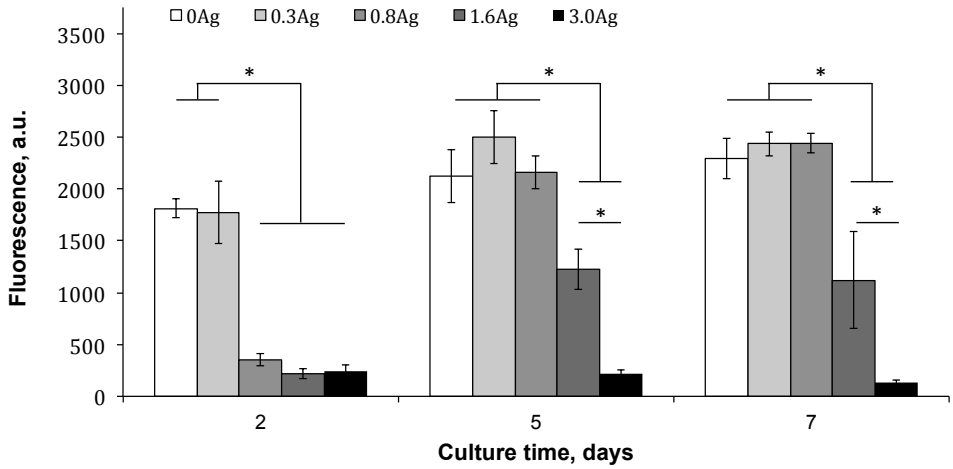

Fig. 5.1. Simian virus 40 (SV40)-immortalized human fetal osteoblasts viability on TiO_2 surfaces bearing different concentrations of Ag nanoparticles.

5.2.2.5. Statistical analyses

Statistical analyses were performed using the one-way Anova test and Tukey–Kramer method to make multiple unplanned comparisons of means based on unequal sample sizes. In the Tukey–Kramer method, the minimum significant difference (MSD) was calculated for each pair of means. If the observed absolute difference between a pair of means was greater than the MSD, the pair of means was declared significantly different.

5.3. Results

The viability of SV-HFO cells cultured on the Ag-free and Ag-bearing surfaces was determined by using the Alamar Blue assay and the results are shown in Fig. 5.1. There was no significant difference in fluorescence signal between 0Ag and 0.3Ag showing no cytotoxic effect for the 0.3Ag surfaces after 2 days of culture. However, the surfaces created using 0.8 g/L, 1.6 g/L and 3.0 g/L Ag nanoparticles in the electrolyte appear to be toxic to SV-HFO cells, after two days of culture, as revealed by Alamar Blue assay. After culturing for 5 and 7 days, the cells on the 0.3Ag and 0.8Ag surfaces showed similar viability with those on 0Ag, indicating that the presence of Ag had no adverse effect on osteoblast viability. Still, the 1.6Ag and 3.0Ag specimens appeared to be toxic for the SV-HFO cells showing low viability after 5 and 7 days in culture.

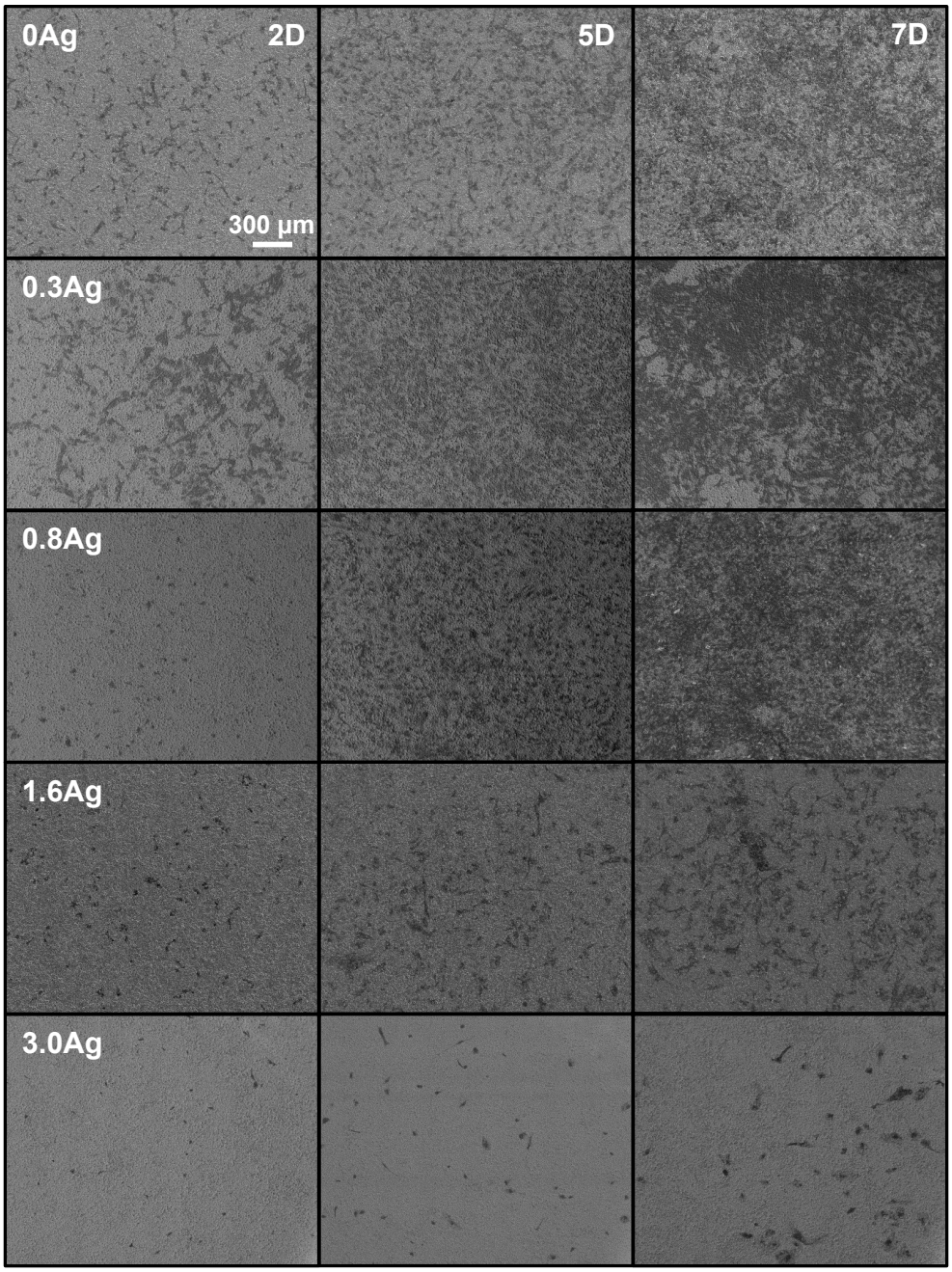

Fig. 5.2. SEM observation of the SV-HFO cells cultured on the Ag-bearing coatings for 2, 5 and 7 days.

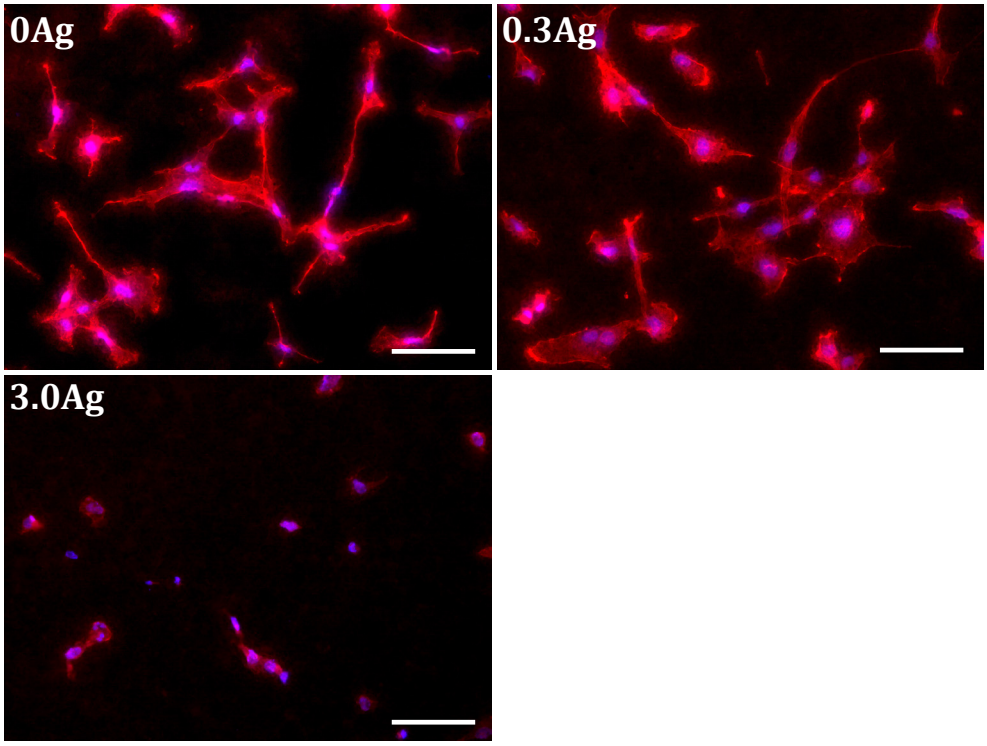

Fig. 5.3. Fluorescence microscopy images of actin-stained (phalloidin) (red) and nuclei-stained (DAPI) (blue) human fetal osteoblasts cultured for 48 hours on Ag-free and Ag-bearing coatings. Scale bar - 100 μm.

These observations were further confirmed by the SEM images of the SV-HFO cells cultured on the Ag-free and Ag-bearing TiO_2 surfaces for 2, 5 and 7 days (Fig. 5.2).

Epifluorescence microscopy of the SV-HFO cells (Fig. 5.3) revealed a well-defined actin cytoskeletal organization and numerous stress fibers throughout the cells for the 0Ag and 0.3Ag surfaces. The cells on 0Ag and 0.3Ag exhibited a stellate polygonal morphology with multidirectional spreading while on the 3Ag the cells were round and lower in number, indicating apoptosis.

5.4. Discussion

In this work, Ag-bearing TiO_2 coatings with different Ag nanoparticles contents were produced by PEO process using the calcium acetate/calcium glycerophosphate

electrolyte bearing 0, 0.3, 0.8, 1.6 and 3.0 g/L Ag nanoparticles. Incorporation of various concentrations of Ag nanoparticles in the TiO_2 matrix, apparently, did not change the morphology of the coatings. All layers produced were porous, with well-defined pores ranging from a few nanometers up to 5 μm in size (Chapters 2 and 3). Moreover, the coatings showed the same thickness and elemental composition, regardless of the Ag nanoparticles content. Therefore, the effect of Ag nanoparticles, embedded in the TiO_2 coatings in various concentrations, on the viability of the SV-HFO cells could be evaluated without the interference of the other factors.

Many studies have been performed to evaluate the toxicity of Ag nanoparticles using different cell lines, yet little is known about the mechanisms of Ag nanoparticles toxicity [18]. Most of the studies [19-21] concluded that, under specific concentration levels, Ag nanoparticles are not cytotoxic. Kawata *et al.* [19] found that under a concentration of 0.5 μg/mL Ag nanoparticles suspended in the culture medium, the proliferation of HepG2 Human Hepatoma cells was accelerated while higher doses (1 μg/mL) induced abnormal cellular morphology and cellular shrinkage. Kim *et al.* [21] studied the oxidative stress-dependent toxicity of Ag in human hepatoma cells and reported good cell viability at dose levels smaller than 0.7 μg/mL Ag nanoparticles in the medium. Cao *et al.* [22] reported the amount of Ag ions released from titanium samples embedded with Ag nanoparticles to be less than 0.01 μg/mL after 60 days, promoting proliferation of the osteoblast-like cell line MG63. However, there is no indication of the total content of Ag nanoparticles incorporated that may be in contact with the MG63 cells. Also, Hsu *et al.* [23] showed enhanced fibroblast attachment on the polyurethane - Ag nanocomposites bearing 30 ppm Ag nanoparticles and reported a release of 0.00035 μg/mL of both ionic and nanoparticlulate Ag.

Summarizing, the experimental conditions differ and there is a clear distinction between testing the Ag nanoparticles suspended in the culture media and Ag nanoparticles incorporated/attached (in)to a solid substrate. When suspended in the culture media, depending on the dispersion stability, the Ag nanoparticles might settle on the surface of the cells. Thus, Ag nanoparticles toxicity might be due to the direct contact after settlement, or Ag nanoparticles entering the cell membrane by different uptake routes (*i.e.,* endocytosis or diffusion) causing cytoskeleton damage, oxidation of DNA, mitochondrial dysfunction and chromosomal aberrations leading to cell apoptosis [24]. However, there is no control on the concentration of Ag nanoparticles in contact with the cells and it is difficult to estimate the toxic concentration levels.

When incorporated and fixed into a substrate, the mechanism of Ag nanoparticles toxicity might be due to direct contact with the seeded cells disrupting normal cell behavior. However, Ag nanoparticles have a high surface area per unit mass and

always release a continuous level of ionic silver into their environment. Furthermore, according to a study of Liu *et al.* [25] Ag nanoparticles surfaces can adsorb Ag ions. It is generally agreed that both ionic Ag (free or adsorbed), as well as the Ag nanoparticle itself, may contribute to the cytotoxic effects of Ag nanoparticles [19, 20]. However, Navarro *et al.* [26] suggested that Ag nanoparticles contribute to toxicity only by serving as sources of Ag ions and alone are not a direct source of toxicity. On the other hand, Kim *et al.* [21] proposed that Ag nanoparticles cytotoxicity is primarily the result of oxidative stress and is independent of the toxicity of Ag ions.

In the present work, various concentrations of Ag nanoparticles are fused in the TiO_2 matrix and SV-HFO cells are seeded on top of the surfaces. Thus, both direct contact of the Ag-bearing surfaces with the cells as well as the release of Ag ions in the osteogenic medium may contribute to the toxicity of these surfaces.

In the Chapter 4 of this thesis, it has been showed that the cumulative concentrations of Ag ions released from the 0.3Ag surfaces, immersed in deionized water for 2, 5 and 7 days were 0.0077, 0.0096 and 0.012 μg/mL, respectively. Correspondingly, for the 3.0Ag surface the concentrations were 0.05, 0.063 and 0.09 μg/mL. For both 0.3Ag and 3.0Ag samples the released Ag ions concentrations were below the cytotoxic level reported in the literature and presented above.

The viability of SV-HFO cells on the Ag-bearing surfaces was strongly dependent on the concentration of Ag nanoparticles present in the layers. The SV-HFO viability on the 0.3Ag surfaces, assessed by Alamar Blue, SEM and fluorescence microscopy, is not inhibited after 2, 5 and 7 days of culture. However, the 3.0Ag surfaces appear to be very toxic to SV-HFO cells starting with day 2 of culture, despite the low Ag ions concentrations released into the culture medium.

One hypothesis might be that the toxicity of 3.0Ag surfaces is due to the Ag nanoparticles *per se* present in the TiO_2 matrix in a higher concentration as compared with the 0.3Ag surfaces rather due to the release of Ag ions in the osteogenic medium. The testing of the TiO_2 surfaces bearing intermediary concentrations of Ag nanoparticles appears to confirm the hypothesis. A significantly lower number of SV-HFO cells survived on the 0.8Ag and 1.6Ag samples after 2 days of culture. However, the surviving cells on the 0.8Ag showed a rapid proliferation rate reaching the same viability numbers with the 0Ag and 0.3Ag surfaces for day 5 and 7 while the cells on 1.6Ag reached only 50% viability within the same time interval.

5.5. Conclusions

TiO_2 layers with various contents of Ag nanoparticles were successfully formed by PEO on the Ti6Al7Nb medical alloy, in electrolytes bearing different concentrations of Ag nanoparticles (*i.e.,* 0.3Ag, 0.8Ag, 1.6Ag and 3.0Ag).

The viability of SV-HFO cells, studied by AlamarBlue, SEM and fluorescence microscopy, was observed to depend on the concentration of Ag nanoparticles present in the TiO_2 layers. The Ag-free coatings and 0.3Ag coatings showed not to be toxic to SV-HFO cells after 2, 5 and 7 days of culture. On the other hand, the 1.6Ag and 3.0Ag surfaces were found to be toxic to SV-HFO cells, because of the higher concentration of Ag nanoparticles in the TiO_2 matrix.

It is assumed that the direct contact with Ag-bearing surfaces may have strongly contributed to the cytotoxic effect of 1.6Ag and 3.0Ag surfaces rather than the Ag released in the osteogenic medium.

Under these specific experimental conditions, from all the investigated Ag-bearing TiO_2 layers, the 0.3Ag sample was found to be the most promising antibacterial surface, because of its high antibacterial effect and no toxicity to human bone cells.

References

[1] B.D. Ratner, A.S. Hoffman, F.J. Schoen, J.E. Lemons, Biomaterials Science - An Introduction to Materials in Medicine, Third Edition, Elsevier Inc., Amsterdam, 2013.

[2] W. Zimmerli, Infection and musculoskeletal conditions: Prosthetic-joint-associated infections, Best Practice & Research Clinical Rheumatology, 20 (2006) 1045-1063.

[3] G. Walenkamp, Joint prosthetic infections: a success story or a continuous concern?, Acta Orthopaedica, 80 (2009) 629-632.

[4] I.G. Sia, E.F. Berbari, A.W. Karchmer, Prosthetic joint infections, Infectious Disease Clinics of North America, 19 (2005) 885-91.

[5] K.L. Ong, S.M. Kurtz, E. Lau, K.J. Bozic, D.J. Berry, J. Parvizi, Prosthetic Joint Infection Risk After Total Hip Arthroplasty in the Medicare Population, Journal of Arthroplasty, 24 (2009) 105-109.

[6] D. Davies, Understanding biofilm resistance to antibacterial agents, Nature reviews. Drug discovery, 2 (2003) 114-122.

[7] S. Esposito, S. Leone, Prosthetic joint infections: microbiology, diagnosis, management and prevention, International Journal of Antimicrobial Agents, 32 (2008) 287-293.

[8] L. Lidgren, K. Knutson, A. Stefánsdóttir, Infection of prosthetic joints, Best Practice & Research Clinical Rheumatology, 17 (2003) 209-218.

[9] I. Francolini, G. Donelli, Prevention and control of biofilm-based medical-device-related infections, FEMS Immunology & Medical Microbiology, 59 (2010) 227-238.

[10] A. Simchi, E. Tamjid, F. Pishbin, A.R. Boccaccini, Recent progress in inorganic and composite coatings with bactericidal capability for orthopaedic applications, Nanomedicine, 7 (2011) 22-39.

[11] B.S. Necula, L.E. Fratila-Apachitei, A. Berkani, I. Apachitei, J. Duszczyk, Enrichment of anodic MgO layers with Ag nanoparticles for biomedical applications, Journal of Materials Science-Materials in Medicine, 20 (2009) 339-345.

[12] B.S. Necula, I. Apachitei, F.D. Tichelaar, L.E. Fratila-Apachitei, J. Duszczyk, An electron microscopical study on the growth of TiO_2-Ag antibacterial coatings on Ti6Al7Nb biomedical alloy, Acta Biomaterialia, 7 (2011) 2751-2757.

[13] B.S. Necula, L.E. Fratila-Apachitei, S.A. Zaat, I. Apachitei, J. Duszczyk, In vitro antibacterial activity of porous TiO_2-Ag composite layers against methicillin-resistant Staphylococcus aureus, Acta Biomaterialia, 5 (2009) 3573-3580.

[14] D. Seriwatanachai, N. Krishnamra, J. van Leeuwen, Evidence for Direct Effects of Prolactin on Human Osteoblasts: Inhibition-of Cell Growth and Mineralization, Journal of Cellular Biochemistry, 107 (2009) 677-685.

[15] M. van Driel, M. Koedam, C.J. Buurman, M. Roelse, F. Weyts, H. Chiba, A.G. Uitterlinden, H.A.P. Pols, J. van Leeuwen, Evidence that both 1 alpha,25-dihydroxyvitamin D-3 and 24-hydroxylated D-3 enhance human osteoblast differentiation and mineralization, Journal of Cellular Biochemistry, 99 (2006) 922-935.

[16] H. Chiba, N. Sawada, T. Ono, S. Ishii, M. Mori, Establishment and characterization of a Simian-Virus 40-Immortalized osteoblastic cell line from normal human bone, Japanese Journal of Cancer Research, 84 (1993) 290-297.

[17] M. Eijken, S. Swagemakers, M. Koedam, C. Steenbergen, P. Derkx, A.G. Uitterlinden, P.J. van der Spek, J.A. Visser, F.H. de Jong, H.A. Pols, J.P. van Leeuwen, The activin A-follistatin system: potent regulator of human extracellular matrix mineralization, The Journal of the Federation of American Societies for Experimental Biology, 21 (2007) 2949-2960.

[18] H. Cao, X. Liu, Silver nanoparticles-modified films versus biomedical device-associated infections, Wiley Interdisciplinary Reviews: Nanomedicine and Nanobiotechnology, 2 (2010) 670-684.

[19] K. Kawata, M. Osawa, S. Okabe, In Vitro Toxicity of Silver Nanoparticles at Noncytotoxic Doses to HepG2 Human Hepatoma Cells, Environmental Science & Technology, 43 (2009) 6046-6051.

[20] P.V. AshaRani, G. Low Kah Mun, M.P. Hande, S. Valiyaveettil, Cytotoxicity and genotoxicity of silver nanoparticles in human cells, ACS Nano, 3 (2009) 279-290.

[21] S. Kim, J.E. Choi, J. Choi, K.H. Chung, K. Park, J. Yi, D.Y. Ryu, Oxidative stress-dependent toxicity of silver nanoparticles in human hepatoma cells, Toxicology In Vitro, 23 (2009) 1076-1084.

[22] H.L. Cao, X.Y. Liu, F.H. Meng, P.K. Chu, Biological actions of silver nanoparticles embedded in titanium controlled by micro-galvanic effects, Biomaterials, 32 (2011) 693-705.

[23] S.H. Hsu, H.J. Tseng, Y.C. Lin, The biocompatibility and antibacterial properties of waterborne polyurethane-silver nanocomposites, Biomaterials, 31 (2010) 6796-6808.

[24] P.V. Asharani, M.P. Hande, S. Valiyaveettil, Anti-proliferative activity of silver nanoparticles, BMC Cell Biology, 10 (2009) 65.

[25] J.Y. Liu, R.H. Hurt, Ion Release Kinetics and Particle Persistence in Aqueous Nano-Silver Colloids, Environmental Science & Technology, 44 (2010) 2169-2175.

[26] E. Navarro, F. Piccapietra, B. Wagner, F. Marconi, R. Kaegi, N. Odzak, L. Sigg, R. Behra, Toxicity of Silver Nanoparticles to Chlamydomonas reinhardtii, Environmental Science & Technology, 42 (2008) 8959-8964.

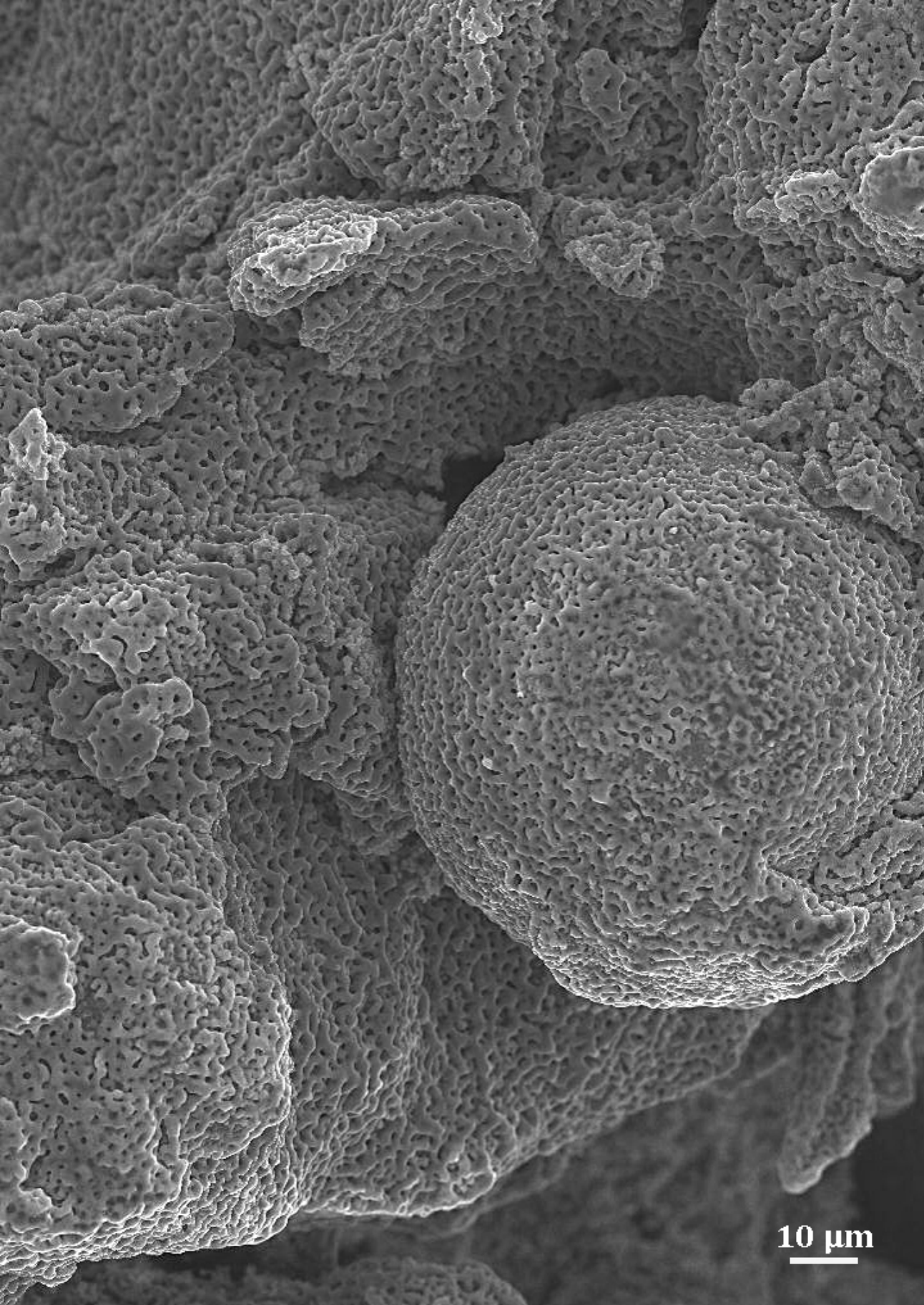
10 µm

Chapter 6

Ag-based antibacterial TiO_2 layers on commercially available bone implants*

Can Ag-bearing TiO_2 layers be applied on commercially available bone implants?

6.1. Introduction

Titanium and its alloys are widely used as biomaterials for bone implants in orthopaedic and dental applications due to their high biocompatibility, low Young modulus, high specific strength, good corrosion resistance and machinability [1, 2].

The clinical long-term success of the cementless titanium implants depends on the ability to establish secure osseointegration of the implant *i.e.,* the direct bone-implant contact without a fibrous connective tissue interface. Despite all long-term successes, bone implants may be accompanied by serious complications such as (i) aseptic loosening caused by particle disease or micromotion of the prosthesis due to insufficient initial fixation and (ii) septic loosening due to implant associated infections (IAI) [3-5].

*Based on:
B.S. Necula, I. Apachitei, L.E. Fratila-Apachitei, E.J. van Langelaan, J. Duszczyk, Titanium bone implants with superimposed micro/nano-scale porosity and antibacterial capability, Applied Surface Science, 273 (2013) 310–314.

To overcome these problems, intense research efforts are directed towards surface modification of titanium implants (topography and chemistry). Thus, implant surfaces that stimulate osteogenesis, bone in-growth and prevent bacterial infections are expected to have beneficial effects on long-term success of the implant.

In terms of topography for tissue in-growth, rough and macro-porous (100 - 400 μm) surfaces proved to be effective whereas for osteogenesis, micro/nano pores are considered potential stimuli for osteogenic differentiation of stem cells and new bone formation [2, 6-10]. Because both bone in-growth and osteoinduction are beneficial for osseointegration, porous architectures combining macro with micro and nano features would be the most attractive. In addition, the superimposed micro/nano surface porosity can act as a reservoir for specific bioactives (*e.g.,* growth factors, antimicrobial agents, etc.) thus adding a drug-delivery function to the medical device itself. Currently, dental and orthopaedic implant systems use plasma spraying as a surface modification technique to provide rough and macro-porous surfaces for bone anchoring [2, 11].

In terms of surface chemistry, hydroxyapatite and β-tricalcium phosphate layers are plasma sprayed (PS) on the titanium implants due to their ability to provide osteoconductive surfaces for enhanced bone growth [12]. However, these coatings are very brittle and may impair the mechanical properties of titanium implants like fatigue strength [13].

One approach to minimize the problem of IAI is to render the surface of implant antibacterial. Thus, using various surface modification techniques, a titanium surface can be made bactericidal by means of releasing an antibacterial agent directly at the site of implantation [14-22]. Among antibacterial agents, Ag is a suitable choice because (i) bacteria do not develop resistance to Ag, as in the case of antibiotics and (ii) it is known to kill a wide range of bacteria strains including multi-drug resistant microorganisms, such as methicillin-resistant *Staphylococcus aureus* (MRSA) [15, 23-25].

As described in Chapters 2 and 3, plasma electrolytic oxidation (PEO) process proved to have the capability to create interconnected TiO_2 micro and nano porous structures on titanium surfaces [26], which can be attractive features for cell attachment and growth [27, 28] as well as reservoirs for the antibacterial agents [14, 15, 29].

The aim of this chapter was to investigate the possibility of PEO process to grow TiO_2 layers on rough and macro-porous PS titanium coatings and subsequent incorporation of Ag nanoparticles to render the surface antibacterial. This is the first study that explores the ability of the PEO process to grow multifunctional layers on

plasma-sprayed titanium implants. Such surfaces may be of a great interest to enhance the biological performance of titanium orthopaedic and dental implants like hip prostheses and tooth roots.

6.2. Experimental

6.2.1. Plasma-sprayed samples preparation and characterization

A 60 mm diameter PS acetabular cup (Biomet, NL) was cut in small pieces (approx. 1 x 1 x 0.4 cm^3) using a Struers cutting machine. To avoid damaging of the coating structure and morphology, the cutting was performed at low speed. After cutting, the samples were cleaned in acetone, ethanol and deionized water using an ultrasonic bath. The PS samples were attached to a copper wire and the connection was insulated with a water and temperature resistant lacquer.

Before the PEO layer synthesis, the PS samples were characterized with respect to surface morphology using a Jeol 6500F-D scanning electron microscope (SEM) operated at an electron beam energy of 15 kV. Coupled with the energy dispersive X-ray spectroscopy (EDX) technique, SEM was used to determine the elemental composition of the PS samples.

6.2.2. TiO_2 layer synthesis on plasma-sprayed samples

The PEO process was performed on a custom made laboratory scale set-up consisting of an AC power supply, type ACS 1500 (ET Power Systems Ltd., UK), and a double wall glass electrolytic cell cooled by a mixture of water and glycerol using a Haake V15 thermostatic bath. The electrolytic cell was filled with an electrolyte comprised of 24 g/L calcium acetate (≥ 99%, Sigma-Aldrich) and 4.2 g/L calcium glycerophosphate (Dr. Paul Lohmann, Germany) with and without 0.3 g/L Ag nanoparticles. The PEO layers synthesis was performed under galvanostatic conditions using a current of 3.5 A for 120 s. The temperature of the electrolyte solution was maintained at 10°C. Fig. 6.1 depicts the cross-sectional view of the cathode/electrolyte/anode interfaces and emphasizes the main reactions taking place during PEO process. Overall, two different PEO surfaces were formed on PS samples *i.e.,* with embedded Ag nanoparticles and particles-free, respectively. After the PEO process the oxidized samples were rinsed for 5 min under running tap water followed by ultra-sonication in 70% ethanol and deionized water.

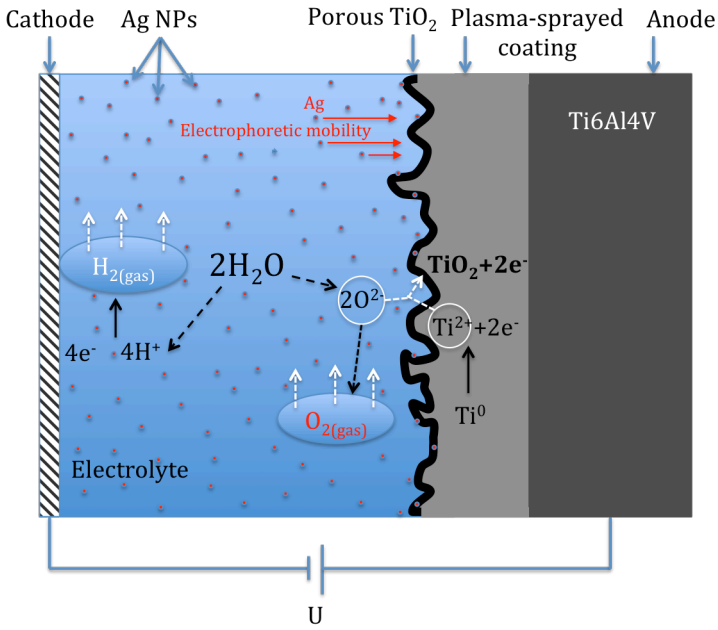

Fig. 6.1. Cross-sectional view of the cathode/electrolyte/anode interface during PEO of a PS sample in electrolytes bearing Ag nanoparticles.

6.2.3. Characterization of Ag-based TiO_2 layers superimposed on plasma-sprayed samples

The morphological characteristics of the PEO treated PS samples, with or without Ag nanoparticles, were examined through SEM analysis. Prior to SEM imaging, the samples were coated with a 12 nm layer of carbon using an Agar automatic sputter coater. For each condition (*i.e.,* no PEO treatment, PEO treatment in the absence of Ag nanoparticles and PEO treatment in the presence of Ag nanoparticles) a number of 4 different samples were used (n=4).

The chemical composition of the PS samples, before and after the PEO treatment, was determined using the SEM equipped with an EDX detector.

Identification of the Ag nanoparticles on the PEO layers was achieved by studying the high-resolution micrographs obtained using a SEM coupled with a back-scattering detector.

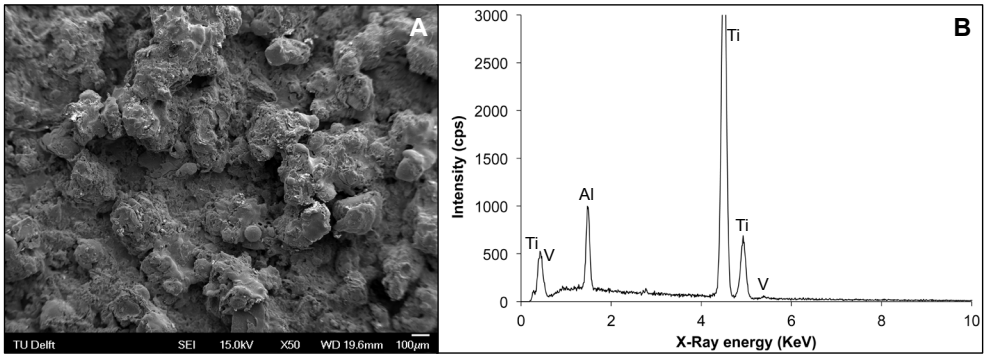

Fig. 6.2. SEM micrograph displaying the surface morphology of a PS sample (A) and the EDX pattern showing the presence of Ti, Al and V elements (B).

6.3. Results

6.3.1. Surface morphology and chemical composition of plasma-sprayed specimens

Prior to the PEO layer synthesis, the PS samples were characterized with respect to surface morphology and chemical composition. Fig. 6.2A illustrates a typical SEM micrograph of the PS sample and the corresponding EDX pattern showing the elemental composition (Fig. 6.2B).

The SEM morphology of the PS samples shows a rough and porous coating surface with fully and partially melted metallic particles. The chemical composition of the surface layer revealed the alloy composition of Ti6Al4V powder *i.e.,* 6 wt.% Al, 4 wt.% V, with the rest being Ti.

6.3.2. Surface morphology and chemical composition of Ag-based TiO_2 layers superimposed on plasma-sprayed samples

The SEM micrographs of different sections of the porous layer produced by PEO technique on the PS coating are shown in Fig. 6.3, in contrast with the PEO untreated samples. At low SEM magnification it appears that the PEO treatment did not alter the macroscopic structure of the PS coating (Fig. 6.3A1 *vs.* Fig. 6.3B1). However, at a high SEM resolution (Fig. 6.3B2 and Fig. 6.3B3), it can be seen that a fine network of interconnected, round or elongated pores, with sizes ranging from 0.07 up to 5 µm, is

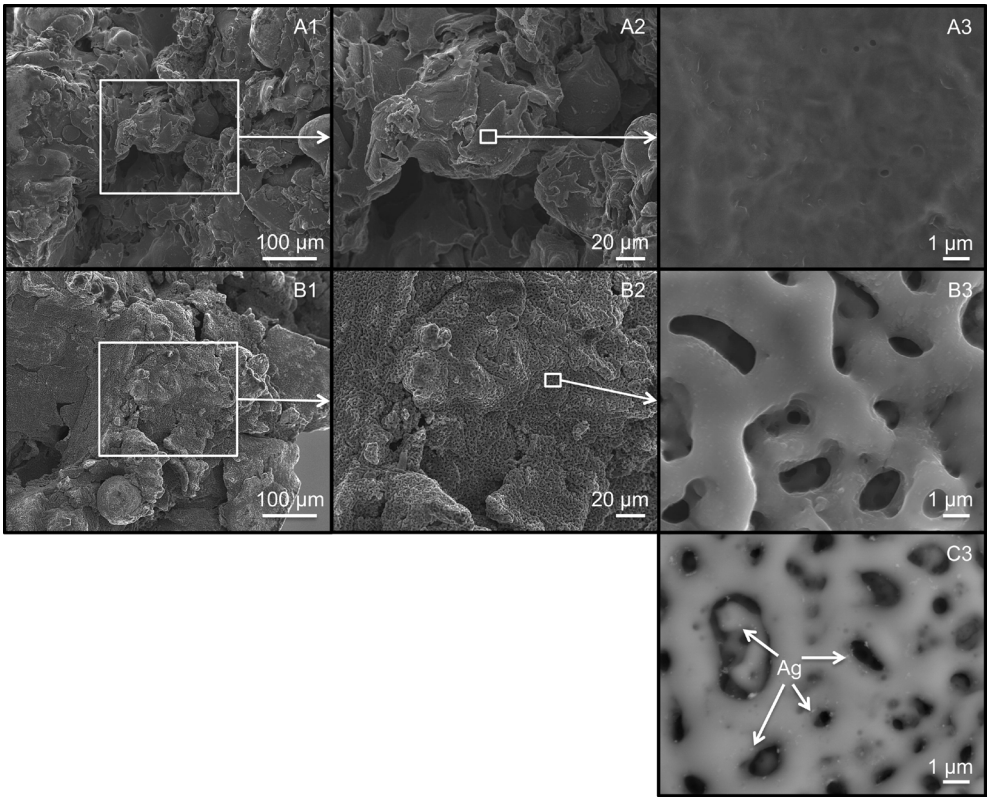

Fig. 6.3. Surface morphology of PEO untreated PS samples at different magnifications (A1, A2, A3), PEO porosity superimposed on PS samples (B1, B2, B3) and Ag nanoparticles incorporated in PEO layer superimposed on PS samples (C3).

superimposed on the structure of the PS sample. When the PEO process was performed in the electrolyte bearing Ag nanoparticles, the resulting porous layers contain Ag particles on the surface of the TiO_2 layer, as can be seen in Fig. 6.3C3. The Ag particles seem to be present on top of the TiO_2 layer and inside the pores, that is in line with the previous studies on smooth Ti6Al7Nb surfaces (Chapter 3, [29]).

The chemical composition of the PEO layers superimposed on PS samples was analyzed by EDX. According to the recorded EDX patterns (typical pattern showed in Fig. 6.4A) calcium and phosphorus species are present in the PEO layers next to Ti, Al and V elements from the substrate. The EDX point analysis on the PEO surfaces revealed a Ca/P atomic ratio of 1.72 ± 0.13, which is slightly higher than that of bone apatite (*i.e.,* 1.67). The EDX pattern and the table with the elemental composition

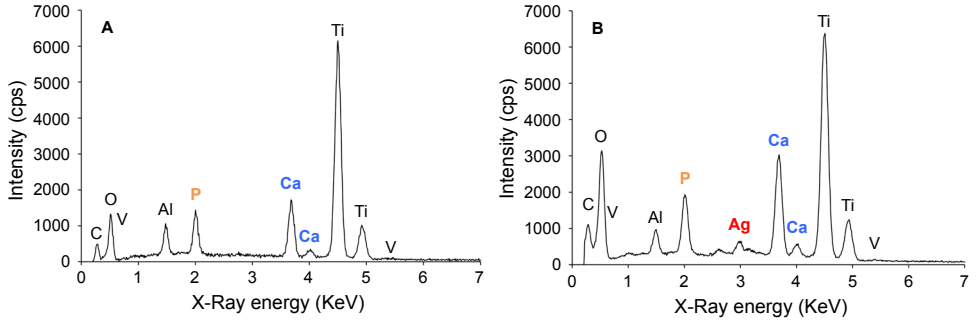

Element	C	O	Al	V	P	Ca	Ag	Ti
Atomic %	13.12	39.42	2.31	1.36	3.50	5.98	-	34.31
Atomic % error	0.44	0.66	0.06	0.20	0.07	0.15	-	0.33

Element	C	O	Al	V	P	Ca	Ag	Ti
Atomic %	11.12	46.72	1.49	1.32	3.77	8.29	0.75	26.54
Atomic % error	0.33	0.39	0.04	0.09	0.05	0.08	0.04	0.15

Fig. 6.4. Typical EDX pattern and chemical composition of the PEO treated PS samples (A) typical EDX scan on an Ag nanoparticle incorporated in PEO layer superimposed on a PS sample (B).

corresponding to a point analysis on a single Ag nanoparticle is shown in Fig. 6.4B and confirms the presence of Ag in the PEO layers.

6.4. Discussion

In order to establish secure osseointegration of bone prostheses, several factors related to implant must be further controlled and improved, *i.e.,* surface topography of the implant (micro/nano-texture) and surface chemistry to provide bioactivity and antibacterial activity. In this study, a multifunctional bone implant surface combining macro, micro, submicron and nano-scale porosity, a tailored chemical composition (Ca/P ratio close to that of bone apatite) and an antibacterial function is produced on a PS titanium surface using the PEO process.

The PEO process enables the generation of a micro and nano porous oxide layer with pore sizes ranging between 0.07 and 5 µm, on the complex geometry of the PS specimens. The top layer of the PS titanium substrate is converted to TiO_2 via electrochemical and plasma-assisted thermochemical reactions. A schematic illustration combining the electrochemical reactions taking place during the PEO process and the experimental set-up is shown in Fig. 6.1.

A closer inspection of the SEM micrographs of the PEO layer superimposed on PS samples (Fig. 6.3) indicated the formation of a fine network of micro, submicron and nano pores on the top of the macro-porous construction of the PS coatings. Surface texture, roughness and porosity, are essential factors influencing the success of the biologically fixed implants [30]. PS coatings on titanium bone implants are already known to exhibit enhanced mechanical interlocking with the bone due to their increased surface area and porous structure [2, 30]. However, the key to regulate the cell response including cell adhesion, migration, proliferation and differentiation is nano, submicron and micro-scale porosity. Thus, interactions between cells, extracellular matrix and the metallic substrate take place at the nano/micro-scale levels. Habibovic *et. al.* [31] demonstrated that the presence of micro-pores within macro-pore walls is necessary to make the biomaterial osteoinductive.

As a surface modification technique, the PEO process can be explored also to modify the surface chemistry of treated substrates. Thus, depending on the selected electrolytes the PEO process allows formation of porous layers with tailored chemical composition. In this study, the PEO process was performed in an electrolyte based on calcium acetate and calcium glycerophosphate bearing Ag nanoparticles. The resulting TiO_2 layers have chemical characteristics suitable for eliciting enhanced bioactivity due to the Ca/P ratio close to that of bone apatite (*i.e.,* 1.67) and antibacterial activity due to the incorporation of Ag nanoparticles. Being fused on the surface of the oxide layers and into the pore walls, Ag nanoparticles are expected to kill a wide range of bacteria strains including the multi-drug resistant microorganisms, locally, at the site of implantation. As described in Chapter 4, one possible bactericidal mechanism of the Ag-based antibacterial surface is the release of Ag ions that penetrate the cell wall and interact with sulfur- and phosphorous-containing molecules thus impeding the DNA replication of bacteria. Ag nanoparticles can also directly interact with the microbial cells causing degradation of the lipopolysaccharide molecules and forming ‘‘pits’’ leading to large increases in membrane permeability [15, 16].

Overall, this research shows that PEO is a suitable technique for creating surfaces with multiple functionalities on titanium medical devices. Few distinctive capabilities of the PEO process can be identified: (i) a good ability to grow uniform TiO_2 layers on rough and complex surface geometries with micro, submicron and nano-scale porosity, (ii) the ability to render the surface of the implant bioactive by changing its chemical composition and (iii) the possibility to incorporate antibacterial agents in the layers for their on-site delivery in the peri-implant area. These are essential features for the future designs of orthopaedic and dental implants that will need, for a

better clinical performance, to have an accelerated biological fixation coupled with an antibacterial function.

6.5. Conclusions

This study explored the ability of PEO process to grow TiO_2 layers on rough and macro-porous PS titanium coatings in order to further enhance their surface bioactivity and create reservoirs for antibacterial agents. The PEO process has been performed in calcium acetate and calcium glycerophosphate electrolytes with and without additions of Ag nanoparticles.

The results showed formation of a fine (0.07 - 5 μm) porous network of round and elongated pores superimposed on the macro-porous structure of the PS coating.

The porous network followed accurately the surface topography of PS coating. In addition, the surface chemistry of the PS coating has been changed by incorporation of Ca and P species and Ag nanoparticles in the TiO_2 layer. A Ca/P atomic ratio of 1.72 ± 0.13 close to that of bone apatite (1.67) has been detected.

Furthermore, the Ag nanoparticles were found to be present on top as well as in the porous structure of TiO_2 layer.

References

[1] T.P. Brunette DM, Textor M, Thomsen P, Titanium in Medicine, Springer, 2001.

[2] Y. Yang, N. Oh, Y. Liu, W. Chen, S. Oh, M. Appleford, S. Kim, K. Kim, S. Park, J. Bumgardner, W. Haggard, J. Ong, Enhancing osseointegration using surface-modified titanium implants, JOM Journal of the Minerals, Metals and Materials Society, 58 (2006) 71-76.

[3] E.B. Benz, M. Federman, J.J. Godleski, B.E. Bierbaum, T.S. Thornhill, M. Spector, Transmission electron microscopy of intracellular particles of polyethylene from joint replacement prostheses: size distribution and cellular response, Biomaterials, 22 (2001) 2835-2842.

[4] M. Jasty, C. Bragdon, W. Jiranek, H. Chandler, W. Maloney, W.H. Harris, Etiology of osteolysis around porous-coated cementless total hip arthroplasties, Clinical Orthopaedics and Related Research, (1994) 111-126.

[5] P. Aspenberg, P. Herbertsson, Periprosthetic bone resorption. Particles versus movement, Journal of Bone and Joint Surgery - British Volume, 78 (1996) 641-646.

[6] R.A. Gittens, T. McLachlan, R. Olivares-Navarrete, Y. Cai, S. Berner, R. Tannenbaum, Z. Schwartz, K.H. Sandhage, B.D. Boyan, The effects of combined micron-/submicron-scale surface roughness and nanoscale features on cell proliferation and differentiation, Biomaterials, 32 (2011) 3395-3403.

[7] E.K. Yim, K.W. Leong, Significance of synthetic nanostructures in dictating cellular response, Nanomedicine, 1 (2005) 10-21.

[8] Y.T. Sul, B.S. Kang, C. Johansson, H.S. Um, C.J. Park, T. Albrektsson, The roles of surface chemistry and topography in the strength and rate of osseointegration of titanium implants in bone, Journal of Biomedical Materials Research Part A, 89A (2009) 942-950.

[9] J. Isaac, J.C. Hornez, D. Jian, M. Descamps, P. Hardouin, D. Magne, beta-TCP microporosity decreases the viability and osteoblast differentiation of human bone marrow stromal cells, Journal of Biomedical Materials Research Part A, 86 (2008) 386-393.

[10] S. Verrier, M. Peroglio, C. Voisard, B. Lechmann, M. Alini, The osteogenic differentiation of human osteoprogenitor cells on Anodic-Plasma-Chemical treated Ti6Al7Nb, Biomaterials, 32 (2011) 672-680.

[11] G. Rizzi, A. Scrivani, M. Fini, R. Giardino, Biomedical coatings to improve the tissue-biomaterial interface, The International Journal of Artificial Organs, 27 (2004) 649-657.

[12] S.R. Paital, N.B. Dahotre, Calcium phosphate coatings for bio-implant applications: Materials, performance factors, and methodologies, Materials Science & Engineering R-Reports, 66 (2009) 1-70.

[13] Y. Yang, J.L. Ong, K. Bessho, Plasma-sprayed hydroxyapatite-coated and plasma-sprayed titanium-coated implants, in: M.J. Yaszemski, D.J. Trantolo, K.U. Lewandrowski, V. Hasirci, D.E. Altobelli, D.L. Wise (Eds.) Biomaterials in Orthopedics, Marcel Dekker Inc., New York, 2004, pp. 401-423.

[14] B.S. Necula, L.E. Fratila-Apachitei, A. Berkani, I. Apachitei, J. Duszczyk, Enrichment of anodic MgO layers with Ag nanoparticles for biomedical applications, Journal of Materials Science-Materials in Medicine, 20 (2009) 339-345.

[15] B.S. Necula, L.E. Fratila-Apachitei, S.A. Zaat, I. Apachitei, J. Duszczyk, *In vitro* antibacterial activity of porous TiO_2-Ag composite layers against methicillin-resistant Staphylococcus aureus, Acta Biomaterialia, 5 (2009) 3573-3580.

[16] B.S. Necula, J.P. van Leeuwen, L.E. Fratila-Apachitei, S.A. Zaat, I. Apachitei, J. Duszczyk, *In vitro* cytotoxicity evaluation of porous TiO_2-Ag antibacterial coatings for human fetal osteoblasts, Acta Biomaterialia, (2012).

[17] M. Teller, U. Gopp, H.G. Neumann, K.D. Kuhn, Release of gentamicin from bone regenerative materials: an *in vitro* study, Journal of Biomedical Materials Research Part B: Applied Biomaterials, 81 (2007) 23-29.

[18] S. Radin, P. Ducheyne, Controlled release of vancomycin from thin sol-gel films on titanium alloy fracture plate material, Biomaterials, 28 (2007) 1721-1729.

[19] H.L. Cao, X.Y. Liu, F.H. Meng, P.K. Chu, Biological actions of silver nanoparticles embedded in titanium controlled by micro-galvanic effects, Biomaterials, 32 (2011) 693-705.

[20] B.J. Nablo, A.R. Rothrock, M.H. Schoenfisch, Nitric oxide-releasing sol-gels as antibacterial coatings for orthopedic implants, Biomaterials, 26 (2005) 917-924.

[21] A. Simchi, E. Tamjid, F. Pishbin, A.R. Boccaccini, Recent progress in inorganic and composite coatings with bactericidal capability for orthopaedic applications, Nanomedicine, 7 (2011) 22-39.

[22] H. Hu, W. Zhang, Y. Qiao, X. Jiang, X. Liu, C. Ding, Antibacterial activity and increased bone marrow stem cell functions of Zn-incorporated TiO_2 coatings on titanium, Acta Biomaterialia, 8 (2012) 904-915.

[23] M. Rai, A. Yadav, A. Gade, Silver nanoparticles as a new generation of antimicrobials, Biotechnology Advances, 27 (2009) 76-83.

[24] H.H. Lara, E.N. Garza-Trevino, L. Ixtepan-Turrent, D.K. Singh, Silver nanoparticles are broad-spectrum bactericidal and virucidal compounds, Journal of Nanobiotechnology, 9 (2011).

[25] J.R. Morones, J.L. Elechiguerra, A. Camacho, K. Holt, J.B. Kouri, J.T. Ramirez, M.J. Yacaman, The bactericidal effect of silver nanoparticles, Nanotechnology, 16 (2005) 2346-2353.

[26] Q. Dong, C.Z. Chen, D.G. Wang, Q.M. Ji, Research status about surface modification of biomedical Ti and its alloys by micro-arc oxidation, Surface Review and Letters, 13 (2006) 35-43.

[27] P. Whiteside, E. Matykina, J.E. Gough, P. Skeldon, G.E. Thompson, *In vitro* evaluation of cell proliferation and collagen synthesis on titanium following plasma electrolytic oxidation, Journal of Biomedical Materials Research Part A, 94 (2010) 38-46.

[28] J.Z. Chen, H.Y. Peng, X.L. Zhang, Effects of the micro-arc oxidized film on pure titanium surface on attachment and growth of BMSCs, Shanghai Kou Qiang Yi Xue, 18 (2009) 81-85.

[29] B.S. Necula, I. Apachitei, F.D. Tichelaar, L.E. Fratila-Apachitei, J. Duszczyk, An electron microscopical study on the growth of TiO_2-Ag antibacterial coatings on Ti6Al7Nb biomedical alloy, Acta Biomaterialia, 7 (2011) 2751-2757.

[30] X. Liu, P. Chu, C. Ding, Surface modification of titanium, titanium alloys, and related materials for biomedical applications, Materials Science and Engineering: R: Reports, 47 (2004) 49-121.

[31] P. Habibovic, H. Yuan, C.M. van der Valk, G. Meijer, C.A. van Blitterswijk, K. de Groot, 3D microenvironment as essential element for osteoinduction by biomaterials, Biomaterials, 26 (2005) 3565-3575.

Summary

Total hip arthroplasty (THA) is the most effective and safest method for treating severe degenerative, post-traumatic and other diseases of the joints. With an aging population that is increasingly active, the use of biomedical implants will continue to rise. It is estimated that more than 1,000,000 THAs are performed each year globally. Consequently, the threat posed by implant associated infections (IAI) will affect a large percentage of this populace. IAI are serious complications, caused by infectious bacteria that colonize the implant surface, rapidly proliferate and secrete a matrix of polysaccharides known as a biofilm. Once formed, the biofilm is extremely resistant to host-defense mechanisms or antibiotics, and ultimately will lead to implant loosening and revision surgery with devastating effects on the patient. Currently, no solutions are clinically available to prevent IAI on cementless implants. Therefore, intense research efforts are focused on development of antibacterial surfaces that will kill any adherent bacteria and thus, prevent the bacteria from generating a biofilm.

The aim of this PhD thesis was to develop a novel antibacterial surface for cementless implants. The research was focused on the synthesis, physicochemical characterization and biological evaluation of an Ag-based antibacterial surface on the Ti6Al7Nb biomedical alloy. Using the plasma electrolytic oxidation (PEO) process, various concentrations of Ag nanoparticles were incorporated into a microporous TiO_2 layer grown on the Ti6Al7Nb alloy to render its surface antibacterial. Following synthesis, thorough characterization of the novel oxide layers with regard to Ag nanoparticles distribution, chemical and phase composition, surface roughness, coating porosity, pore density, pore size distribution, and surface free energy was performed. Furthermore, their antibacterial effectiveness and toxicity to human bone cells were assessed *in vitro*. Finally, a feasibility study assessing whether Ag-based antibacterial surfaces can be applied on commercially available bone implants such as plasma sprayed titanium hip components was also performed.

The thesis comprises six chapters starting with an introduction in *Chapter 1* that provides the background, as well as the state of the art information on implant

associated infections and current biomaterial-based strategies to prevent this problem. Furthermore, a description of the PEO process, as a possible process for generating antibacterial surfaces for bone implants, and the motivation of using Ag nanoparticles as antibacterial agent are also presented. Finally, the aim of the research and the thesis outline are defined.

The experimental conditions and the required equipment for the synthesis and characterization of novel Ag-based antibacterial layers on the Ti6Al7Nb alloy are presented in *Chapter 2*. In addition, the main results on surface characterization are reported in this chapter. During the PEO process, the Ti6Al7Nb disk was immersed in an aqueous calcium acetate/calcium glycerophosphate-based electrolyte bearing dispersed Ag nanoparticles and connected to a high-voltage power supply. A stainless steel plate served as the counter-electrode. When the applied voltage exceeded a certain critical value, dielectric breakdown of the anodic barrier TiO_2 layer occurred on the surface of the Ti6Al7Nb alloy thereby resulting in a modified surface. The morphological investigations by scanning electron microscopy (SEM) revealed the presence of a porous TiO_2 layer with well-separated round/elongated pores, ranging from a few nanometers up to 10 μm in size. The presence of Ag nanoparticles in the porous TiO_2 layers was confirmed by high-resolution SEM coupled with the back-scattering and energy dispersive X-ray spectroscopy (EDX) detectors. Except the presence of different concentrations of Ag nanoparticles in the TiO_2 layers, the other surface characteristics such as chemical and phase composition, surface roughness, porosity, pore density, pore size distribution, mean pore size and surface free energy remained unchanged as compared with the Ag-free TiO_2 layers. Therefore, the effect of Ag nanoparticles embedded in the TiO_2 coatings in various concentrations, on the bacteria killing ability and viability of the bone cells could be evaluated without the interference of the other factors.

The challenge addressed in *Chapter 3* was the investigation of the mechanism of Ag nanoparticles incorporation in the TiO_2 layers during the PEO process. How and where are the Ag nanoparticles incorporated in the porous TiO_2 layer were the main research questions addressed. Thus, the Ag-bearing TiO_2 layers were grown at different oxidation times *i.e.,* 10, 30, 60, 90, 120, 180, 240 and 300 seconds and thoroughly studied in plan view and cross-section using state of the art imaging techniques such as high-resolution transmission electron microscopy and SEM coupled with EDX analyses for chemical composition. It was observed that Ag nanoparticles could be incorporated in the growing TiO_2 layers starting with very initial stages of oxidation (*i.e.,* 10 seconds) with further incorporation as the PEO process was continued for longer durations. Thorough investigation of the coatings for evidence of particles revealed three different locations of Ag within the oxide: (i)

fused on the surface of the oxide (with some particles protruding from the layer), (ii) fused into the pore walls (both open and closed pores), and (iii) embedded across the thickness of the dense oxide layer (starting just above the barrier-like layer). The morphology of the Ag nanoparticles found in the layers seemed to match that of the nanoparticles used in the electrolyte. As far as the mechanism of Ag nanoparticles incorporation is concern, four main steps were proposed:

(i) transport of Ag nanoparticles at the TiO_2/electrolyte and Ti6Al7Nb/TiO_2 interfaces by mechanical agitation and electrophoretic mobility through short-circuit channels, open pores and cracks;
(ii) attachment/adsorption of Ag nanoparticles to the sites of coating growth, where under the local heating generated by the sparking events the layer is relatively soft;
(iii) fusion of Ag nanoparticles into the soft oxide once the sparks extinguish and the site is cooled by the electrolyte;
(iv) encroachment of the already embedded Ag nanoparticles during the coating growth as the new coating formed close to the Ti6Al7Nb/TiO_2 interface might be extruded through the breakdown channels causing the molten material to fill the previously created pores and cracks moving along the Ag nanoparticles that were fused in a previous discharge event.

The particular focus of *Chapter 4* was to perform *in vitro* tests to evaluate the antibacterial activity of the TiO_2 layers bearing different concentrations of Ag nanoparticles. The main challenge was to find and use the proper antibacterial assays to investigate the antibacterial activity of solid surfaces. Considering that the current available assays do not reflect the precise conditions under which the bacteria will come in close contact with a potentially bactericidal surface, new assays for surface antibacterial activity as well as leachable antibacterial activity were proposed and tested. The pathogen used for the tests was methicillin-resistant *Staphylococcus aureus* (MRSA), one of the most prevalent and virulent microorganism responsible for implant associated infections. Surface antibacterial activity, tested by a direct contact assay, revealed 98% and 99.75% reduction in bacteria colony forming units (CFU) for 0.3Ag and 3.0Ag surfaces, respectively. In contrast, the untreated Ti6Al7Nb and Ag-free (0Ag) surfaces showed a 1000-fold increase in bacterial CFU. Testing of leachable antibacterial activity revealed a well-defined inhibition zone around the Ag-bearing samples due to the release of Ag ions after 24 hours of incubation with MRSA. Quantification of Ag ions release and determination of total Ag content in the layers, together with the antibacterial tests, led to the conclusion that both Ag nanoparticles *per se* as well as Ag ions release contributed to the bactericidal activity of the TiO_2 surfaces.

The next step in the development of antibacterial surfaces for bone implants was to check their toxicity to human cells. Whether or not the Ag-bearing TiO_2 layers were toxic to osteoblast cells was described in *Chapter 5*. For this, a Simian Virus 40 (SV40)-immortalized human fetal osteoblast (SV-HFO) cell line was used. Cell viability, cell morphology and spreading, and the actin cytoskeletal organization and nucleus were studied *in vitro* using the Alamar Blue assay, SEM and fluorescence microscopy, respectively on TiO_2 surfaces bearing different concentrations of Ag nanoparticles (*i.e.,* 0.3Ag, 0.8Ag, 1.6Ag and 3.0Ag). The results showed that the viability of osteoblast cells was strongly dependent on the concentration of Ag nanoparticles in the layers. The 3.0Ag surfaces, because of the higher concentration of Ag nanoparticles in the TiO_2, were found to be toxic to osteoblast cells. In contrast, the osteoblasts viability on the 0.3Ag surfaces, assessed by Alamar Blue, SEM and fluorescence microscopy, was not inhibited after 2, 5 and 7 days of culture. The testing of the TiO_2 surfaces bearing intermediate concentrations of Ag nanoparticles appeared to follow the same trend. A significantly lower number of bone cells survived on the 0.8Ag and 1.6Ag samples after 2 days of culture.

Chapter 6 covers a feasibility study to see whether the PEO process, used to render the surface of a Ti6Al7Nb alloy antibacterial, can be applied on commercially available cementless bone implants such as plasma-sprayed titanium hip components. Such implants have very complex geometries and the main challenge was to create an Ag-bearing antibacterial TiO_2 layer that covers accurately the topography of such implants. A titanium plasma-sprayed acetabular cup was chosen as a substrate and PEO was performed using the Ag-bearing calcium acetate/calcium glycerophosphate electrolyte. The superimposed layers were then characterized with respect to surface morphology and chemistry using SEM and EDX. The surface morphology results showed the successful creation of the TiO_2 layer, with its fine network of interconnected, round or elongated pores, superimposed on the macro-porous structure of the plasma-sprayed coating. The PEO antibacterial layer followed accurately the surface topography of the plasma-sprayed sample. Furthermore, the Ag nanoparticles were found to be present on top as well as in the porous structure of TiO_2 layer.

The work performed in this thesis leads to the final conclusions that (i) TiO_2 layers bearing Ag nanoparticles can be produced on titanium biomedical alloys and on titanium-based bone implants using the plasma electrolytic oxidation process and (ii) the resultant novel layers can be a suitable engineering solution for the clinical problem of implant associated infections of cementless bone implants.

Samenvatting

Totale heup arthroplastiek (THA) is de veiligste en meest effectieve methode voor het behandelen van ernstige degeneratieve, posttraumatische en andere gewrichtsaandoeningen. Met een vergrijzende bevolking, die steeds actiever wordt, zal het gebruik van biomedische implantaten aanhoudend stijgen. Volgens schattingen worden er jaarlijks wereldwijd 1.000.000 THAs uitgevoerd. Dientengevolge zal het gevaar van implantaat geassocieerde infecties (IGI) een groot percentage van deze populatie treffen. IGI zijn ernstige complicaties veroorzaakt door infectieuze bacteriën die het implantaatoppervlak bevolken, snel prolifereren en een matrix van polysacharide afscheiden, ook wel biofilm genoemd. Eenmaal gevormd, is een biofilm extreem resistent tegen antibiotica of verdedigingsmechanismen van de gastheer en zal uiteindelijk leiden tot loslating van het implantaat en revisiechirurgie, met desastreuze gevolgen voor de patiënt. Op dit moment is er geen remedie klinisch beschikbaar die IGI kunnen voorkomen op cementloze implantaten. Daarom zijn intensieve onderzoeksinspanningen toegespitst op de ontwikkeling van antibacteriële oppervlakken die elke aanhechtende bacterie doodt en als gevolg voorkomt dat bacteriën een biofilm kunnen vormen.

De doelstelling van dit doctoraatsproefschrift was het ontwikkelen van innovatieve antibacteriële oppervlakken voor cementloze implantaten. De focus van het onderzoek lag op de synthese, fysicochemische karakterisering en biologische evaluatie van een op-Ag-gebaseerde antibacteriële oppervlak op de biomedische Ti6Al7Nb legering. Met behulp van het plasma elektrolytische oxidatie (PEO) proces werden verschillende concentraties Ag-nanodeeltjes in een microporeuze TiO_2-laag ingelijfd, die op de Ti6Al7Nb legering werd gegroeid, om zo het oppervlak om te vormen naar een antibacteriële. In navolging van de synthese werden de innovatieve oxidelagen diepgaand gekarakteriseerd met betrekking op verdeling van Ag-nanodeeltjes, chemische- en fasesamenstelling, oppervlakteruwheid, coatingporositeit, poriedichtheid, poriegrootte-distributie en oppervlakte vrije energie. Verder werden de antibacteriële effectiviteit en toxiciteit voor humane botcellen van de lagen *in vitro* beoordeeld. Ten slotte werd er een haalbaarheidsstudie

uitgevoerd waarin werd beoordeeld of op-Ag-gebaseerde antibacteriële oppervlakken toegepast konden worden op commercieel verkrijgbare botimplantaten zoals plasma-spray titanium heup componenten.

Het proefschrift beslaat zes hoofdstukken, aanvangend met een introductie in *Hoofdstuk 1* dat de achtergrond maar ook de state-of-the-art informatie verschaft op het gebied van implantaat geassocieerde infecties en de huidige op-biomateriaal-gebaseerde strategieën behandeld om dit probleem te voorkomen. Verder wordt het PEO proces als een potentieel proces voor het genereren van antimicrobiële oppervlakken voor botimplantaten beschreven en de motivatie voor het gebruik van Ag-nanodeeltjes als antimicrobiële agens gegeven. Voorts wordt de doelstelling van het onderzoek gedefinieerd en met een beknopt overzicht van de inhoud en opbouw van het proefschrift afgesloten.

De experimentele condities en de benodigde apparatuur voor de synthese en karakterisering van innovatieve op-Ag-gebaseerde antibacteriële lagen op de Ti6Al7Nb legering worden in *Hoofdstuk 2* gepresenteerd. Bovendien worden de voornaamste resultaten van de oppervlaktekarakterisering in dit hoofdstuk gerapporteerd. Tijdens het PEO proces was de Ti6Al7Nb schijf ondergedompeld in een waterige, op-calciumacetaat/calciumglycerofosfaat-gebaseerd elektrolyt die gedispergeerde Ag-nanodeeltjes bevatte en aangesloten aan een hoogspanningsvoeding. Een roestvaststalen plaat diende als tegenpool. Wanneer de toegepaste spanning een bepaalde kritische waarde oversteeg, ontstond er diëlektrische afbraak van de anodische barrière TiO_2-laag op het oppervlak van de Ti6Al7Nb legering wat resulteerde in een gemodificeerd oppervlak. Het onderzoek naar de morfologie, door middel van scanning elektronenmicroscopie (SEM), liet de aanwezigheid van een poreuze TiO_2-laag zien met afzonderlijke ronde/langwerpige poriën, variërend van een paar nanometers tot 10 µm in grootte. De aanwezigheid van Ag-nanodeeltjes in de poreuze TiO_2-lagen werd bevestigd door hoge-resolutie SEM gekoppeld met detectoren voor terugverstrooiing en energie dispersieve röntgenspectroscopie (EDX). Naast de aanwezigheid van verschillende concentraties Ag-nanodeeltjes in de TiO_2-lagen bleven, vergeleken met de Ag-vrije TiO_2-lagen, de andere kenmerken van het oppervlak zoals chemische- en fasesamenstelling, oppervlakteruwheid, porositeit, poriedichtheid, poriegrootte-distributie, gemiddelde poriegrootte en oppervlakte vrije energie onveranderd,. Hierdoor kon het effect van Ag-nanodeeltjes, ingebed in de TiO_2 coatings in verschillende concentraties, op bacteriedodend vermogen en levensvatbaarheid van de botcellen zonder stoornis van andere factoren geëvalueerd worden.

De uitdaging die in *Hoofdstuk 3* behandeld wordt, was het onderzoek naar de mechanismen van de inlijving van Ag-nanodeeltjes in de TiO_2-lagen tijdens het PEO proces. De voornaamste onderzoeksvragen waren hoe en waar de Ag-nanodeeltjes in de poreuze TiO_2-lagen ingelijfd werden. De Ag-houdende TiO_2-lagen werden daarom op verschillende oxidatietijden aangegroeid, namelijk 10, 30, 60, 90, 120, 180, 240 en 300 seconden en diepgaand bestudeerd in bovenaanzicht en dwarsdoorsnede, waarbij gebruik werd gemaakt van state-of-the-art beeldvormingstechnieken zoals hoge-resolutie transmissie elektronenmicroscopie en SEM gekoppeld met EDX analyses voor chemische samenstelling. Er werd waargenomen dat Ag-nanodeeltjes al op een vroeg stadium van de oxidatie (namelijk 10 seconden) in de groeiende TiO_2-laag ingelijfd konden worden, waarna verdere inlijving plaatsvond, naarmate het PEO proces voortduurde. Diepgaand onderzoek op de coatings voor bewijs van deeltjes onthulde drie verschillende locaties van Ag in de oxide: (i) fusie aan het oppervlak van de oxide (met een aantal deeltjes uit de laag stekend), (ii) fusie in de poriewand (zowel open als gesloten poriën) en (iii) ingebed langs de gehele dikte van de dichte oxide laag (beginnend net boven de barrière-achtige laag). De morfologie van de Ag-nanodeeltjes die in de lagen werden gevonden, leken overeen te komen met die van de nanodeeltjes gebruikt in het elektrolyt. Wat betreft de mechanismen van de inbedding van de Ag-nanodeeltjes werden vier stappen aangedragen:

(i) Transport van de Ag-nanodeeltjes aan de TiO_2/elektrolyt en Ti6Al7Nb/TiO_2 grensvlakken bij mechanische agitatie en elektroforetische mobiliteit door kortsluitingskanalen, open poriën en scheuren;
(ii) Aanhechting/adsorptie van Ag-nanodeeltjes naar het gebied van coatinggroei, waar, door de vonkactiviteit is gegenereerde lokale warmte, de laag relatief zacht is;
(iii) Fusie van Ag-nanodeeltjes in de zachte oxide wanneer de vonken zijn gedoofd en de locatie is gekoeld door de elektrolyt;
(iv) Behoud van de reeds ingebedde Ag-nanodeeltjes tijdens de groei van de coating; de nieuw gevormde coating, dichtbij het Ti6Al7Nb/TiO_2 grensvlak, kan door de afbraakkanalen geëxtrudeerd worden met als gevolg dat het gesmolten materiaal de reeds gevormde poriën en scheuren vult en langs de Ag-nanodeeltjes beweegt die al in een eerdere ontladingsgebeurtenis waren gefuseerd.

De focus van *Hoofdstuk 4* lag op het uitvoeren van *in vitro* testen om de antibacteriële activiteit van de TiO_2-lagen te evalueren die verschillende concentraties Ag-nanodeeltjes bevatte. De voornaamste uitdaging was het vinden en gebruiken van de juiste antibacteriële toetsingen om de antibacteriële activiteiten van oppervlakken van vaste stoffen te onderzoeken. Rekening houdend met het feit dat huidige

beschikbare testen niet de precieze omstandigheden reflecteren waaronder de bacteriën in contact komen met een potentiele bactericidaal oppervlak, werden nieuwe testen voor zowel antibacteriële activiteit aan het oppervlak als uitlogende antibacteriële activiteit voorgedragen en getest. De pathogeen die voor de test werd gebruikt, was meticillineresistente Staphylococcus aureus (MRSA), een van de meest prevalente en virulente micro-organismen verantwoordelijk voor implantaat geassocieerde infecties. De antibacteriële activiteit aan het oppervlak, getest door een direct contact toets, liet een afname zien van 98% en 99.75% in bacterie-kolonievormende eenheden (CFU) voor respectievelijk 0.3Ag en 3.0Ag. In tegenstelling lieten de onbehandelde Ti6Al7Nb en Ag-loze (0Ag) oppervlakken een 1000-voudige toename zien in bacterie CFU. Testen op uitlogende antibacteriële activiteit lieten een goed gedefinieerde inhibitiezone rond de Ag-houdende monsters zien vanwege de vrijgave van Ag-ionen na een incubatie met MRSA van 24 uur. Kwantificatie van de vrijgave van Ag-ionen en bepaling van de totale Ag-samenstelling in de lagen, tezamen met de antibacteriële tests, leidde tot de conclusie dat zowel Ag-nanodeeltjes per se als vrijgave van Ag-ionen bijdroegen aan de bacteriële activiteit van de TiO_2-oppervlakken.

De volgende stap in de ontwikkeling van antibacteriële oppervlakken voor botimplantaten was het controleren van hun toxiciteit voor humane cellen. Of de Ag-houdende TiO_2-lagen wel of niet toxisch waren voor osteoblast cellen is beschreven in *Hoofdstuk 5*. Hiervoor werd gebruik gemaakt van een Simian Virus 40 (SV40) geïmmortaliseerde humane foetale osteoblast (SV-HFO) cellijn. Celviabiliteit, celmorfologie en spreiding en de organisatie van het actine cytoskelet en nucleus werden bestudeerd *in vitro* met behulp van de Alamar Blue test, SEM en fluorescentiemicroscopie respectievelijk op TiO_2-oppervlakken met verschillende concentraties Ag-nanodeeltjes (namelijk 0.3Ag, 0.8Ag, 1.6Ag en 3.0Ag). De resultaten lieten zien dat de viabiliteit van osteoblast cellen sterk afhankelijk was van de concentratie Ag-nanodeeltjes in de lagen. De 3.0Ag oppervlakken, vanwege de hogere concentratie Ag-nanodeeltjes in de TiO_2, bleken toxisch te zijn voor osteoblast-cellen. Echter, de osteoblast-viabiliteit op de 0.3Ag oppervlakken, beoordeeld door Alamar Blue, SEM en fluorescentiemicroscopie, was niet geïnhibeerd na 2, 5 en 7 dagen kweken. Het testen van de TiO_2 oppervlakken die de tussenliggende concentraties Ag-nanodeeltjes bevatte, scheen dezelfde trend te volgen. Een significant lagere hoeveelheid aan botcellen overleefde op de 0.8Ag en 1.6Ag monsters na 2 dagen kweken.

Hoofstuk 6 beslaat een haalbaarheidsstudie waarin wordt bekeken of het PEO proces, gebruikt om het oppervlak van de Ti6Al7Nb legering om te vormen naar een antibacteriële, kan worden toegepast op commercieel verkrijgbare cementloze

botimplantaten zoals plasma-spray titanium heup componenten. Deze implantaten hebben zeer complexe geometrieën en de voornaamste uitdaging was om een Ag-houdende antibacteriële TiO_2-laag te creëren die de topografie van zo'n implantaat accuraat bedekt. Een plasma-spray acetabulaire cup werd als substraat gekozen en PEO werd uitgevoerd met het Ag-houdende calciumacetaat/calciumglycerofosfaat elektrolyt. De oppervlaktemorfologie en samenstelling van gesuperimponeerde lagen werden daarna gekarakteriseerd met behulp van SEM en EDX. De oppervlakte morfologieresultaten lieten de succesvolle fabricage van de TiO_2-laag zien met een fijne maas van aaneengesloten, ronde of langwerpige poriën gesuperimponeerd op de macro-poreuze structuur van de plasma-spray coating. De PEO antibacteriële laag volgde nauwgezet de oppervlaktetopografie van het plasma-spray monster. Bovendien werden de Ag-nanodeeltjes gevonden aan het oppervlak en in de poreuze structuur van de TiO_2-laag.

Het uitgevoerde werk in dit proefschrift leidt tot de eindconclusies dat (i) Ag-nanodeeltjes houdende TiO_2-lagen geproduceerd kunnen worden op titanium biomedische legeringen en op botimplantaten die op titanium gebaseerd zijn, gebruikmakend van het plasma elektrolytische oxidatie proces en (ii) de daaruit volgende innovatieve lagen een geschikte, technische oplossing voor het klinische probleem kunnen zijn van implantaat geassocieerde infecties van cementloze botimplantaten.

Acknowledgements

This thesis could not have been written without the help and support of many people, for whom I would like to express my deep gratitude.

First, I would like to thank Prof. dr. ir. Carmen Teodosiu, Dr. ir. Iulian Apachitei and Assoc. prof. dr. dr. h.c. ir. Jurek Duszczyk for helping me find my way in the Netherlands, at Delft University of Technology. Thank you for involving me in challenging research projects that allowed me to develop a solid scientific background and obtain a PhD degree in the end.

Next, I would like to thank Prof. ir. Laurens Katgerman for his support in getting this thesis ready and for helping with all the paperwork needed for starting the defence procedure.

I would have never been able to write this thesis without the help of my daily supervisors Dr. ir. Iulian Apachitei and Dr. ir. Lidy Fratila-Apachitei. They coached me on a daily basis, both professionally and personally, and provided me with valuable knowledge and ideas from the very beginning of my work at TU Delft to the very end of it. Thank you so much for your constant encouragement, inspiration, guidance and energy to read and improve many drafts of my writings.

Also, this thesis could have never been written without the excellent collaboration of Dr. Sebastian Zaat from Academic Medical Center, Department of Medical Microbiology and Center for Infection and Immunity, Amsterdam and Prof. dr. Hans van Leeuwen from Erasmus Medical Center, Department of Internal Medicine. Thank you for allowing me to perform my research in your labs and for teaching me all the biological assays. I also express my thanks to Dr. ir. Frans Tichelaar for helping me with the TEM measurements and Joop Padmos for helping me with GFAAS measurements.

I would like to thank the technical support of TU Delft, namely Tjeerd Tobi, Lambert Schipperheijn, Sander Leeflang, Kees Kwakernaak and Jan Boomsma. Extra thanks to Tjeerd Tobi for his kind and invaluable help during my first weeks in the Netherlands. Thanks Sander Leeflang for all the Dutch translations in this thesis.

Next, I would like to acknowledge all my colleagues for their continuous support and friendship. I would like to mention especially Floris, Demian, Sander, Jan, He, Tanya and Andre from the LMP group; Lambert, Ziggy, Tungky, Juan-Pablo, Andrea, Allert and Yulia from the MSE group; Bianca, Bram, Claudia B, Claudia N, Viola, Rodrigo and Marijke from the "bone" group; and Leonie, Paul and Martijn from the microbiology group. I had a great time having you around and I enjoyed all the lunch and coffee breaks with you.

Furthermore, I want to thank my friends Andrei, Stefan, Bogdan T, Adriana, Robert, Ruxandra, Marius, Maria, Mihai C, Mihai L, Iulia, George and Madalina who made all my holidays, weekend road-trips and game nights awesome!

Finally, this thesis would not have been possible without the continuous support and encouragement from my parents and family members. There are not enough words to express my gratitude to them.

Since it is not possible to mention here each and every person who contributed to my work in one way or the other, I apologize to these persons for not including them, and thank them all together.

Bogdan Stefan NECULA

Curriculum vitae

Bogdan Stefan NECULA

Date of birth:	December 21, 1979
Place of birth:	Piatra Neamt, Romania
Nationality:	Romanian

Education:

2004 – 2005	**MSc. Environmental Management**
	Gh. Asachi Technical University of Iasi, Romania
	Grade: 9.86 out of 10
1999 – 2004	**BSc. Chemical Engineering**
	Gh. Asachi Technical University of Iasi, Romania
	Grade: 9.8 out of 10

Professional and research experience:

2009 – 2013	**PhD researcher**
	Delft University of Technology, Delft – The Netherlands
	Department of Biomechanical Engineering
2010	**Visiting researcher**
	Academic Medical Center, Amsterdam – The Netherlands
	Center for Infection and Immunity Amsterdam
2009 –2010	**Visiting researcher**
	Erasmus Medical Center, Rotterdam – The Netherlands
	Department of Internal Medicine
2006 – 2009	**Research fellow**
	Delft University of Technology, Delft – The Netherlands
	Department of Materials Science and Engineering

List of publications

Journal publications:

B.S. Necula, I. Apachitei, L.E. Fratila-Apachitei, E.J. van Langelaan, J. Duszczyk, Titanium bone implants with superimposed micro and nano-scale porosity and antibacterial capability, Applied Surface Science, 273 (2013) 310–314.

B.S. Necula, L.E. Fratila-Apachitei, J.P.T.M. van Leeuwen, S.A.J. Zaat, I. Apachitei, J. Duszczyk, *In vitro* cytotoxicity evaluation of porous TiO_2-Ag antibacterial coatings on human fetal osteoblasts, Acta Biomaterialia, 8 (2012) 4191–4197.

G.J.S. Dawes, L.E. Fratila-Apachitei, **B.S. Necula**, I. Apachitei, J.P.T.M. van Leeuwen, J. Duszczyk, M. Eijken, Effects of dexamethasone loaded PLGA microspheres on human fetal osteoblasts, Journal of Biomaterials Applications, 27(4) (2011) 477–483.

B.S. Necula, I. Apachitei, F.D. Tichelaar, L.E. Fratila-Apachitei, J. Duszczyk, An electron-microscopical study on the growth of TiO_2-Ag antibacterial coatings on Ti6Al7Nb biomedical alloy, Acta Biomaterialia, 7 (2011) 2751-2757.

G.J.S. Dawes, L.E. Fratila-Apachitei, **B.S. Necula**, I. Apachitei, G.J. Witkamp, J. Duszczyk, Release of PLGA–encapsulated dexamethasone from microsphere loaded porous surfaces, Journal of Materials Science: Materials in Medicine, 21 (2010) 215–221.

B.S. Necula, L.E. Fratila-Apachitei, S.A.J. Zaat, I. Apachitei, J. Duszczyk, *In vitro* antibacterial activity of porous TiO_2–Ag composite layers against methicillin-resistant Staphylococcus aureus, Acta Biomaterialia, 5 (2009) 3573–3580.

B.S. Necula, I. Apachitei, L.E. Fratila-Apachitei, A. Berkani, J. Duszczyk, Enrichment of anodic MgO layers with Ag nanoparticles for biomedical applications, Journal of Materials Science: Materials in Medicine, 20 (2009) 339–345.

B.S. Necula, I. Apachitei, L.E. Fratila-Apachitei, C. Teodosiu and J. Duszczyk, Stability of nano-/microsized particles in deionized water and electroless nickel solutions, Journal of Colloid and Interface Science 314(2) (2007) 514-522.

Conference publications:

B.S. Necula, I. Apachitei, S.A.J. Zaat, L.E. Fratila-Apachitei, M.A. Leeflang, J. Duszczyk, Loading and distribution of Ag nanoparticles in porous TiO_2 antibacterial layers, Euro PM2012 (ISBN 978-1-899072-25-5), vol. 1, pp. 217-222.

B.S. Necula, L.E. Fratila-Apachitei, J.P.T.M. van Leeuwen, S.A.J. Zaat, I. Apachitei, J. Duszczyk, Bone cell viability and antibacterial efficacy of porous TiO_2-Ag coatings, European Cells and Materials, Vol. 21. Suppl. 2, 2011.

B.S. Necula, L.E. Fratila-Apachitei, S.A.J. Zaat, I. Apachitei, J. Duszczyk, Bactericidal Coatings with Silver Nanoparticles, European Cells and Materials Vol. 20. Suppl. 3, 2010.

B.S. Necula, L.E. Fratila-Apachitei, J.P.T.M. van Leeuwen, I. Apachitei, J. Duszczyk, Effects of microporous Ti6Al7Nb surfaces on the *in vitro* bone cells response, PM2010 Conference Proceedings, Volume 4: PM Biomaterials, p 739-746.

B.S. Necula, L.E. Fratila-Apachitei, S.A.J. Zaat, I. Apachitei, J. Duszczyk, Antibacterial effect of Ag nanoparticles embedded in a porous Ti6Al7Nb surface, EURO PM2009 Conference Proceedings, Volume 2: PM Biomaterials, p 423-428.